Journal of Medicinal Chemistry

pubs.acs.org/jmc

Article

Targeting a Pleckstrin Homology Domain with a Lysine-Reactive Covalent Binder

Rebekah M. West, Radu Costin Bizga Nicolescu, Paul Brear, James Wagstaff, Beata K. Blaszczyk, Tomas Deingruber, Matthew G. Sanders, Francisco Javier Pérez-Areales, David R. Spring,* and Marko Hyvönen*

Cite This: J. Med. Chem. 2026, 69, 12099−12121

Read Online

ACCESS | Metrics & More | Article Recommendations | Supporting Information

ABSTRACT: Bruton's Tyrosine Kinase (BTK) is a validated target for hematological malignancies, with numerous FDA-approved inhibitors on the market. Current therapies target the highly conserved ATP binding site and hence limit the therapeutic index given the site's highly conserved nature across the kinome. We explore a novel approach for BTK inhibition by targeting the PH domain-mediated membrane recruitment and activation of BTK. We have identified a fragment which covalently modifies a lysine in the inositol phosphate (PIP3) binding site and inhibits the binding of a soluble PIP3 headgroup analog to the PH domain. Fragment growth and an extensive structure-binding relationship study uncovered 27 crystal structures and a best-in-class analog, **24**. Evaluation of pK_a values of the targeted lysine in BTK and other PH domains suggests this as a more general approach to PH domain inhibition.

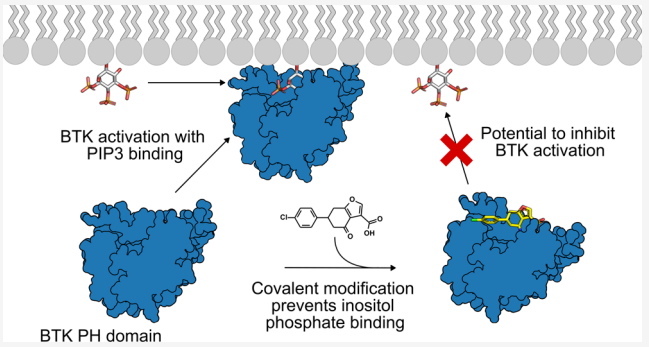

Inhibition of signaling proteins, such as protein kinases, is typically achieved through targeting of their active sites, such as ATP-binding sites in kinases. As these sites tend to be under high evolutionary pressure to preserve binding to natural cofactor ATP, development of specific inhibitors can be challenging. An alternative approach is to identify other functionally important sites in the protein, which would offer better selectivity. Such sites might include protein−protein interaction sites or binding sites for other cofactors. In the case of BCR:ABL inhibition, the myristoyl binding site in the kinase lobe has been successfully used to develop a treatment for chronic myeloid leukemia (CML).[1] We have recently shown how targeting of the TPX2 binding site on Aurora A kinase can result in highly specific inhibition through a novel mechanism.[2]

Many eukaryotic signaling proteins are composed of multiple independent domains that modulate the activity and localization of the proteins. Among these, Pleckstrin Homology (PH) domains are one of the most common, with an estimated 250 of them in the human proteome.[3] PH domains are typically involved in membrane association, through binding to phosphoinositides on the inner leaflet of the plasma membrane. In the case of Akt, the N-terminal PH domain can interact with the kinase domain, rendering it inactive, but can release this activation upon lipid binding. The importance of this mechanism has been highlighted by identification of molecules that inhibit Akt by locking the PH and kinase domains in their inactive state.[4]

The Tec family of tyrosine kinases is another example of PH domain-containing signaling proteins where membrane association is critically important for their activity. As members of the larger Src superfamily, they share a core structure of SH2-SH3-kinase domains, but contain an additional PH domain and a Zn^{2+} binding Tec-homology domain (also called as BTK-motif) in their N-termini (Figure 1A).[5] However, unlike other Src-like kinases, which are usually myristoylated at their N-termini and hence intrinsically membrane associated, the membrane association of Tec kinases is mediated by the PH domain through interactions with phosphatidylinositol (3,4,5)-trisphosphate (PIP3), the product of PI3-kinase activity on the plasma membrane.[6]

Bruton's Tyrosine Kinase (BTK) is one of the best studied Tec family kinases.[7] BTK plays a key role in B-cell maturation and its inactivation by mutations results in X-linked agammaglobulinemia (XLA), a condition in which (typically) male individuals lack B-cells and antibody-mediated humoral immune protection.[5,7]

Received: December 28, 2025
Revised: March 17, 2026
Accepted: May 4, 2026
Published: May 14, 2026

https://doi.org/10.1021/acs.jmedchem.5c03818
J. Med. Chem. 2026, 69, 12099−12121

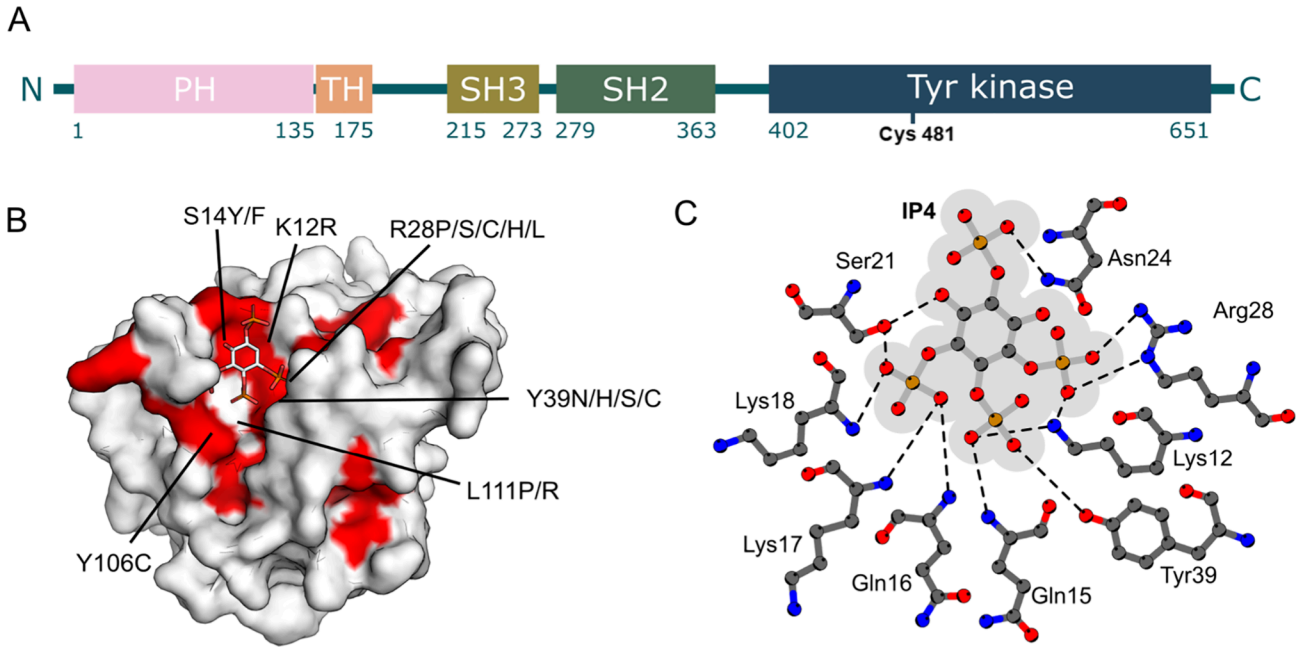

Figure 1. BTK as a target. (A) From N- to C-terminus, the 659 amino acids of BTK are organized into five domains: Pleckstrin homology (PH), Tec homology (TH), Src homology 3 (SH3), Src homology 2 (SH2) and a tyrosine kinase domain. Lysine 12 and cysteine 481, targets of covalentmodifiers from this work and of ibrutinib, respectively, are highlighted. (B) Structure of BTK PH domain in complex with IP4 (PDB: 1B55) with ligand shown as sticks and domain shown as molecular surface. Residues around the IP4 binding site found to cause XLA (as listed in LOVD database https://databases.lovd.nl/shared/genes/BTK) are colored red. (C) Details of the IP4 binding site in BTK PH domain, showing the electrostatic and hydrogen bonding interactions between the ligand and the domain. Figure modified from Ligplot output of PDB: 1B55.

BTK is also studied for its role in cancer. Primarily expressed in hematopoietic cells, aberrant BTK interferes with healthy BCR signaling leading to uncontrolled B-cell survival and proliferation in chronic lymphocytic leukemia (CLL), mantle cell lymphoma (MCL) and other blood cancers.[8] Interestingly, isoforms of BTK (p65BTK) are also thought to drive tumor progression in solid tumors (such as colon, breast and prostate), through promoting resistance to chemotherapy, contributing to tumor-stroma communication and manipulating macrophage activity and immune suppression.[8]

Activation of BTK is dependent on PH domain binding to PIP3. Membrane recruitment mediated dimerization is thought to release BTK from its inhibited form, resulting in trans-autophosphorylation and activation of BTK.[9] Given that a large number of mutations are found in the inositol phosphate binding site and abolishing lipid binding can result in XLA, inhibition of membrane association by small molecules would be a valid approach to BTK inhibition (Figure 1B). For example, R28, one of the key residues involved in PIP3 binding, is mutated in a number of XLA cases[10] and mutation of the same residue to cysteine (R28C) in mice results in X-linked immunodeficiency (XID).[11] In addition to validating the PH domain as a target for BTK inhibition, interaction with these conserved ligand-binding residues would potentially make it difficult for BTK to acquire resistance as their mutation would also disrupt binding to natural ligands.

Targeting PH domains is not expected to be straightforward as the binding site for phosphorylated phosphoinositides is highly charged and their interactions with the PH domain are largely ionic (Figure 1C). Also, the binding occurs in a relatively shallow pocket on the surface of the domain, offering limited three-dimensionality. In the early 2000s, the purine analog, triciribine, was repurposed upon the discovery that its monophosphate active form prevented the membrane recruitment of Akt. As might be expected for inhibitors binding a highly charged pocket, triciribine had limited bioavailability and, disappointingly, was discontinued from clinical trials due to toxicity and poor efficacy.[12] Peptides which are better able to mimic PIP3 interaction motifs have been developed against Akt PH domain E17K mutants, but they suffer from poor stability, permeability, and half-life in comparison to small molecules.[13]

At the time of writing, no direct PH domain inhibitors have advanced to late-stage clinical trials, despite the recent development of preclinical candidates against PDK1[14] and BRAG2.[15] With the PH domain being found in large numbers of human proteins while being relatively poorly conserved, its inhibition has been recognized as an interesting alternative to more conventional target sites in BTK.[3]

With this background in mind, we decided to use BTK as a model for PH domain-targeted inhibitor development. We used fragment-based ligand discovery, aiming to generate from the outset binders that have drug-like properties and are suitable for further development. A reactive lysine residue was discovered in the middle of the PIP3 binding site and used as the anchor point for the development of inhibitors that block PIP3 binding to the PH domain.

RESULTS AND DISCUSSION

Fragment Screening against PH Domain

The fragment screening campaign against the BTK PH domain consisted of a thermal shift assay, followed by validation with X-ray crystallography and biophysical techniques (ITC).

A fragment library from the group of Chris Abell, (Department of Chemistry, Cambridge, unpublished) of 720 fragments was screened against both the wild-type (WT) and mutant (R28C) BTK PH domain constructs by differential

https://doi.org/10.1021/acs.jmedchem.5c03818
J. Med. Chem. 2026, 69, 12099−12121

scanning fluorimetry (DSF). DSF assays have varied success in fragment-based screens; however, soluble PIP3 analogue inositol-1,3,4,5-tetrakisphosphate (IP4) resulted in +20 °C stabilization of the domain, suggesting that productive binding to this site would be detected by thermal shift. As R28 is one of the key residues for IP4 binding and frequently mutated in XLA patients (Figure 1B), we used a PH domain with an R28C mutation as a control to identify hits that bound to the targeted IP4 binding site. A fragment that stabilized the WT PH domain but not the R28C mutant was likely to be binding at the IP4 site. The original screen identified 7 hits that stabilized the WT PH domain by more than 5 °C. These were further validated by DSF and X-ray crystallography. Testing the fragments at different concentrations by DSF identified two compounds (**i**/**1** and **v**) that showed significant stabilization of the WT domain while fully inactive against the R28C mutant. Compound **vii** also showed modest stabilization of the WT PH domain compared to the mutant (Figure 2A).

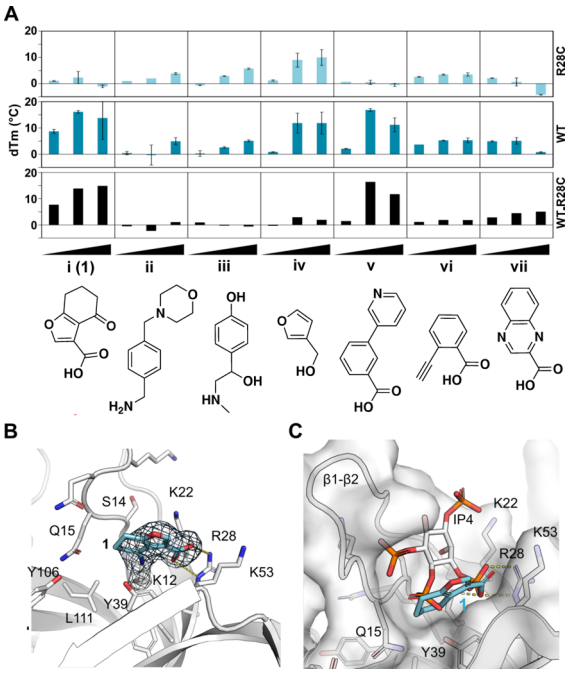

Figure 2. Fragment hit validation. (A) DSF analysis of hit fragments against WT and R28C mutant of BTK PH domain at three different concentrations. (B) Crystal structure of **1** covalently bound to K12 in the BTK PH domain (PDB: 6TUH). (C) Overlay of IP4 (PDB: 1B55) and hit **1**.

While the WT PH domain had not been crystallized before in unliganded form, well diffracting, soakable crystals were obtained through serial seeding using crystals of R28C mutant (PDB: 1BTK)The four fragment hits were soaked to these crystals but data from **v, vi** and **vii** showed only partial density for the fragment, most likely of the carboxylic acid moiety, close to R28 side chain.

In contrast, soaking the crystals with fragment **i**/**1** showed good density for the entire fragment (Figure 2B). Unexpectedly, as the fragment library was not designed to be for covalent modification, **1** forms a reversible iminium covalent bond with the nucleophilic terminal amino group of K12 (PDB: 6TUH) attacking the carbonyl of the ligand's cycloketone. The carboxylic acid of **1** interacts with R28 as expected, confirming its failure to stabilize R28C mutant. The binding site is overlapping with the IP4 binding site, engaging with key residues for IP4 interactions (Figure 2C). Compound **1** is sandwiched between a loop connecting β-strands 1 and 2 (β1-β2 loop) and residues Y39 and K53 from strands 3 and 4. The 1−2 loop undergoes significant reorganization upon binding to IP4 and is seen also in a more closed conformation with Q15 side chain hydrogen binding to Y106, compared to unliganded BTK PH domain. Our crystal system contained four domains in the asymmetric unit, which showed variable levels of modification by **1**, with one of the domains containing a second modified lysine (K19) next to K12. In subsequent elaborations only K12 was ever modified.

Biophysical Validation of Fragments

To further investigate the contribution of covalent bond formation to inhibition of IP4 binding to the BTK PH domain, we characterized this hit using isothermal titration calorimetry (ITC). While direct binding of **1** to the BTK PH domain could not be detected in ITC (data not shown), we could measure binding of IP4 to the PH domain with K_d of ca. 36 nM (Figure 3A). When the same titration was performed in the presence of 1 mM of **1**, IP4 binding was completely inhibited, confirming interaction with the target site (Figure 3B). The same ITC competition study was performed with **1z** where the electrophilic cyclohexanone section of **1** was removed (Figure 3C). As expected, **1z** did not inhibit the binding of IP4 to BTK PH and confirmed the importance of the covalent interaction observed in the crystal structure.

Mixed solvent molecular dynamics (MxMD) were performed to assess the druggability of the BTK PH domain. Given its function as a membrane anchor, the PH domain is a positively charged domain with shallow, charged pockets. Probing the surface of BTK PH domain with three cosolvents (isopropanol, pyrimidine and acetonitrile) 5% in water uncovered a pocket immediately adjacent to the three position of the cyclohexanone ring of the analogues (with a promising MxMD score of 31000). The pocket has an area of 286 Å^2 and a volume of 94 Å^3, with strong pyrimidine and isopropanol clustering. Importantly, this highlighted the potential of growing with *ortho* substituted phenyl rings, which productively fill the uncovered pocket with pi-stacking potential and hydrophobicity (Figure S108). Virtual screening and R-group enumeration using this phenyl scaffold also indicated that *ortho* substitutions may be advantageous (Figure S109).

Development of Fragment Hit 1 to Give Parent 2

The crystal structure of **1** showed significant space at the end of the six-membered ring, toward Y106 (Figures 4A and S2A). Given the flexibility of β1-β2 loop, as seen in the unliganded and IP4 bound structures before, we anticipated a more substantial pocket could open up with a suitable ligand. To explore this, a synthetic route was developed to grow the fragment from the six-membered ring. The most obvious derivative of **1** was to add a phenyl ring to it, yielding **2**. Soaking this into BTK PH domain crystals yielded a high-resolution cocrystal structure of a singly covalently modified target protein. Like fragment **1**, **2** shows the crystal ligand covalently bound to K12 (Figures 4B and S2B) and making a salt bridge with R28, but with the β1-β2 loop moving away from the binding site, making space for the phenyl ring. The phenyl ring is lying on top of L111, sandwiched between β1-β2 loop and Y106 side chain.

Importantly, the phenyl group of **2** presents various potential growing vectors as illustrated by analogues **4** and **5** (Figure

https://doi.org/10.1021/acs.jmedchem.5c03818
J. Med. Chem. 2026, 69, 12099−12121

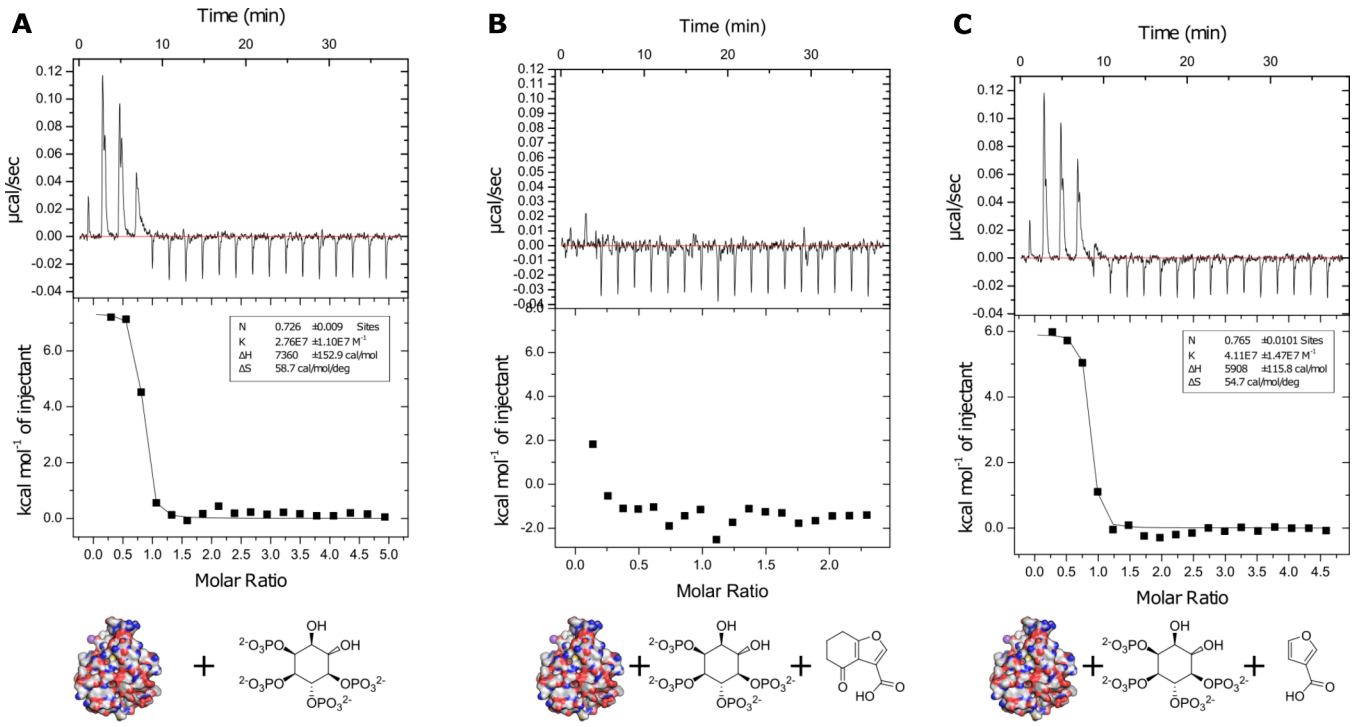

Figure 3. Isothermal titration calorimetry experiments. (A) BTK PH domain titrated with IP4. (B) Pretreatment with 1 mM furan fragment **1**. (C) Pretreatment with 1 mM furan fragment without ketone **1z**.

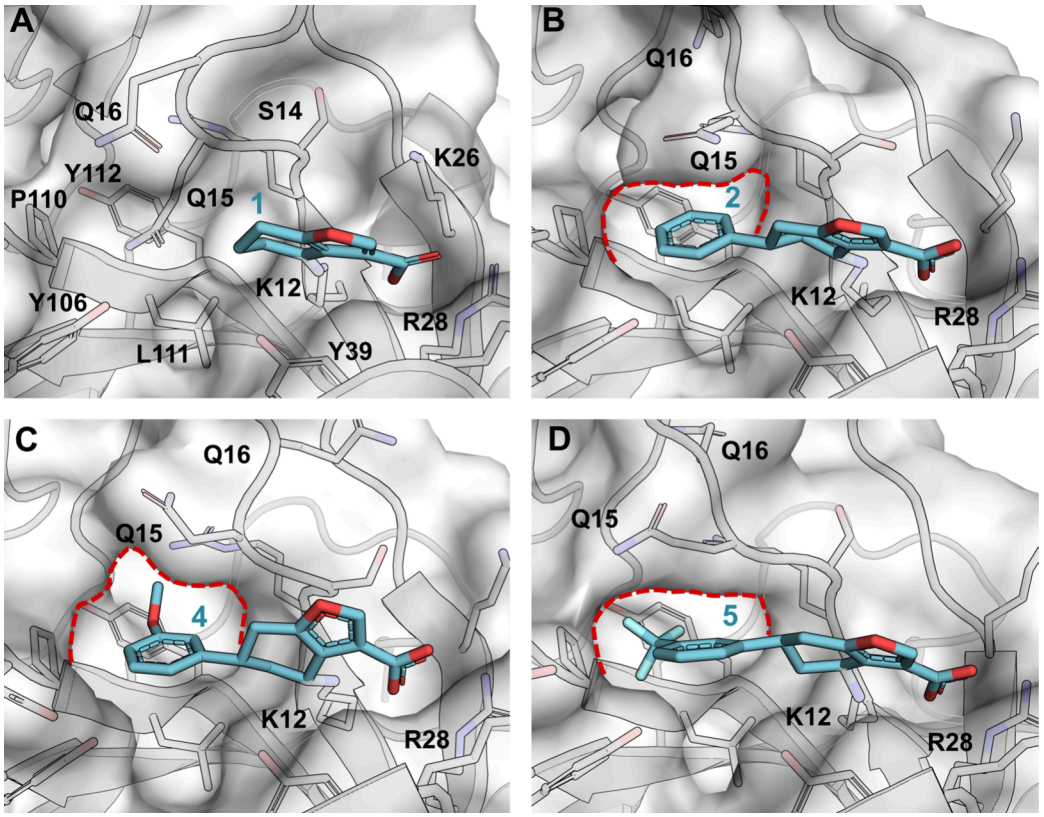

Figure 4. First iteration analogues. (A) Complex of **1** with BTK PH domain with semitransparent surface of the domain and key binding site residue shown as sticks and labeled (PDB: 6TUH). (B) Complex of **2** with BTK PH domain in the same view as in A showing expanded pocket to accommodate the phenyl ring (PDB: 7I9I). (C) Complex of **4** with BTK PH domain in the same view as in A (PDB: 7I96). (D) Complex of **5** with BTK PH domain in the same view as in A (PDB: 9T23). The pocket that opens up with β1-β2 loop moving away is indicated with red dotted line in panels B, C, and D.

https://doi.org/10.1021/acs.jmedchem.5c03818
J. Med. Chem. 2026, 69, 12099−12121

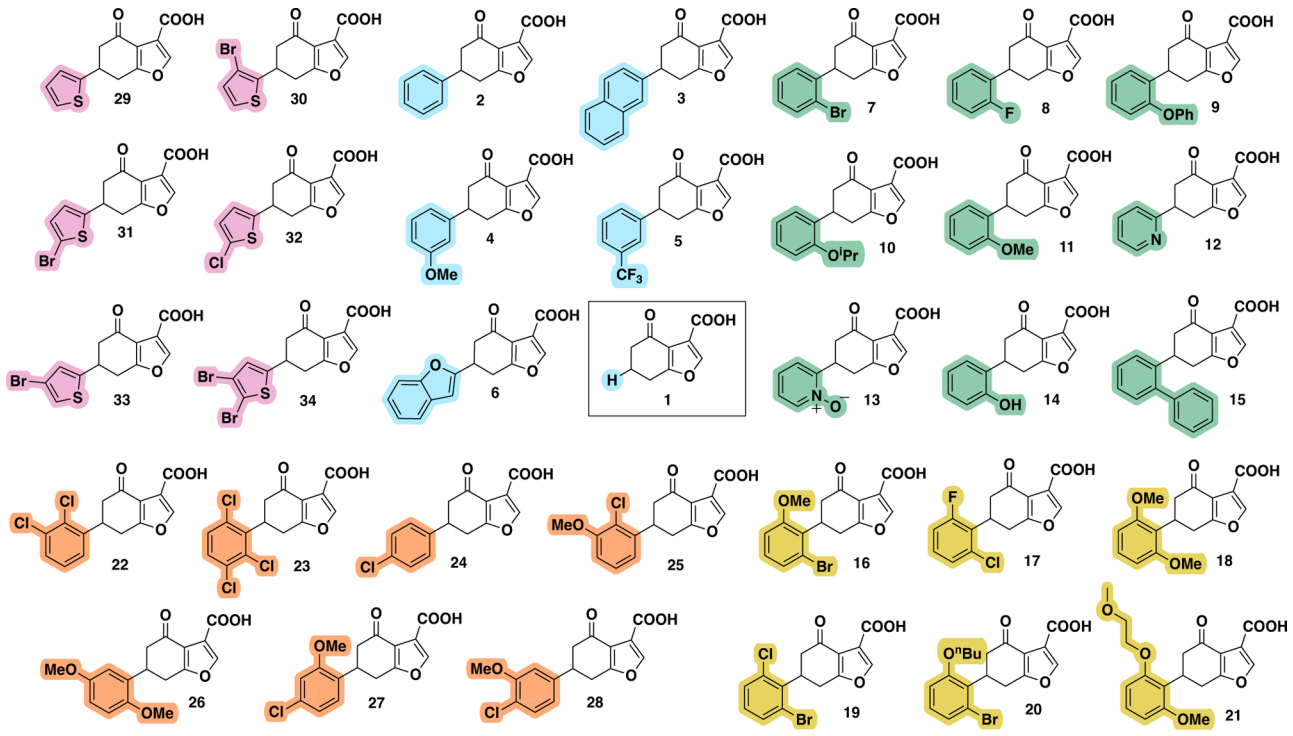

Figure 5. All analogues. The fragment hit **1**, surrounded by first-iteration analogues (compound **2**-**6**, pale blue) exploring fused rings and *meta* substitution, second-iteration analogues (compound **7**-**15**, green) exploring *ortho* substitution, third-iteration analogues (compound **16**-**21**, yellow) exploring 2,6 *ortho* disubstitution, fourth-iteration analogues (compound **22**-**28**, orange) exploring other substitution patterns on a benzene scaffold and fifth-iteration analogues (compound **29**-**34**, pink) exploring substitution on a thiophene scaffold.

4C,D). First, a large hydrophobic pocket gated by Y39 could potentially hydrogen bond with substituents in the *ortho* position. Varying ring substitution patterns would also perturb electron distribution and could influence C−H···π interactions between the side chain of Q15 and the aromatic system. The potential substitution of the phenyl ring and scaffold hopping to investigate key interactions provided scope for our subsequent structure-binding relationship study and led to the synthesis of several iterations of analogues (Figure 5).

Chemistry

The furan fragment hit **1** could be synthesized in one step from readily available diketone starting material **1c** (Scheme 1). Potassium hydroxide generates the enolate of the diketone to attack ethyl bromopyruvate forming a furan ester which is hydrolyzed in situ.

Scheme 1. Synthesis of the Furan Fragment Hit 1[a]

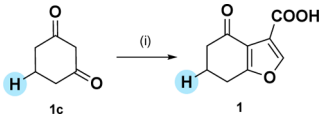

[a]Reagents and conditions: (i) ethyl bromopyruvate (2 equiv), KOH (3 equiv), EtOH, rt; 50 wt % NaOH (4.5 equiv).

The synthetic route was extended to access the phenyl parent compound **2**, for which the diketone **2c** had to be synthesized from α,β-unsaturated compound **2b** in three stages (Scheme 2a). The diethyl malonate Michael addition product cyclizes under the reaction conditions to give the 1,3-cyclohexanedione moiety with an additional ester group after the first stage. The additional ester is removed in the final two stages by hydrolysis and decarboxylation to form diketone **2c** (Scheme 2b). As before, the furan **2** is formed with ethyl bromopyruvate, however solubility issues were addressed by using a stronger base (NaOEt) (Scheme 2c).

One main synthetic route was then developed to obtain subsequent analogues **3**−**12**, **16**−**34** (Scheme 3). The α,β-unsaturated compounds (**b**) were synthesized from aldehydes (**a**) by Wittig reactions.

In order to interrogate the functionalities on the molecule, matched-pair compounds were synthesized and tested. Diketones **16c**, **24c** and **33c** were subjected to furan formation conditions without subsequent hydrolysis to yield esters **16d**, **24d** and **33d** respectively (Scheme 3). For analogue **17**, the electrophilic ketone was reduced to an alcohol to form **17e**. The aldehyde precursors of the O-alkylated analogues **11a**, **20a**, **21a** were synthesized by adding an alkylation step before the Wittig reaction (Scheme 4a). Similarly, the aldehyde for the methoxy analogue **16a** could not be obtained commercially so was synthesized by methylating the respective hydroxy form **16f** (Scheme 4b). Analogues **13**, **14** and **15** were synthesized via oxidation of **12** (Scheme 4c), demethylation of **11** (Scheme 4d) and cross-coupling with **7**, respectively (Scheme 4e). Finally, negative control **37**, based on the structure of alpha tetralone **35** but with a carboxylic acid to mimic that in the fragment hit, was synthesized (Scheme 5). The lead compounds were fully soluble up to 1 mM concentrations in buffer and were stable in DMSO at room temperature (>three months).

Structure−Binding Relationship Study

Crystal structures were obtained for 24 analogues (Supporting Information S1 X-ray Crystallography). All show similar binding modes as illustrated with the phenyl parent, **2** (Figures

https://doi.org/10.1021/acs.jmedchem.5c03818
J. Med. Chem. 2026, 69, 12099−12121

Scheme 2. (a) Synthesis of the Parent Phenyl 2[a,b]

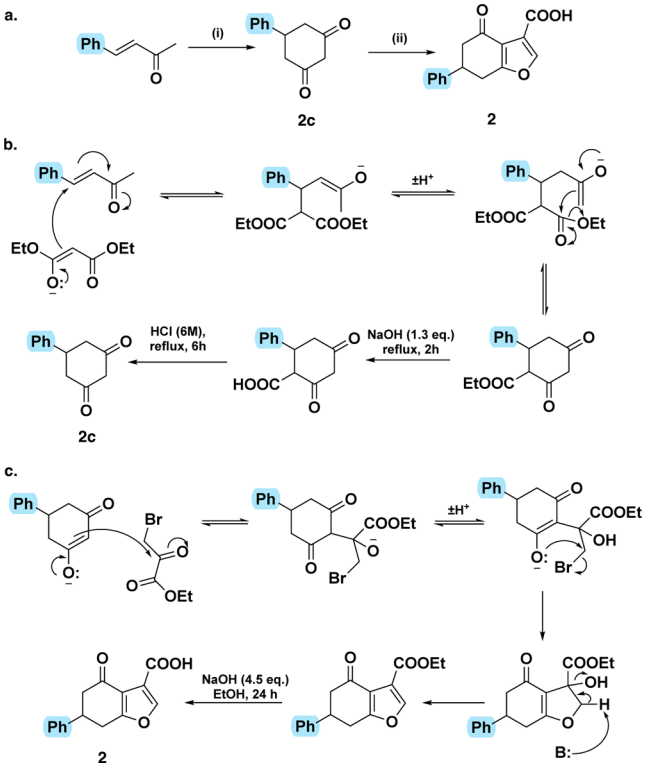

[a](b) Reaction pathway toward diketone formation. (c) Furan formation from diketone. [b]Reagents and conditions: (i) diethyl malonate (1.1 equiv), 7% NaOEt in EtOH (1.1 equiv), rt; 50 wt % NaOH (1.3 equiv), reflux; 1−6 M HCl, reflux; (ii) ethyl bromopyruvate (1.3 equiv), 7% NaOEt in EtOH (1.1 equiv), rt/reflux; 50 wt % NaOH (4.5 equiv), rt.

Scheme 3. General Synthetic Route to Analogues 3−12 and 16−34[a]

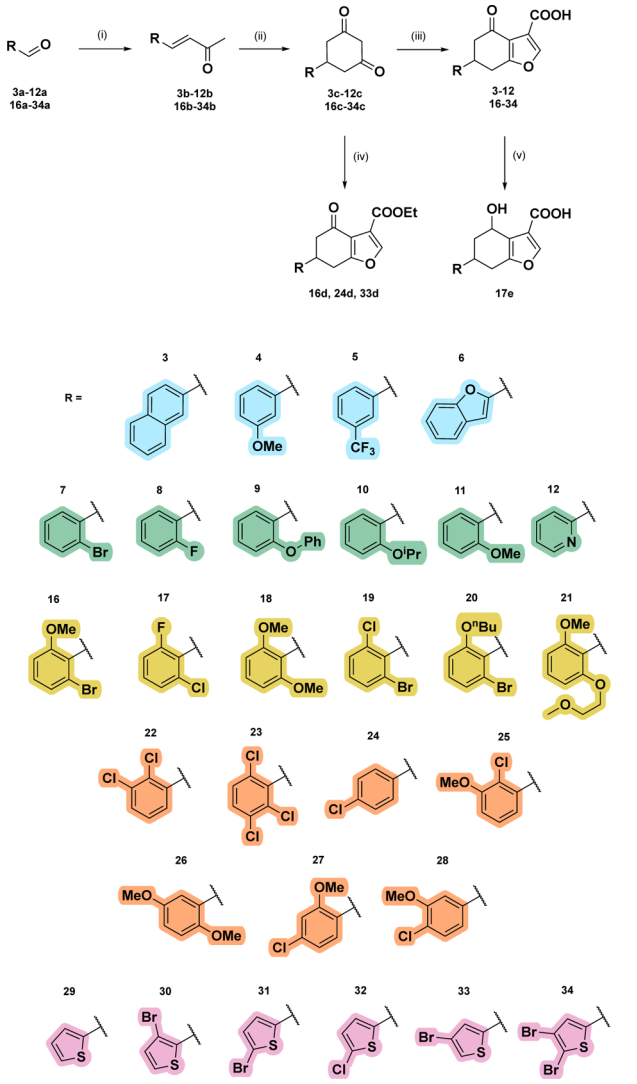

[a]Reagents and conditions: (i) 1-(triphenyl-λ5-phosphaneylidene)-propan-2-one (1 equiv), THF, reflux; (ii) diethyl malonate (1.1 equiv), 7% NaOEt in EtOH (1.1 equiv), rt; 50 wt % NaOH (1.3 equiv), reflux; 1−6 M HCl, reflux; (iii) ethyl bromopyruvate (1.3 equiv), 7% NaOEt in EtOH (1.1 equiv), rt/reflux; 50 wt % NaOH (4.5 equiv), rt; (iv) ethyl bromopyruvate, 7% NaOEt in EtOH (1.1 equiv), rt/reflux; (v) $NaBH_4$ (1.5 equiv), EtOH, 0 °C − rt.

4B and S2B). As well as the covalent label at K12, the salt bridge of the carboxylic acid with R28 is preserved in all cases; no crystal structures could be obtained for the ethyl ester precursors **16d**, **27d** and **33d**.

The first-iteration analogues (**3**−**6**) were designed to explore accessibility to a pocket next to the *meta* position of the phenyl ring. Crystal structures were obtained for **4** and **5**, which show the methoxy and trifluoromethyl group expand the pocket opened up by the phenyl group of **2**, with Q15 in β1-β2 loop making room for the ligands. The pocket is lined by P110, L111, and Y112, with the aliphatic part of R13 side chain at the far end (Figures 4 and S2C,D). The fused rings in **3** and **6** appear to be too large or having nonideal geometry for this malleable pocket and we were unable to get crystal structures with these compounds.

The second-iteration analogues (**7**−**15**) explored the *ortho* position and yielded promising results with well-defined binding pose evident in crystal structures for **7**−**14** (Figures S1 and S2E−L). No crystal structures were obtained for the biphenyl analogue **15**, suggesting that the rigid system was not accommodated. However, with an oxygen spacer, the phenoxy substituted **9** projects the phenyl ring further into the pocket lined by R13 and Y106, underneath Q15 (Figure 6A). This pocket is also occupied by the *ortho* halogens in **7** (Figure 6B) and **8**. Notably, the bromine atom in **7** creates a strong water-mediated halogen bond with the backbone carbonyl of R13, indicating a strong preference for bulky, soft halogens in the ortho position. Pyridine-containing analogue **12** and its oxidized counterpart, **13**, project their heteroatoms toward the same protein pocket and β1-β2 loop, as does the hydroxyl group of **14**.

The alkoxy substituted analogues behave differently. The isopropoxy group of **10** and methoxy of **11** project in the opposite direction, toward Y39 (Figure S2H,I), without making additional contacts with the protein. Given the propensity of *ortho* substituents to point toward either inside (**7** Br, **8** F, **9** OPh, **12** N, **13**, N^+-O^-, **14** OH) or outside (**10** OiPr, **11** OMe,) of the protein, a third series of analogues with 2,6-disubstitutions (**16**−**21**) was constructed.

The crystal structures of **16**, **17** and **19** demonstrate that larger halogen atoms (bromo or chloro) go into the hydrophobic pocket adjacent to the *ortho* position, while the smaller substituents (methoxy and, respectively, fluoro and

https://doi.org/10.1021/acs.jmedchem.5c03818
J. Med. Chem. 2026, 69, 12099−12121

Scheme 4. Additional Synthetic Steps toward 10a, 20a, 21a, 16a, and 13−15[a]

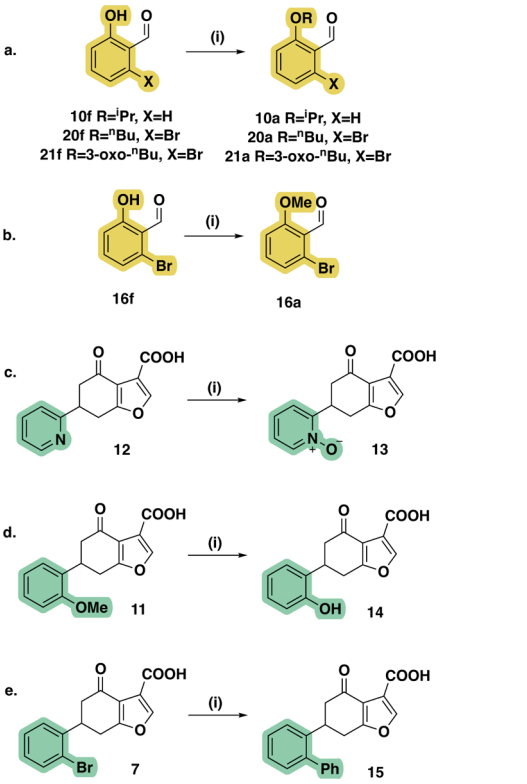

[a]Reagents and conditions: (a) (i) RBr (1.5 equiv), DMF, K_2CO_3 (2 equiv), 0 °C − rt. (b) (i) K_2CO_3 (3.8 equiv), MeI (17 equiv), acetone, rt. (c) (i) mCPBA (1.5 equiv), DCM, rt. (d) (i) BBr_3 (2.3 equiv), DCM, −78 °C − rt. (e) (i) Phenyl boronic acid (1.2 equiv), $Pd(OAc)_2$ (0.075 equiv), s-phos (0.1 equiv), K_3PO_4 (2 equiv), 20:3 toluene/H_2O, μwave, 60 °C.

Scheme 5. Synthetic Route to Negative Control 37[a]

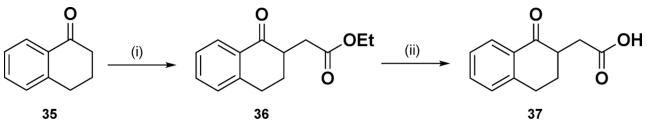

[a]Reagents and conditions: (i) LDA (1.1 equiv), ethyl 2-bromoacetate (1.1 equiv), THF, hexane, −60 °C − rt; (ii) 3 M NaOH (3 equiv), 2:1 THF/MeOH, rt.

chloro) point toward Y39 (Figure 6C). The second substituent causes the phenyl ring to move toward the $\beta1$-$\beta2$ loop, pushing the loop further back. The halogen interaction made by **7** and **8** with a water is subsequently lost. The symmetric analogue **18** with two methoxy groups binds in a similar manner to the halogenated analogues. The methoxy group on the opposite side of the $\beta1$-$\beta2$ loop is inserted into a small pocket between the terminal hydroxyl groups of Y39 and Y106, lined by I56 and L111 side chains (Figure S2M−P).

The fourth-iteration analogues explored various chloro and methoxy substitution patterns on the phenyl ring. With adjacent *ortho* and *meta* positions occupied in **22** and **25**, the substituents were forced inside the hydrophobic pocket toward L111. The nonadjacent *ortho* and *meta*-methoxy substituents of **26** oriented in the same way as the monosubstituted analogues **11** and **4**, with the methoxy in the *ortho* position pointing into the small pocket between Y39 and Y106, while the methoxy in the *meta* points toward the hydrophobic pocket by the $\beta1$-$\beta2$ loop (Figure S2Q−U).

The crystal structure of **24** reveals that the system tolerates also a chloro substituent in the *para* position, pushing residue E108 by ca. 1 Å, to make space for the halogen, with the phenyl ring shifting further toward Y106 compared to ortho-substituted compounds (Figure 6D,E). With the *para*-substitution $\beta1$-$\beta2$ loop is also folding over the compound, creating a partially closed cavity for the modifier. Retaining the interaction the chlorine makes, a methoxy group was added to decorate the *ortho* position in **27** and it points, expectedly, toward Y106 and shifts the phenyl ring slightly more to that same direction. Interestingly, the *para*-chloro halogen bond allows a *meta*-methoxy, which was previously observed to point toward $\beta1$-$\beta2$ loop in analogues **11** and **26**, to also point toward Y39 in **28**.

Scaffold hopping at the phenyl ring led to a series of thiophene analogues, beginning with **29**. The introduction of a 3-bromo substituent on the thiophene in **30** allows an interaction with S14, similar to that with the *ortho* halogenated phenyls in **17** and **19**. 4-Bromo substitution in **33** flips the ring suggesting the bulky Br atom is not accommodated in the *meta* position without flipping the heterocycle (Figure 6F). In the 5-bromo and 5-chloro thiophene analogues, **31** and **32**, the halogen interacts with a pocket formed by the main chain carbonyls of E108, G109, and P110 and the side chain of Y106. Like **33**, **32** is ring flipped relative to the unsubstituted thiophene recapitulating the preference for a *para*-chloro substituted phenyl ring. We were unable to obtain a well-defined structure of double-brominated thiophene **34** bound to the target, even though there appears to be room for a second substituent.

Overall, while the binding is dominated by ionic interactions with R28 and covalent linkage to K12, the binding site with its highly flexible $\beta1$-$\beta2$ loop offers significant opportunities for further elaboration. The $\beta1$-$\beta2$ loop seems to be able to mold itself to many different substitutions, with Q15 either engaging with the ligand directly or moving away from the binding site, as exemplified most dramatically by bromo-substitutions in the *ortho* position of the phenyl ring (e.g. in **19**) opening a new pocket where large substitutions can be accommodated (Figure 6C).

Mass Spectrometry

All analogues were tested at a concentration of 150 μM with 2.5 μM of WT BTK PH domain and, with the exception of the fifth iteration compounds, using R28C mutant as a negative control. The complexes were incubated at 37 °C for 5 min. Given the short LC gradient (5 min) and fast ionization (milliseconds), no reductive stabilization was performed prior to MS analysis and our imines were assumed to be stable on LCMS time scales.

With compound **2**, these conditions gave rise to mostly a singly labeled covalent ligand-protein complex (Figure 7), while a small proportion of the protein showed a second labeling. All analogues labeled the BTK WT protein and compounds **1**-**4** failed to covalently label the R28C mutant. This suggests that the analogues specifically label K12 and occupy the native inositol phosphate binding site, relying on the key ionic interaction between R28 and the carboxylic acid in the binders, which is disrupted in the R28C mutant.

Intact protein mass spectrometry has been previously used for approximating the extent of protein labeling by a covalent

https://doi.org/10.1021/acs.jmedchem.5c03818
J. Med. Chem. 2026, 69, 12099−12121

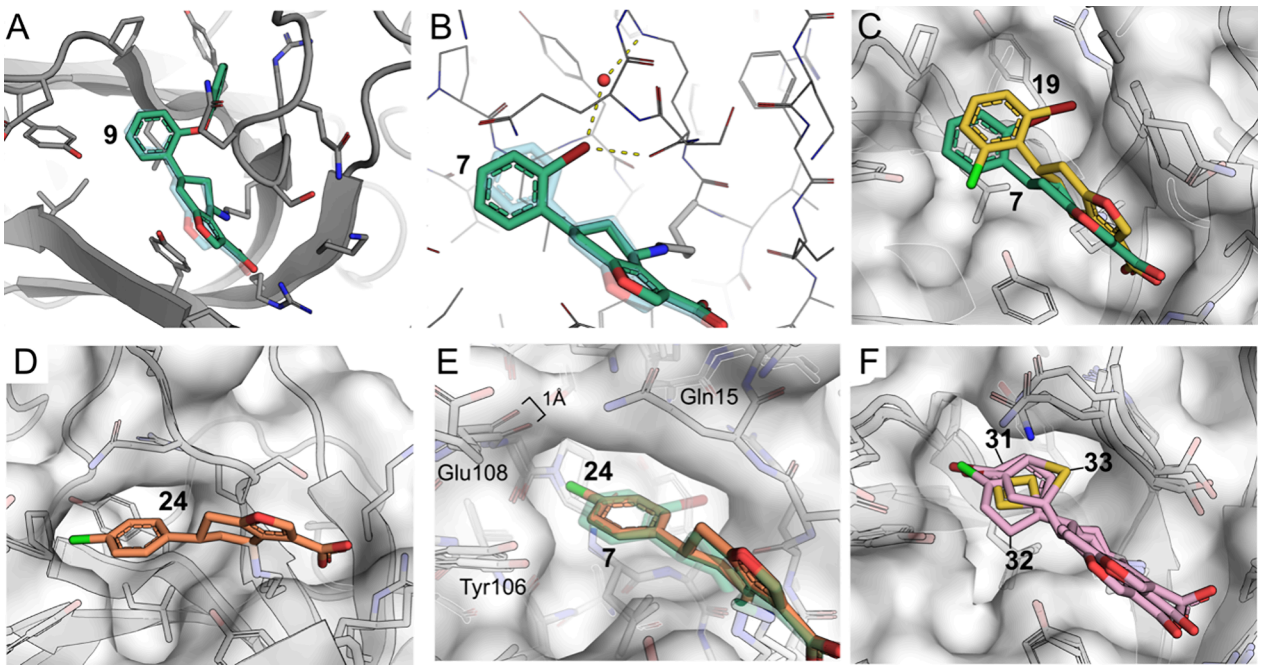

Figure 6. Elaborated covalent modifiers. (A) Second- iteration analogue **9** (green) overlaid with transparent **2**. An oxygen spacer allows the large phenyl group to point into the hydrophobic pocket under Q15 (PDB: 7I92). (B) Structure of **7** demonstrating *ortho* halogens also occupying this pocket and the possibility of halogen bonds with water or carbonyl of S14 PDB: 7I90). (C) A third-iteration analogue **19** with the larger halogen (Br) points deeper than monosubstituted **7** into the hydrophobic pocket, possibly pushed by the chloro substituent on the other side of the ring (PDB: 9T0T). (D) *Para*-chloro analogue **24** makes a weak halogen bond with backbone carbonyl of E108 (PDB: 9RL9). (E) Comparison of **7** and **24** showing how **24** pushes E108 by 1 Å to make room for the *para*-chloro group, with Q15 from the β1-β2 loop folding over **24**. (F) Halogenated thiophenes **31**, **32** and **33** all form similar halogen bonds with backbone of E108, with thiophene ring flipping depending on the position of the halogen (PDB: 9RM0, 7I9B, 9RN5).

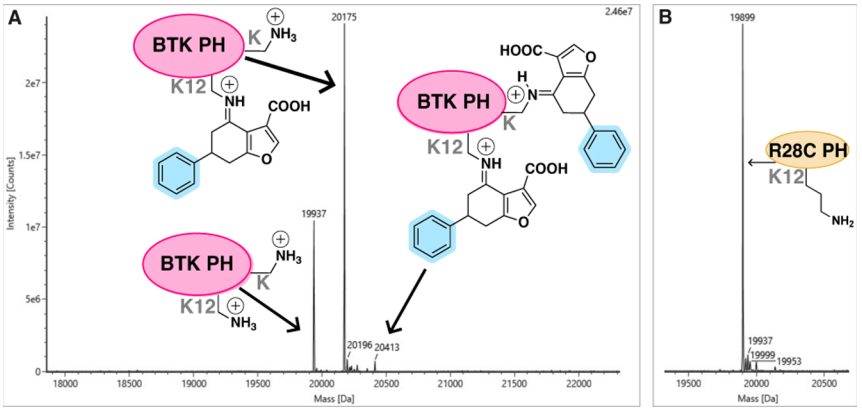

Figure 7. Protein mass spectrometry. Compound **2** (150 μM) labels the WT BTK PH domain (2.5 μM) after 5 min incubation (shaking at 37 °C).

modifier.[16] In our study, relative peak intensities corresponding to unlabeled, singly labeled, and multiply labeled BTK PH domain were quantified. Single labeling relative intensity refers to the percentage of protein bearing one covalent modification, whereas multiple labeling relative intensity denotes species containing more than one modification. Because multiply labeled species are assumed to include modification at Lys12 in addition to nonspecific labeling at other lysine residues, the total labeling relative intensity was defined as the sum of the single and multiple labeling relative intensities, representing the overall proportion of covalently modified K12 under the assay conditions. The relative intensities of peaks of mass corresponding to singly, multiply and unlabeled WT protein were recorded after 5 min incubation with the first- to fourth-iteration analogues (Figures 8A and S42−S70).

The total labeling relative intensity of parent analogue **2** is almost three times that of the initial hit **1** (86% compared to 27%), demonstrating the benefit of introducing the phenyl ring. Fused ring analogues **3** and **6** also show efficient labeling relative to **1**. The other first-iteration analogues display less desirable behavior with *meta* substituents [*meta*-methoxy (**4**) and trifluoromethyl (**5**)] giving relatively low peak intensities for labeled species (52 and 34%, respectively).

The *ortho* analogues of the second-iteration display a range of outcomes. Halogens, bromo **7** and fluoro **8**, exhibit high total labeling relative intensities of 94 and 87% respectively with minimal nonspecific binding (and hence minimal multiple labeling relative intensity). However, the alkoxy substituents yield moderate responses, 62% with the isopropoxyl analogue **10** and 67% with the methoxy analogue **11**. The oxygen spacer

https://doi.org/10.1021/acs.jmedchem.5c03818
J. Med. Chem. 2026, 69, 12099−12121

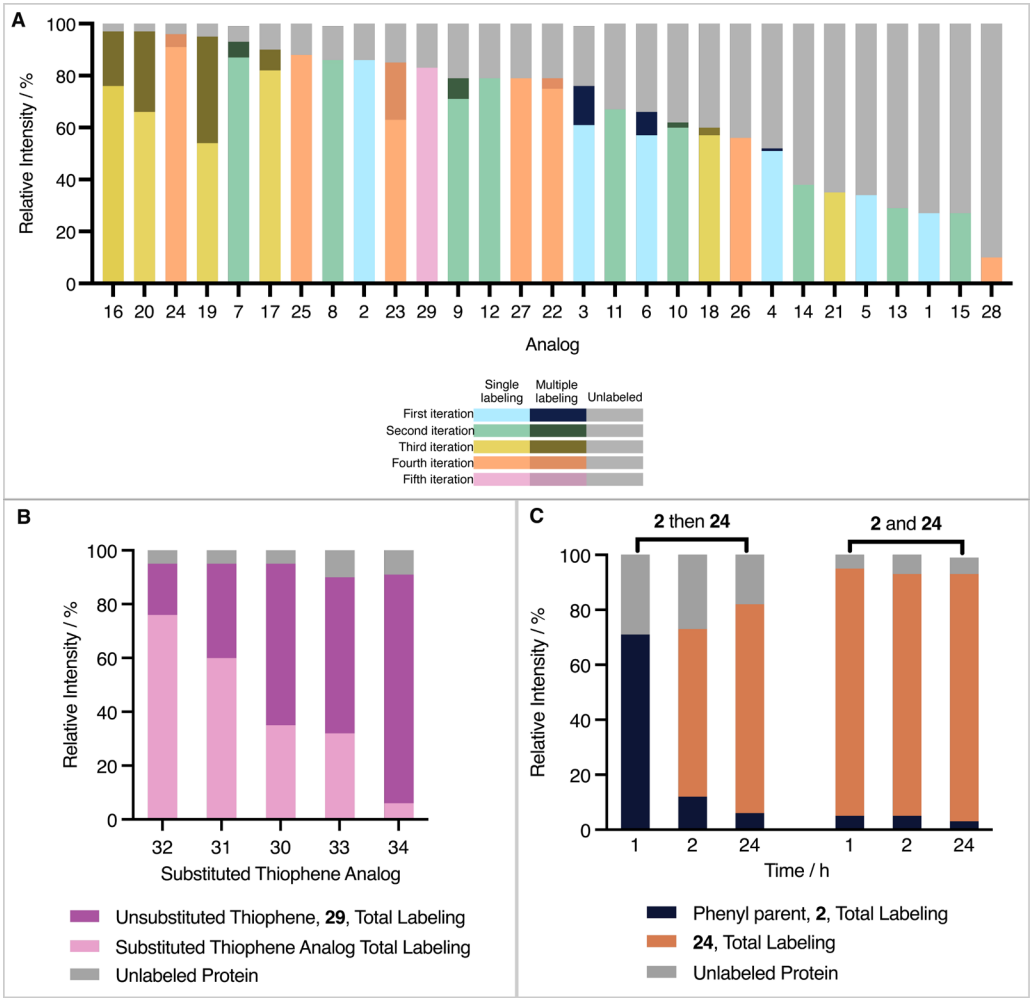

Figure 8. Mass spectrometry studies. (A) Mass spectrometric evaluation of WT protein labeling after 5 min. First- to fourth-iteration analogues **1**–**28** and thiophene **29** (150 μM) were incubated with WT BTK (2.5 μM) for 5 min, with shaking, at 37 °C. The intensities of peaks were compared within each sample to show the proportion of unlabeled and singly, doubly and triply labeled proteins. (B) Thiophene analogue competition experiments. Each fifth-iteration thiophene analogue (150 μM) was incubated along with the unsubstituted thiophene **29** (150 μM) and WT BTK PH domain (2.5 μM) and shaken at 37 °C for 1 h. The intensity of single labeling peaks for the unsubstituted and substituted thiophenes relative to the total protein intensity are shown in dark and pale purple, respectively. (C) A graph to summarize the results of the three treatments in reversibility studies. The protein (2.5 μM) was incubated at 37 °C for 1 h with either analogue **2** (150 μM), analogue **24** (150 μM) or both (150 μM each). A mass spectrum was recorded before addition of analogue **24** (150 μM), addition of analogue **2** (150 μM) or no addition, respectively, and further incubation for 1 h. A second mass spectrum was recorded for each treatment. The samples were incubated at 37 °C with no further additions for another 22 h. In each case, the same equilibrium is reached indicating the reversibility of the labeling.

in the phenoxy group of **9** improves the relative intensity of total K12 labeling (79%) compared to the larger, more rigid biphenyl system in **15** (27%). Total binding of the pyridine analogue **12** (78%) is reduced by oxidation to **13** (29%) and the hydroxy analogue **14**, structurally similar to N-oxide **13**, also behaves poorly (38%).

The third and fourth generations achieve relatively high intensities for total labeling, except for disubstituted analogues **18**, **21** and **26** (59, 35, and 56% respectively) which all contain *ortho*-methoxy and alkoxy substituent. Interestingly, *ortho*-bromo methoxy **16** and *ortho*-bromo n-butoxy **20** show the highest relative intensity of total labeling (both 97%) albeit inducing high intensity multiple labeling (21 and 31% respectively). Disubstituted *ortho*-chloro containing analogues **17**, **19**, **22**, and **25** performed well (90, 95, 78, and 88%) as do disubstituted *para* chloro containing analogues **27** and **28** (79 and 83%) and trichloro analogue **23** (84%). Finally, singly substituted *para*-chloro analogue **24** shows the highest relative intensity of total labeling (96%) with minimal nonspecific binding events (relative intensity of multiple labeling is 4%).

Scaffold hopping at the phenyl ring to give thiophene analogue **29** proved successful and the relative intensities of labeled protein peaks are comparable to the phenyl series in mass spectrometry. The subsequent thiophene analogues (**30**-**34**) were incubated in succession with the unsubstituted thiophene **29** to create a competition study (Figure 8B, Table S2). Based on labeling efficiency, the analogues show clear ranking **32** > **31** > **30** > **33** > **34**, with **31** and **32** outperforming the unsubstituted thiophene **29**.

The reversibility of the reaction was studied by using two ligands in succession. The total labeling relative intensity of the phenyl parent analog, **2**, reached approximately 75% after 1 h incubation at 37 °C. Subsequent incubation with high performing *para*-chloro analog, **24**, caused the system to re-equilibrate. Irrespective of order of addition, the same distribution of labeling was achieved after 24 h incubation at

https://doi.org/10.1021/acs.jmedchem.5c03818
J. Med. Chem. 2026, 69, 12099−12121

37 °C suggesting an equilibrium is reached, indicative of reversible imine formation (Table S3, Figures 8C, and S71–S79).

The time and pH dependence of protein labeling was further explored to investigate the nature of the covalent bond between the ligand and the protein (Figure S80–S92). Basic pH environments favor the reaction, which was found to reach >95% completion in less than 20 min for pH values of 9 and 7.8. While the reaction is slower at physiological pH 7.4, the protein labeling reaches >90% completion in less than an hour, highlighting the potential of our compounds for in vivo labeling of K12. As expected for lysine labeling, the reaction becomes significantly slower at pH = 6, where a significant proportion of K12 is protonated, and reaches 50% conversion after 1 h.

Mass spectrometry was also used to determine the effect of scaffold hopping and chirality on binding. All ester (**16d**, **24d**, **33d**), reduced (**17e**) and alpha tetralone based (**37**) analogues showed no binding to the target (Figures S93–S95). The covalent binding of the parent phenyl, **2**, was further confirmed using MALDI (Figure S100).

To evaluate the overall reactivity of lysines in BTK PH domain, we used a nonspecific electrophilic lysine label 4-methylbenzenesulfonyl fluoride **38** (150 μM), as a probe. We observed no covalent adduct when the reaction was incubated at 37 °C for 5 min (Figure S96). With increased concentration, up to 1 mM, and overnight incubation at room temperature, **38** gave barely detectable labeling (Figure S97) This is in stark contrast to the nearly 100% labeling by **24** under the same conditions (Figure S98) indicating that the labeling of lysine 12 by our lead compound is specific and driven by bespoke interactions with the protein.

Differential Scanning Fluorimetry

The analogues were screened against the WT BTK PH domain (Tables S4, S5, and Figure S101A) and the R28C mutant (Table S6 and Figure S101B). The upper limit of the ligand concentration was around 1.5 mM in the assay, constrained by solubility of the compounds. All analogues induce different thermal shift profiles in the WT versus R28C, indicating the specificity of binding in the IP4 binding site, consistent with the requirement for the salt bridge between R28 and the modifier carboxylate for labeling of K12.

The first-iteration analogues (**3** and **5**) induce small shifts in protein melting point (T_m) compared to parent **2** (ΔT_m at 750 μM ligand = 7 °C), indicating weaker binding to the protein (Table S5, Figure S101A). Higher T_m shifts (ΔT_m at 750 μM ligand = 7.5–10.5 °C) are seen for all second-iteration analogues (**7**–**15**) except the phenoxy and biphenyl analogues, **9** and **15** (ΔT_m at 750 μM ligand = 1 and 3 °C respectively). Notably, **16**, **17** and **19** in the third iteration produce even larger shifts (ΔT_m at 750 μM ~ 14 °C), with selectivity confirmed by the R28C mutant. The fourth-iteration analogues (**22**–**28**) induce significant stabilization of the protein (all ΔT_m at 750 μM > 8 °C) with the exception of **22** and **28**, which induce small shifts (ΔT_m at 750 μM = 3–5 °C) performing poorly as in mass spectrometry.

K_d values were approximated from the DSF data (Table S7) to be used only as a metric for comparison with mass spectrometry. Encouragingly, approximate log(K_d) correlates well with total labeling relative intensities from mass spectrometry (Pearson, r = −0.56, R squared = 0.32, P value [two tailed] = 0.003, Figure S102, Tables S8, and S9), indicating higher K_d values for compounds with low total labeling relative intensities. One does need to treat this correlation with some caution as thermal stabilization will rely on all the interactions a compound makes, and the correlation with labeling efficiency is not necessary always true.

To further evaluate the importance of the covalent interaction between the compounds and the target, we synthesized **17e**, an analogue of **17** in which the ketone has been reduced to an alcohol (Figure 9). This compound failed to induce a potent positive response in the WT BTK, instead inducing a negative shift of −5 °C. This suggests **17e** engages the with the PH domain in an alternative binding mode, confirming the ketone moiety is essential for covalent binding at K12 through an imine forming carbonyl group.

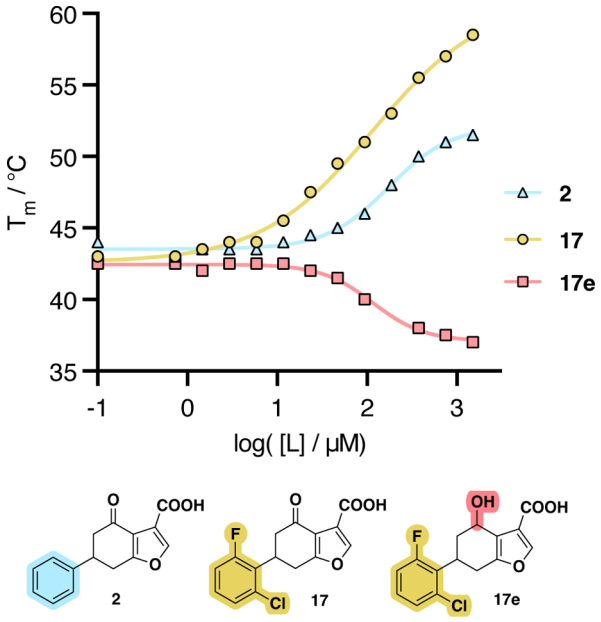

Figure 9. Differential scanning fluorometric evaluation of binders. A dose–response curve of selected modifiers, measured as change in melting temperature, T_m, measured using 5 μM BTK PH domain. Numerical data in Table S4.

From the crystal structures, the stereochemistry at the chiral carbon in the binders cannot be ascertained, thus the enantiomers of **19** were separated to investigate binding. As expected, the enantiomers (**19p1** and **19p2**) were shown not to interconvert in HEPES buffer (Figures S103–S107). **19p1**, showed a higher total labeling after 5 min than the other **19p2** in protein mass spectrometry (Figure S99), which was in line with the electron density in X-ray crystallography.

DISCUSSION

We herein report the discovery of a novel mode of targeting BTK through its PH domain. A reversible covalent binding mode was uncovered, with crystallographic analysis proving an iminium bond formation through K12 with the ketone electrophile.

X-ray crystal structures of BTK PH domain with various analogues demonstrate how the binding mode of the furan fragment is consistently determined by the imine formation with K12 and the salt bridge interaction with R28 – both of which are key residues interacting with PH domain ligand IP4.

https://doi.org/10.1021/acs.jmedchem.5c03818
J. Med. Chem. 2026, 69, 12099–12121

The phenyl ring of the analogues is versatile with respect to the orientation of its *ortho* substituents relative to the protein backbone. Soft halogens (bromine and chlorine) in **17** and **19** point toward the protein backbone, with bromine displaying a water-mediated halogen bond with the carbonyl of R13. The large phenoxy substituent in **9** unexpectedly points in the same direction, albeit with notable $\beta1$-$\beta2$ loop rearrangement (Figure 10). On the other hand, alkoxy substituents (methoxy, isopropoxy) and hydroxyl substituents orient their donor atoms toward the hydroxyl of Y106, indicating a propensity toward H bonding.

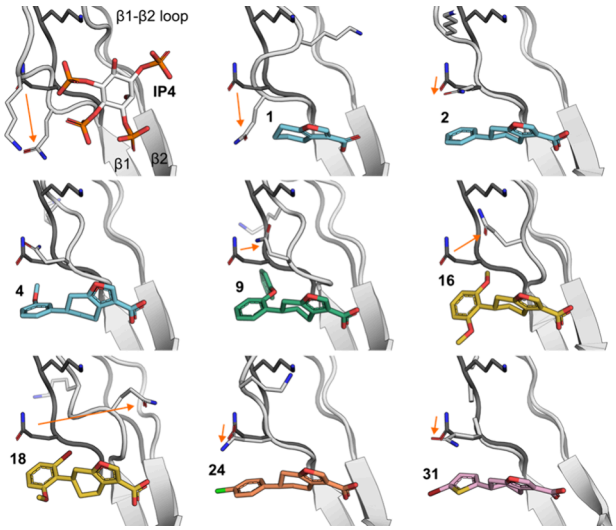

Figure 10. Movement of $\beta1$-$\beta2$ loop. Representative compounds in complex with BTK PH domain are shown with $\beta1$-$\beta2$ loop and Q15 residue. In each panel the $\beta1$-$\beta2$ loop with **1** is shown with darker gray and movement of Q15 in each complex relative to that is indicated with a red arrow. PDBs: 1B55, 6TUH, 7I9I, 7I96, 7I92, 7I9F, 7I9E, 9RL9, 9RM0).

The trends at the *meta* position are less defined with respect to the in-or-out positioning relative to the protein backbone. Notably, the methoxy and trifluoromethyl groups in **4** and **5** point inward and induce a pocket via $\beta1$-$\beta2$ loop rearrangement, whereas in **28** the *meta*-methoxy group points toward the solvent.

The *para* position emerges as a privileged one for halogens, with the chlorine in **28** forming a halogen bond with the backbone carbonyl of Gly109. Thiophene analogues in the fifth generation proved to be potent bioisosteres of the phenyl ring and are well tolerated, while introducing a slightly different angularity around substituents.

One of the key features in our exploration of structure−activity relationship around our compounds is the movement of $\beta1$-$\beta2$ loop. It has been seen to be highly mobile and adopt significantly different conformations in unliganded and IP4-bound structures.[17] Depending on the compound presented here, the $\beta1$-$\beta2$ loop can either engage with the compound or move away, exposing a wider pocket underneath it where substituents can go, with Q15 as one of the most mobile residues (Figure 10).

This work demonstrates the feasibility to design small molecule modifiers for PH domains in general and acts as a springboard for the development of more potent and selective BTK PH domain inhibitors. We expect this to act also as a proof-of-concept for inhibition of the PH domain:inositol phosphate binding more broadly.

In general, clear trends emerged from MS and DSF, indicating that certain bulky groups or ring systems are not tolerated on the phenyl ring, while halogens and alkoxy substituents are. Straight carbon to nitrogen swaps are also tolerated in the ring. The binding specificity of the analogues was confirmed by the point mutant R28C which ablates the key arginine-carboxylate salt bridge. Mass spectrometry studies converge with DSF studies and point to *ortho* and *para* halogen substituted phenyl rings being the most beneficial for binding. The covalent labeling was proven to be highly dependent on the pH of the reaction buffer, with higher pHs inducing faster kinetics. The reversible covalent nature of the binding was proven by the reversibility study, in which **24** fully labeled the protein regardless of the order of addition.

This novel class of BTK PH domain modifiers represents an important starting point for further development. With binding specificity validated by crystallography, MS and DSF, further medicinal chemistry modifications have the potential to yield potent and selective BTK inhibitors, complementary to the current ATP binding site targeting ones.

Two obvious questions arise from this as well. First, why is Lys12 modified? Is it particularly reactive? Following on from that, could this be more generalized method for targeting PH domains?

To answer the first question, we analyzed 12 BTK PH domain structures (PDBs 1B55, 1BWN, 2Z0B, 4Y94) using two computational pK_a calculation methods, DeepKa[18] and pyPKa.[19] Both methods predicted significantly lowered pK_a compared to the other 14 lysines in this domain. pK_a of K12 was predicted to be 7.05 ± 1.29 and 8.82 ± 0.80, with the two methods, respectively, while other lysines had average pK_as of 10.50 ± 0.97 and 10.77 ± 0.90 (Figure S110, Table S10). This suggests K12 is particularly reactive in BTK PH domain. To answer the second question, we analyzed also other PH domains (Akt, Grb1, DAPP1 and pRex1) for which structures are available and which bind inositol phosphates in the same site using the DeepKa server. In all cases, the lysines that are equivalent to K12 in BTK PH domain were unique in having their pK_a values 2.2−3.2 units lower than other lysines in those structures. Despite the known limitations of protein pK_a calculations, this suggests the covalent approach we describe here as a more universal approach to PH domain inhibition.

Lysine-directed covalent chemistry can raise concerns regarding selectivity in cellular environments. Without in vivo validation for our micromolar binders, we acknowledge possible off-target reactivity. Reversible imines, however, pose a lower risk than irreversible electrophiles because formation is slow and requires preorganization. Only lysines that are both accessible for kinetics and properly positioned to stabilize the iminium transition state can form adducts.

While extremely abundant and solvent-exposed lysines exist on proteins in the cell (e.g., human serum albumin), most surface lysines remain protonated and are poor nucleophiles. Catalytically active lysines, however, can transiently form Schiff bases (e.g., K252 in the porphobilinogen synthase ALAD of stimulated immune cells[20]) so are inherently primed to undergo covalent modification. Importantly, the present system relies not only on an unusually reactive lysine, but also its positioning within a highly structured ligand-binding site. The requirement for simultaneous noncovalent recognition, specifically the conserved arginine−carboxylate inter-

https://doi.org/10.1021/acs.jmedchem.5c03818
J. Med. Chem. 2026, 69, 12099−12121

action and precise geometric alignment within the PIP3 binding pocket, strongly constrains off-target reactivity.

Local microenvironmental effects within the PH domain, such as hydrogen bonding, electrostatics, and solvent accessibility, lower the pK_a of the target lysine, increasing the fraction of nucleophilic neutral amine and promoting selective covalent reactivity under near-physiological conditions. This is distinct from nonspecific reactivity, which would require changes in bulk pH and is unlikely in cells.

Overall, local pK_a modulation and the requirement for precise binding suggest that selective covalent modification could be possible cellularly, resulting in a homogeneous lysine-modified population which, in principle, exhibits more predictable pharmacokinetics.

CONCLUSIONS

In conclusion, we developed a novel class of lysine targeting covalent modifiers against the PH domain of BTK, a previously unreported strategy. Five families of analogues were generated in a structure-binding relationship study incrementally guided by emerging X-ray crystallographic data. Following on from the unsubstituted phenyl of parent compound **2**, *ortho* and *meta* substituents were explored, as well as fused rings. *Meta* substituents and fused rings turned out to be detrimental for binding, while *ortho* substituents proved to be beneficial (particularly halogens and alkoxy groups). Scaffold hopping at the phenyl ring to give thiophene analogue **29** proved successful, bringing the total number of ligand-bound crystal structures to 24.

The binding selectivity was validated by protein mass spectrometry and differential scanning fluorimetry, whereby all analogues induce expected responses with the WT BTK, but fail to induce a response with the loss of function mutant R28C. The DSF results suggest an increase in binding affinity of slightly more than 2 orders of magnitude from hit compound **1** to lead compound **24** (Table 1).

These modifiers target a lysine in the center of the binding site for inositol phosphates, the primary function of PH domains. these modifiers inhibit BTK PH domain binding to PIP3 headgroup and thereby also be expected to prevent membrane association and thereby prevent BTK activation. Mutations in and around the PIP3 binding site are known to cause XLA, further strengthening our hypothesis that ligands binding to this site can act as functional inhibitors of BTK.

Table 1. Summary Table of Key Compounds

Compound	 1	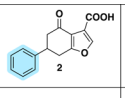 2	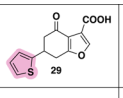 29	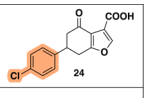 24
Total Labeling Relative Intensity[a] / %	27	86	83	97
K_d from DSF[b] / μM	796	191	35	6
PDB Code for Crystal Structure	6TUH	7I9I	9T21	9RL9
CLogP[c]	1.04	2.60	2.25	3.32

[a]Protein MS of BTK PH domain (2.5 μM) with ligand(s) (150 μM) in 20 mM HEPES buffer (pH 8.0, 100 mM NaCl, 0.5 mM TCEP). Total volume 25 μL; 1.5% DMSO. Samples were incubated shaking at 37 °C for 5 min. [b]Differential scanning fluorimetry (DSF) with protein (5 μM) and ligand (varying concentrations) in 20 mM HEPES buffer (pH 8.0) containing SYPRO Orange (8×) and 5% DMSO (total volume 25 μL). Fluorescence readings gave DTm and nonlinear regression for "One site − Specific Binding" (performed in Prism10; GraphPad Software Inc.[21]) fit the data to the simplest saturation model, $Y = B_{max} \times X/(K_d + X)$. [c]CLogP values were generated using ChemDraw Professional, Version 20.1.0.112 (PerkinElmer, Waltham, MA, 2023).[22]

METHODS

Expression and Purification

WT and R28C mutant of the BTK PH-Btk motif construct (residues 1−170, Uniprot: Q06187) was expressed and purified as described previously,[5] with the exception that final ion exchange chromatography could be left out without compromising the quality of the preparations. To facilitate crystallization, a variant form of the protein was produced in which exposed C145 in the TH domain was mutated to a serine or alanine, creating proteins Btk_S and Btk_A, respectively.

X-ray Crystallography

Btk_wt/Btk_S/Btk_A were crystallized at 20−25 mg/mL in 100 mM NaCl, 20 mM CHES-NaOH, pH 9.5. The reservoir used was 0.1 M TRIS 8.5 pH, 32.5% w/v PEG 3350, 200 mM $MgCl_2$ in a 1:0.9 ratio with a total volume of 0.4 μL by the site-in drop method using the mosquito robotics system (SPT Labtech). In the absence of suitable crystals, previously described crystals of R28C mutant were used as the start for serial seeding process.[5] Seeds were generated from past crystal screens and diluted in 0.1 M TRIS 8.5 pH, 32.5% w/v PEG 3350, 200 mM $MgCl_2$. Seeds were added to the drop at 0.01 μL using the mosquito robotics system (SPT Labtech) The fragments were soaked as singletons at 2−100 mM into these crystals for 15−20 h in 0.1 M TRIS 8.5 pH, 32.5% w/v PEG 3350, 200 mM $MgCl_2$ after which the crystals were cryo-cooled in liquid nitrogen for data collection. X-ray diffraction data was collected at Diamond synchrotron radiation sources and then processed using the pipedream package by Global Phasing Ltd.; structures were solved using Phaser[23] from the CCP4 package.[24] Models were iteratively refined and rebuilt by using Refmac,[25] Buster[26] and Coot[27] programs. Ligand coordinates and restraints were generated from their SMILES strings using the AceDRG[28] software from the CCP4 package. Statistics of crystallographic data processing and refinement are shown in Table S1. Electron densities for the compounds are shown in Figure S1 and structures of all the compounds in identical orientation in Figure S2.

Isothermal Titration Calorimetry

All ITC experiments were performed at 25 °C using a MicroCal iTC200 instrument (GE Healthcare). WT BTK PH domain (20 mg/mL, 50 mM HEPES pH 8.0, 100 mM NaCl) was diluted in HEPES buffer (50 mM HEPES pH 8.0, 100 mM NaCl, 5% DMSO, **1**/**1z** 1 mM/0 mM) and concentrated to 5 μM of WT BTK PH domain. IP4 in 10 mM stock solutions was diluted into the buffer to 100 μM (50 mM HEPES pH 8.0, 100 mM NaCl, 5% DMSO, 1/1z 5 mM/0 mM), ensuring that the DMSO concentrations were carefully matched. In a typical experiment WT BTK PH domain (5 μM) was loaded into the sample cell and 100 μM of the ligand was titrated in 18 2 μL injections of 2 s duration at 150 s intervals, stirring at 750 rpm. Heats of dilution were determined in identical experiments, but without protein in the cell. The data fitting was performed with a single-site binding model using the Origin software package.

Protein MS Experiments

2.5 μM of BTK PH domain was incubated with 150 μM ligand(s), 20 mM HEPES buffer, 100 mM NaCl and 0.5 mM TCEP, pH 8.0 in 25 μL total volume. The DMSO concentration was kept constant throughout all experiments, at 1.5%. The samples were then incubated at 37 °C either for five minutes (individual ligand experiments) or one hour (competition ligand experiments). All samples were injected directly into the liquid chromatography mass spectrometer and analyzed. Protein MS measurements were performed on a Waters LCT Premier Time of Flight mass spectrometer, with errors within ±5 ppm. All mass spectra are shown in Supporting Information,

https://doi.org/10.1021/acs.jmedchem.5c03818
J. Med. Chem. 2026, 69, 12099−12121

Figures S42−S70. Example of MALDI-TOF data is shown in Figure S100.

Defining Relative Intensity Terms from MS

The un-, singly, doubly and triply labeled protein peaks can be described as P, P+L, P+2L and P+3L with intensities of I_P, I_{P+L}, I_{P+2L} and I_{P+3L} respectively. The total protein intensity is the sum of these intensities.

$$\text{Total Protein Intensity, } I_{TP} = I_P + I_{P+L} + I_{P+2L} + I_{P+3L}$$

Under the assumption that the primary label is happening in all labeled cases, the relative intensities can be calculated (by dividing by the total protein intensity) as follows:

$$\text{Single Labeling Relative Intensity} = I_{P+L}/I_{TP} \times 100$$

$$\text{Multiple Labeling Relative Intensity} = (I_{P+2L} + I_{P+3L})/I_{TP} \times 100$$

$$\text{Total Labeling Relative Intensity} = (I_{P+L} + I_{P+2L} + I_{P+3L})/I_{TP} \times 100$$

MALDI Analysis

ZipTip Pipette tips (Merck Millipore, C18 resin, bed volume 0.6 μL, tip volume 10 μL) were washed by aspirating and dispensing MeCN (2 × 10 μL) and 98% H_2O, 2% MeCN, 0.1% TFA (2 × 10 μL). The protein (2.5 μM) was bound by aspirating samples (10 μL) from mass spectrometry 3−7 times. The tip was washed with 98% H_2O, 2% MeCN, 0.1% TFA (2 × 10 μL). The sample was eluted by aspirating and dispensing 3 uL of matrix solution, 2-cyano-4-OH-cinnamic acid in 30% MeCN: H_2O (0.1% TFA). This was pipetted (1.5−2 μL) on a stainless steel target plate, which was dried under vacuum and analyzed on a Bruker UltrafleXtreme MALDI-TOF.

Differential Scanning Fluorimetry

Protein (5 μM) was mixed with corresponding ligand (range of concentrations), in the presence of SYPRO orange (8×), in pH 8 HEPES (20 mM) buffer. The total concentration of DMSO was 5% in all the samples. The total volume of each sample was 25 μL. The samples were incubated in a RT-qPCR machine fitted with a fluorescent plate reader. Fluorescence was constantly measured while the temperature increased following a gradient defined as follows: 15 min at 25 °C, then a constant increase of 1.15 degrees/min between at 25 and 100 °C. DSF measurements were performed on a Bio-Rad CXF96 RT-qPCR machine, with fluorescent readings taken every 15 s.

Determination of Approximate K_d Values from DSF

The T_m values for each concentration of ligand were converted to ΔT_m values, by subtracting T_m with no ligand present. Nonlinear regression for "One site − Specific Binding" (performed in Prism10; GraphPad Software Inc.[21]) fit the data to the simplest saturation model, $Y = B_{max} \times X/(K_d + X)$.

CLogP Values

Chemical structures and calculated properties (CLogP) were generated using ChemDraw Professional, Version 20.1.0.112 (PerkinElmer, Waltham, MA, 2023).[22]

Statistics

For statistical comparisons of total labeling relative intensity from MS and approximate log(K_d) values from DSF, normal distribution of data was confirmed using Shapiro−Wilk's tests and analyzed using Pearson correlation tests; P value (two-tailed) < 0.05 is significant. Analysis was performed in Prism10; GraphPad Software Inc.[21]

Mixed Solvent Molecular Dynamics (MxMD)

Simulations were conducted in Maestro (Schrödinger, release 2025-2[29]) using Desmond with the OPLS4 force field to probe ligandable hotspots on the prepared protein. The holo structure was protein-prepared, then stripped of ligands, waters and nonessential cofactors; essential ions/waters were retained as needed. For each selected probe (default set: acetonitrile, isopropanol, pyrimidine), independent systems were built by placing a ∼7 Å shell of the cosolvent around the solute and solvating in water to achieve ∼5% cosolvent (v/v). Each system was minimized and equilibrated by the built-in MxMD workflow, followed by production MD on Linux GPU nodes; frames were saved for analysis. Probe occupancy maps were computed on a 3 Å grid, clustered into probe "spots," and merged across probes to define "hotspots." Hotspots were ranked by the MxMD score (aggregate probe occupancy) and characterized by surface area, volume and probe composition; predicted hotspots were compared to the cocrystallized ligand.

Virtual Screening and R-Group Enumeration

Covalent docking, virtual screening and R-group enumeration were performed in Maestro (Schrödinger, release 2025-3[30]) using Glide and Prime. The receptor (BTK PH domain, PDB 7I9I) was protein-prepared (hydrogens added, termini capped, missing loops built with Prime), and ligands were standardized and converted to 3D with LigPrep at physiological pH. A covalent docking model was defined with Lys12 as the reactive residue and a predefined chemistry for imine condensation; the cocrystal-derived template was first docked in Pose Prediction (thorough) mode to validate covalent bond formation and pose fidelity, with outputs ranked by Prime energies and Glide cdock metrics. For library design, a template scaffold was enumerated at the *ortho*, *meta* and *para* positions of the phenyl ring, using a curated R-group library to generate analogues. This was followed by LigPrep and covalent docking in Virtual Screening (fast) mode under the validated receptor grid and reaction settings. Docked complexes were analyzed in Pose Viewer and cdock affinity/docking score distributions were compared across *ortho*, *meta* and *para* substitution patterns to assess substituent positioning, pocket compatibility and covalent pose quality.

Synthetic Chemistry

All experiments were performed in oven-dried glassware and under an atmosphere of nitrogen, unless stated otherwise. Commercial starting materials were used without further purification. Dry solvents were distilled from mixtures containing CaH_2 or $LiAlH_4$ as drying agents. Yields refer to spectroscopically and chromatographically pure compounds unless otherwise specified. Analytical thin layer chromatography (TLC) was carried out on glass Merck Kieselgel 60 F254 plates. The plates were visualized under direct UV irradiation (254 nm). R_f values are quoted to the nearest 0.1. Preparative thin layer chromatography was performed on commercially available Analtech plates. Flash column chromatography was undertaken on silica gel 60 (230−400 mesh) under a positive air pressure. The eluent systems are reported as % (v/v) of the solvent components.

Reversed-phase column chromatography was carried out using a Combiflash Rf200 automated chromatography system with Redisep reverse-phase C18-silica flash columns (20−40 μm). Preparative high-performance liquid chromatography (HPLC) was performed on an Agilent 1260 infinity machine. The samples were eluted using a Supelcosil ABZ+PLUS column (250 mm × 21.2 mm, 5 μm). The linear gradient used (for 20 min and a flow rate of 20 mL/min) was: solvent A - 0.1% (v/v) TFA in water, solvent B - 0.05% (v/v) TFA in MeCN. The diodes used the wavelengths of 220 and 254 nm to detect absorbance. Analytical HPLC was performed on Agilent 1260 Infinity Series, fitted with a binary pump, using Supelco Supelcosil ABZ+PLUS (4.6 mm × 150 mm, particle size 3 μm, porosity 120 Å) column and operated by ChemStation C.01.03 software; or Agilent 1200 Series, fitted with a quaternary pump, using Agilent Eclipse Plus C18 (4.6 mm × 150 mm, particle size 3.5 μm, porosity 95 Å) column and operated by ChemStation B.04.03 software. The analytical LC systems used a linear gradient of solvent B (acetonitrile with 0.05% TFA) in solvent A (water with 0.05% TFA) run over 15 min, flow rate 1 mL min^{-1}, and UV absorption was measured using a diode-array detector and extracted wavelengths of 220 and 254 nm. Unless otherwise specified, the gradient of 5 to 95% solvent B was used. The retention time t_R was quoted to 0.01 min on the HPLC traces of all key compounds in the Supporting Information, Figures S3−S41. The purity of all lead compounds, determined by HPLC, was ≥95%.

https://doi.org/10.1021/acs.jmedchem.5c03818
J. Med. Chem. 2026, 69, 12099−12121

^{1}H NMR spectra were recorded under an internal deuterium lock at rt on Bruker Advance III HD (400 MHz, 500 MHz, 700 MHz; Smart probe). Assignments are supported by ^{1}H−^{1}H COSY, ^{1}H−^{13}C HSQC and ^{1}H−^{13}C HMBC spectra. Chemical shifts (δ) are given in ppm quoted to the nearest 0.01 ppm (δ_H). The residual solvent peaks are 7.26 for $CDCl_3$, 5.32 for CD_2Cl_2, 3.31 for CD_3OD and 2.51 for $(CD_3)_2SO$. Coupling constants for mutually coupling protons are reported in Hertz, rounded to the nearest 0.1 Hz. Data are reported as chemical shift, multiplicity (br, broad; s, singlet; d, doublet; t, triplet; q, quartet; m, multiplet; or a combination of them), coupling constants, number of nuclei. Spectra were processed using TopSpin v.4.0.6(Bruker) or MestReNova v 14.3.3−33362 (Mestrelab Research S.L.). ^{13}C NMR spectra were recorded using an internal deuterium lock at rt on Bruker Avance III HD (101 MHz) with broadband proton decoupling. Chemical shifts (δ_C) are quoted to the nearest 0.1 ppm and the solvent reference peaks (in ppm) are 77.2 ($CDCl_3$), 53.5 (CD_2Cl_2), 49.1 (CD_3OD), 33.0 $(CD_3)_2SO$). ^{19}F NMR spectra were recorded using an internal deuterium lock at rt on Bruker Avance III HD (101 MHz) with broadband proton decoupling. Chemical shifts (δ_F) are quoted to the nearest 0.1 ppm. For fluorine containing compounds, data are reported as chemical shift, multiplicity, coupling constant. Spectra were processed using TopSpin v.4.0.6(Bruker). All key spectra are shown in the supplementary data file.

High resolution mass spectrometry (HRMS) was performed on a Waters LCT Premier Time of Flight mass spectrometer, with errors within ± 5 ppm.

Analysis of chiral species was performed analytically with the Agilent 1260 Infinity II supercritical fluid chromatography (SFC) system: Chiralpak IC-3 (0.3 cm × 10 cm). Mobile phase: sc-CO_2/2-propanol = 70/30, flow rate = 1.2 mL/min, wavelength = 254 nm, column temperature = 40 °C. For preparative separation, the chiral species were dissolved in 1:2 MeOH/DMSO and purified on Sepiatec using the following SFC conditions: Column: Chiralpak AD, 21 × 250 mm, 5 μm, Mobile phase: 40% MeOH/60% scCO_2, Flow rate: 60 mL/min, BPR: 120 bar, Column temperature: 40 °C, UV max 265 nm.

General Synthetic Procedure for Aldehydes 10a, 20a, 21a. To a stirred suspension of K_2CO_3 (2 equiv) in DMF was added corresponding aldehyde (1 eq., 0.4 M) and the solution was left stirring at room temperature for 1 h. Alkyl halide (1.5 equiv) was added dropwise, on ice, at a rate of 0.1 mL/min and the solution stirred at room temperature for 24 h. Subsequently, the reaction was refluxed for 8 h until full conversion of the starting material. The solution was filtered and subsequently solvent removed in vacuo, before purification by silica gel chromatography (hexane/EtOAc and mixtures) to yield the corresponding aldehydes **a**.

General Synthetic Procedure for Enones 3b−12b, 16b−34b. A solution of 1-(triphenyl-λ5-phosphaneylidene)propan-2-one (1 equiv) and corresponding aldehydes **a** (1 eq., 0.4 M) in THF was refluxed for 48 h. The solvent was subsequently removed in vacuo before purification by silica gel chromatography (hexane/EtOAc mixtures) to yield the corresponding α,β unsaturated ketones **b**.

General Synthetic Procedure for Diketones 2c−12c, 16c−34c. To a stirred solution of 7% EtONa in EtOH (1.1 equiv) was added a solution of diethyl malonate (1.1 eq., 1.2 M in EtOH) dropwise, on ice, at a rate of 0.4 mL/min. The solution was subsequently left stirring at room temperature for 30 min. A solution of corresponding α,β unsaturated ketone **b** in EtOH (0.8 M) was added dropwise on ice, at a rate of 0.4 mL/min. The solution was stirred at rt for 24 h, and subsequently a solution of 50 wt % NaOH (1.3 equiv) was added. The resulting mixture was refluxed for 3 h and the solvent subsequently removed in vacuo. Six M HCl (150 mL) was added and the mixture subsequently refluxed for 6 h. The solution was extracted with EtOAc, dried over anhydrous Na_2SO_4 and the solvent removed in vacuo. The mixtures were purified by reversed-phase column chromatography (2% HCOOH in H_2O/MeCN 9:1 − 1:1) to yield the corresponding 1,3 diketones **c** as white powders.

General Synthetic Procedure for Carboxy Furans 2−12, 16−34. To a stirred solution of 7% NaOEt (1.1 equiv) was added a solution of corresponding 1,3 diketone **c** (1 eq., 0.4 M in EtOH) dropwise, on ice, at a rate of 0.4 mL/min. The mixture was subsequently stirred at rt for 30 min before ethyl bromopyruvate† (1.3 equiv) was added dropwise, on ice, at a rate of 0.4 mL/min. The mixture was subsequently stirred at rt for 24 h before 50% NaOH (4.5 equiv) was added. The reaction was subsequently stirred at rt for 24 h before the solvent was removed in vacuo and the resulting mixture dissolved in water. The mixture was acidified to pH 1 using HCl 3 M. The solution was extracted with EtOAc, dried over anhydrous Na_2SO_4 and the solvent removed in vacuo. The mixtures were purified by reversed-phase column chromatography (H_2O/MeCN 9:1 − 1:1) to yield the corresponding carboxy-furans as white powders.

General Synthetic Procedure for Esters 16d, 24d, 33d. To a stirred solution of 7% NaOEt (1.1 equiv) was added a solution of corresponding 1,3 diketone **c** (1 eq., 0.4 M in EtOH) dropwise, on ice, at a rate of 0.4 mL/min. The mixture was subsequently stirred at rt for 30 min before ethyl bromopyruvate† (1.3 equiv) was added dropwise, on ice, at a rate of 0.4 mL/min. The mixture was subsequently stirred at rt for 24 h before adding water and acidifying to pH 3 using 3 M HCl. The solution was extracted with EtOAc, dried over. anhydrous Na_2SO_4 and the solvent removed in vacuo. The mixtures were purified by reversed-phase column chromatography (H_2O/MeCN 9:1 − 1:1) to yield the esters as white powders.

*4-Oxo-4,5,6,7-tetrahydrobenzofuran-3-carboxylic Acid (**1**).* (3.3 mg, 18 μmol, 2%) **^{1}H NMR** (400 MHz, $CDCl_3$) δ 13.22 (s, 1H), 8.08 (s, 1H), 2.99 (t, *J* = 6.3 Hz, 2H), 2.69 (dd, *J* = 7.1, 5.9 Hz, 2H), 2.29 (p, *J* = 6.4 Hz, 2H). **^{13}C NMR** (101 MHz, $CDCl_3$) δ 199.42, 170.67, 161.50, 150.40, 118.20, 117.47, 36.69, 23.40, 22.55. **HRMS** (ESI+): *m*/*z* $[M + H]^+$ calculated for $C_9H_9O_4$ 181.0501, found: 181.0495, error: −3.3 ppm. **HPLC purity** 99%.

*5-Phenylcyclohexane-1,3-dione (**2c**).* (221 mg, 1.17 mmol, 12%). **^{1}H NMR** (500 MHz, CD_3OD) δ 7.33−7.23 (m, 5H), 3.37 (m, 1H), 2.68 (dd, *J* = 17.1, 11.7 Hz, 2H), 2.55 (dd, *J* = 17.1, 4.7 Hz, 2H). Five % open form impurity [δ 1.99 (s, methyl ketone)]. **^{13}C NMR** (125 MHz, CD_3OD) δ 143.0, 128.3, 126.6, 126.5, 102.7, 39.5, 39.4.

*3-Carboxy-6-phenyl-4,5,6,7-tetrahydrobenzofuran-4-one (**2**).* (3.4 mg, 13 μmol, 2%) **^{1}H NMR** (500 MHz, $CDCl_3$) δ 13.14 (s, 1H), 8.15 (s, 1H), 7.41 (t, *J* = 7.8 Hz, 2H), 7.36−7.31 (m, 3H), 3.70 (m, *J* = 5.0 Hz, 1H), 3.32 (dd, *J* = 17.6, 5.0 Hz, 1H), 3.20 (dd, *J* = 17.6, 11.0 Hz, 1H), 2.99 (s, 1H), 2.98 (d, *J* = 3.6 Hz, 1H). **^{13}C NMR** (125 MHz, $CDCl_3$) δ 197.5, 169.6, 161.2, 150.7, 140.8, 129.2, 127.9, 126.7, 118.1, 117.3, 43.8, 41.3, 31.1. **HRMS** (ESI−): *m*/*z* $[M - H]^-$ calculated for $C_{15}H_{11}O_4^-$ 255.0663, found: 255.0642, error: 2.1 ppm. **HPLC purity** 96%.

*(E)-4-(Naphthalen-2-yl)but-3-en-2-one (**3b**).* (610 mg; 3.09 mmol; 33%), white solid. **^{1}H NMR** (500 MHz, $CDCl_3$) δ 7.98 (s, 1H), 7.91−7.83 (m, 3H), 7.73−7.67 (m, 1H), 7.70 (d, *J* = 16.3 Hz, 1H), 7.58−7.52 (m, 2H), 6.86 (d, *J* = 16.3 Hz, 1H), 2.45 (s, 3H). **^{13}C NMR** (126 MHz, $CDCl_3$) δ 198.3, 143.5, 134.3, 133.3, 131.9, 130.3, 128.8, 128.5, 127.8, 127.4, 127.3, 126.8, 123.5, 27.6.

*5-(Naphthalen-2-yl)cyclohexane-1,3-dione (**3c**).* (158 mg; 0.66 mmol; 26%). **^{1}H NMR** (500 MHz, d_6-DMSO) δ 7.93−7.79 (m, 4H), 7.56 (dd, *J* = 8.5, 1.8 Hz, 1H), 7.54−7.43 (m, 2H), 5.34 (s, 1H), 3.50 (tt, *J* = 11.7, 4.4 Hz, 1H), 2.92 (dd, *J* = 7.2, 1.4 Hz, 2H), 2.59 (dd, *J* = 15.7, 8.7 Hz, 2H). **^{13}C NMR** (126 MHz, d_6-DMSO) δ 141.6, 133.5, 132.4, 128.4, 128.0, 127.9, 126.6, 126.2, 126.1, 125.4, 104.0, 30.7.

*6-(Naphthalen-2-yl)-4-oxo-4,5,6,7-tetrahydrobenzofuran-3-carboxylic Acid (**3**).* (12 mg; 0.04 mmol; 6%). **^{1}H NMR** (500 MHz, $CDCl_3$) δ 13.15 (s, 1H), 8.17 (s, 1H), 7.92 (d, *J* = 8.5 Hz, 1H), 7.90−7.83 (m, 2H), 7.74 (s, 1H), 7.58−7.51 (m, 2H), 7.44 (dd, *J* = 8.5, 1.8 Hz, 1H), 3.92−3.82 (m, 1H), 3.41 (dd, *J* = 17.6, 5.2 Hz, 1H), 3.31 (dd, *J* = 17.6, 10.9 Hz, 1H), 3.16−3.05 (m, 2H). **^{13}C NMR** (126 MHz, $CDCl_3$) δ 197.8, 169.6, 161.2, 150.71, 138.1, 133.4, 132.8, 129.1, 127.74, 127.72, 126.7, 126.4, 125.4, 124.5, 118.1, 117.3, 43.8, 41.4, 31.0. **HRMS** (ESI+): *m*/*z* $[M + H]^+$ calculated for $C_{19}H_{15}O_4$ 307.0965; found 307.0970. error: 1.6 ppm. **HPLC purity** 98%.

*(E)-4-(3-methoxyphenyl)but-3-en-2-one (**4b**).* (2.45 g; 13.91 mmol; 93%). **^{1}H NMR** (500 MHz, $CDCl_3$) δ 7.50 (d, *J* = 16.3 Hz, 1H), 7.34 (t, *J* = 7.9 Hz, 1H), 7.16 (d, *J* = 7.6 Hz, 1H), 7.10−7.07 (m, 1H), 6.97 (ddd, *J* = 8.3, 2.6, 0.8 Hz, 1H), 6.72 (d, *J* = 16.3 Hz, 1H),

https://doi.org/10.1021/acs.jmedchem.5c03818
J. Med. Chem. 2026, 69, 12099−12121

3.86 (s, 3H), 2.41 (s, 3H). **^{13}C NMR** (126 MHz, $CDCl_3$) δ 198.4, 159.9, 143.3, 135.8, 129.9, 127.4, 121.0, 116.4, 113.0, 55.3, 27.5.

*5-(3-Methoxyphenyl)cyclohexane-1,3-dione (**4c**).* (140 mg; 0.64 mmol; 6%). **^{1}H NMR** (500 MHz, CD_3CN) δ 7.28 (t, J = 7.9 Hz, 1H), 6.94−6.80 (m, 3H), 5.39 (s), 3.82 (s, 3H), 3.37 (tt, J = 11.8, 4.7 Hz, 1H), 2.63 (dd, J = 16.8, 11.9 Hz, 2H), 2.51 (dd, J = 17.1, 4.6 Hz, 2H). **^{13}C NMR** (126 MHz, CD_3CN) δ 159.9, 145.3, 129.7, 119.1, 112.8, 111.9, 103.9, 54.8, 39.3.

*6-(3-Methoxyphenyl)-4-oxo-4,5,6,7-tetrahydrobenzofuran-3-carboxylic Acid (**4**).* (2.4 mg; 8.17 μmol; 2%) **^{1}H NMR** (500 MHz, $CDCl_3$) δ 13.1 (s, 1H), 8.15 (s, 1H), 7.34 (t, J = 7.9 Hz, 1H), 6.9−6.8 (m, 3H), 3.83 (s, 3H), 3.7−3.6 (m, 1H), 3.31 (dd, J = 17.6, 5.1 Hz, 1H), 3.19 (dd, J = 17.6, 11.1 Hz, 1H), 3.00−2.90 (m, 2H). **^{13}C NMR** (126 MHz, $CDCl_3$) δ 197.8, 169.6, 161.2, 160.1, 150.7, 142.4, 130.3, 118.8, 118.1, 117.2, 113.1, 112.5, 55.3, 43.8, 41.3, 31.0. **HPLC purity** 98%.

*(E)-4-(3-(Trifluoromethyl)phenyl)but-3-en-2-one (**5b**).* (3.48 g; 16.2 mmol; 85%) **^{1}H NMR** (500 MHz, $CDCl_3$) δ 7.81 (d, J = 0.4 Hz, 1H), 7.74 (d, J = 7.8 Hz, 1H), 7.67 (d, J = 7.8 Hz, 1H), 7.55 (t, J = 7.8 Hz, 1H), 7.54 (d, J = 16.4 Hz, 1H), 6.79 (d, J = 16.3 Hz, 1H), 2.42 (s, 3H). **^{13}C NMR** (126 MHz, $CDCl_3$) δ 197.8 (s), 141.3 (s), 135.3 (s), 131.5 (q, J = 32.6 Hz), 131.2 (q, J = 1.3 Hz), 129.5 (s), 128.5 (s), 126.8 (q, J = 3.7 Hz), 124.8 (q, J = 3.8 Hz), 124.5 (q, J = 273.6 Hz), 27.8 (s). **^{19}F NMR** (470 MHz, $CDCl_3$) δ −63.9.

*5-(3-(Trifluoromethyl)phenyl)cyclohexane-1,3-dione (**5c**).* (117 mg; 0.456 mmol; 4%) **^{1}H NMR** (500 MHz, CD_3OD) δ 7.70−7.60 (m, 2H), 7.61−7.45 (m, 2H), 3.60−3.50 (m, 1H), 2.74 (dd, J = 17.5, 11.7 Hz, 2H), 2.74 (dd, J = 17.5, 4.7 Hz, 2H) Open ring impurities are present (20%). **^{13}C NMR** (126 MHz, CD_3OD) δ 144.6 (s), 130.5 (d, J = 33 Hz), 130.5 (s), 129.2 (s), 124.2 (q, J = 274 Hz), 123.4 (q, J = 4.1 Hz), 39.2 (s), 38.0 (s). **^{19}F NMR** (470 MHz, $CDCl_3$) δ −65.0 (-CF_3). **HRMS** (ESI+): m/z $[M + H]^+$ calculated for $C_{13}H_{12}F_3O_2$ 257.0784; found 257.0782. error: −0.7 ppm.

*4-Oxo-6-(3-(trifluoromethyl)phenyl)-4,5,6,7-tetrahydrobenzofuran-3-carboxylic Acid (**5**).* (1.7 mg; 5.25 μmol; 1%). **^{1}H NMR** (500 MHz, $CDCl_3$) δ 13.0 (s, 1H), 8.17 (s, 1H), 7.64 (d, J = 7.7 Hz, 1H), 7.61−7.47 (m, 3H), 3.77−3.71 (m, 1H), 3.36 (dd, J = 17.5, 5.1 Hz, 1H), 3.23 (dd, J = 17.5, 11.2 Hz, 1H), 3.05−2.93 (m, 2H). **^{13}C NMR** (126 MHz, $CDCl_3$) δ 197.0 (s), 169.0 (s), 161.0 (s), 150.9 (s), 141.7 (s), 131.5 (q, J = 32.7 Hz), 130.1 (s), 129.8 (s), 124.9 (q, J = 3.5 Hz) 123.5 (q, J = 3.5 Hz), 124.0 (q, J = 274 Hz), 118.0 (s), 117.3 (s), 43.5 (s), 41.0 (s), 30.9 (s). **^{19}F NMR** (470 MHz, $CDCl_3$) δ −63.7. **HRMS** (ESI+): m/z $[M + H]^+$ calculated for $C_{15}H_{12}F_3O_4$ 325.0682; found 325.0686. error: 1.2 ppm. **HPLC purity** 96%.

*(E)-4-(Benzofuran-2-yl)but-3-en-2-one (**6b**).* (3.10 g, 16.7 mmol, 81%) **^{1}H NMR** (400 MHz, $CDCl_3$) δ 7.57 (d, J = 7.5 Hz, 1H), 7.47 (dd, J = 7.5, 1.0 Hz, 1H), 7.38 (d, J = 15.7 Hz, 1H), 7.36 (td, J = 7.5, 1.0 Hz, 1H), 7.24 (td, J = 7.5, 1.0 Hz, 1H), 6.97 (s, 1H), 6.86 (d, J = 15.7 Hz, 1H), 2.37 (s, 3H). **^{13}C NMR** (101 MHz, $CDCl_3$) δ 197.5, 155.6, 152.4, 129.5, 128.4, 126.7, 126.7, 123.4, 121.8, 112.0, 111.4, 28.3.

*5-(Benzofuran-2-yl)cyclohexane-1,3-dione (**6c**).* (338 mg, 1.87 mmol, 50%) **^{1}H NMR** (400 MHz, CD_3OD) δ 7.50 (d, J = 7.5 Hz, 1H), 7.41 (d, J = 8.0 Hz, 1H), 7.22 (td, J = 8.0, 1.4 Hz, 1H), 7.17 (td, J = 7.5, 1.2, 1H), 6.55 (t, J = 0.80 Hz, 1H), 5.42 (s, weak), 3.64 (m, J = 5.0 Hz, 1H), 2.80 (dd, J = 17.0, 5.2 Hz, 2H), 2.73 (dd, J = 17.0, 3.9 Hz, 2H). **^{13}C NMR** (101 MHz, CD_3OD) δ 160.5, 156.1, 129.8, 124.9, 123.8, 121.8, 111.7, 102.9, 38.6, 34.5. Open form impurity 30%. HRMS (ESI+): m/z $[M + H]$+ calculated for $C_{14}H_{13}O_3^+$: 229.0859, found: 229.0865, error: 0.4 ppm

*4′-Oxo-4′,5′,6′,7′-tetrahydro-[2,6′-bibenzofuran]-3′-carboxylic Acid (**6**).* (24 mg, 81 μmol, 8.7%). **^{1}H NMR** (500 MHz, CD_3OD) δ 8.11 (s, 1H), 7.52 (dd, J = 7.7, 0.8 Hz, 1H), 7.43 (dd, J = 8.0, 0.8 Hz, 1H), 7.25 (td, J = 8.0, 1.5 Hz, 1H), 7.19 (td, J = 7.7, 0.8 Hz, 1H), 6.65 (t, J = 1.0 Hz, 1H), 3.97 (m, 1H), 3.48 (dd, J = 17.3, 5.3 Hz, 1H), 3.35 (dd, J = 17.6, 9.3 Hz, 1H), 3.07 (s, 1H), 3.05 (d, J = 4.8 Hz, 1H). **^{13}C NMR** (125 MHz, CD_3OD) δ 128.3, 123.9, 122.5, 120.6, 110.5, 102.2, 40.9, 34.4, 27.4. **HRMS** (ESI+): m/z $[M + H]^+$ calculated mass for $C_{17}H_{13}O_5^+$: 297.0757, found: 297.07423, error: 1.4 ppm. **HPLC purity** 97%.

*(E)-4-(2-Bromophenyl)but-3-en-2-one (**7b**).* (6.8 g; 30.2 mmol; 78%). **^{1}H NMR** (500 MHz, $CDCl_3$) δ 7.91 (d, J = 16.3 Hz, 1H), 7.69−7.61 (m, 2H), 7.40−7.33 (m, 1H), 7.26 (dd, J = 7.8 Hz, 1.7 Hz, 1H), 6.64 (d, J = 16.3 Hz, 1H), 2.45 (s, 3H). **^{13}C NMR** (126 MHz, $CDCl_3$) δ 198.3, 141.9, 134.4, 133.4, 131.4, 129.8, 127.8, 127.7, 125.6, 27.2.

*5-(2-Bromophenyl)cyclohexane-1,3-dione (**7c**).* (387 mg; 1.448 mmol; 5%). **^{1}H NMR** (500 MHz, CD_3OD) δ 7.63 (dd, J = 8.0, 1.2 Hz, 1H), 7.46 (dd, J = 7.8, 1.6 Hz, 1H), 7.39 (td, J = 7.7, 1.2 Hz, 1H), 7.19 (td, J = 7.8, 1.7 Hz, 1H), 3.84 (tt, J = 11.5, 4.6 Hz, 1H), 2.69 (dd, J = 17.1, 11.5 Hz, 2H), 2.60 (dd, J = 17.1, 4.7 Hz, 2H). **^{13}C NMR** (126 MHz, CD_3OD) δ 141.4, 133.0, 128.4, 127.8, 127.3, 123.7, 38.5, 37.9. **HRMS** (ESI+): m/z $[M + H]^+$ calculated for $C_{12}H_{12}{}^{79}BrO_2$ 267.0015; found 267.0018. error: 1.0 ppm.

*6-(2-Bromophenyl)-4-oxo-4,5,6,7-tetrahydrobenzofuran-3-carboxylic Acid (**7**).* (143 mg; 0.426 mmol; 30%) **^{1}H NMR** (500 MHz, $CDCl_3$) δ 13.10 (s, 1H), 8.16 (s, 1H), 7.66 (dd, J = 8.0, 1.2 Hz, 1H), 7.39 (td, J = 7.6, 1.2 Hz, 1H), 7.34 (dd, J = 7.8, 1.7 Hz, 1H), 7.22 (ddd, J = 8.0, 7.4, 1.7 Hz, 1H), 4.22−4.13 (m, 1H), 3.39 (dd, J = 17.6, 5.1 Hz, 1H), 3.15 (dd, J = 17.6, 10.8 Hz, 1H), 3.02−2.97 (m, 2H). **^{13}C NMR** (126 MHz, $CDCl_3$) δ 197.5, 169.4, 161.1, 150.8, 139.5, 133.8, 129.4, 128.3, 127.1, 124.2, 118.1, 117.2, 42.4, 40.0, 29.6. **HRMS** (ESI+): m/z $[M + H]^+$ calculated for $C_{15}H_{12}{}^{79}BrO_4$ 334.9913; found 334.9926. error: −3.8 ppm. **HPLC purity** 97%.

*(E)-4-(2-Fluorophenyl)but-3-en-2-one (**8b**).* (2.34 g; 14.26 mmol; 74%). **^{1}H NMR** (500 MHz, $CDCl_3$) δ 7.69 (d, J = 16.5 Hz, 1H), 7.59 (td, J = 7.6, 1.7 Hz, 1H), 7.39 (dddd, J = 8.3, 7.2, 5.3, 1.7 Hz, 1H), 7.19 (td, J = 7.6, 0.9 Hz, 1H), 7.13 (ddd, J = 10.6, 8.3, 1.1 Hz, 1H), 6.80 (d, J = 16.5 Hz, 1H), 2.42 (s, 3H). **^{13}C NMR** (126 MHz, $CDCl_3$) δ 198.4 (s), 161.4 (d, J = 254 Hz), 135.7 (d, J = 3.5 Hz), 131.9 (d, J = 8.8 Hz), 129.2 (d, J = 5.4 Hz), 128.7 (d, J = 2.8 Hz), 124.5 (d, J = 3.7 Hz), 122.5 (d, J = 11.6 Hz), 116.2 (d, J = 21.8 Hz), 27.5 (s). **^{19}F NMR** (376 MHz, $CDCl_3$) δ −115.8.

*5-(2-Fluorophenyl)cyclohexane-1,3-dione (**8c**).* (350 mg; 1.7 mmol; 12%). **^{1}H NMR** (500 MHz, CD_3OD) δ 7.39 (td, J = 7.7, 1.5 Hz, 1H), 7.30 (tdd, J = 7.3, 5.3, 1.7 Hz, 1H), 7.18 (td, J = 7.6, 0.8 Hz, 1H), 7.15−7.08 (m, 1H), 3.68 (tt, J = 11.7, 4.6 Hz, 1H), 2.74 (dd, J = 17.1, 11.7 Hz, 2H), 2.57 (dd, J = 17.2, 4.6 Hz, 2H). **^{13}C NMR** (126 MHz, CD_3OD) δ 160.9 (d, J = 247 Hz), 129.5 (d, J = 13.6 Hz), 128.4 (d, J = 8.6 Hz), 127.8 (d, J = 4.5 Hz), 124.3 (d, J = 3.5 Hz), 115.2 (d, J = 23 Hz), 37.7 (s), 33.1 (d, J = 2.5 Hz). **^{19}F NMR** (376 MHz, $CDCl_3$) δ −120.2. **HRMS** (ESI+): m/z $[M + H]^+$ calculated for $C_{12}H_{12}FO_2$ 207.0816; found 207.0817. error: 0.7 ppm.

*6-(2-Fluorophenyl)-4-oxo-4,5,6,7-tetrahydrobenzofuran-3-carboxylic Acid (**8**).* (250 mg; 0.912 mmol; 53%). **^{1}H NMR** (500 MHz, $CDCl_3$) δ 13.12 (s, 1H), 8.15 (s, 1H), 7.39−7.31 (m, 1H), 7.31−7.25 (m, 1H), 7.20 (td, J = 7.6, 1.1 Hz, 1H), 7.14 (ddd, J = 10.8, 8.2, 1.1 Hz, 1H), 3.99−3.88 (m, 1H), 3.32 (dd, J = 16.8, 5.2 Hz, 1H), 3.27 (dd, J = 16.8, 9.3 Hz, 1H), 3.08 (dd, J = 17.2, 12.3 Hz, 1H), 2.96 (dd, J = 17.2, 4.2 Hz, 1H). **^{13}C NMR** (126 MHz, $CDCl_3$) δ 197.8 (s), 169.6 (s), 161.2 (s), 160.8 (d, J = 246 Hz), 150.7 (s), 129.6 (d, J = 8.6 Hz), 128.0 (d, J = 4.3 Hz), 127.6 (d, J = 13.4 Hz), 124.8 (d, J = 3.6 Hz), 118.1 (s), 117.2 (s), 116.3 (d, J = 22.1 Hz), 42.1 (d, J = 1.8 Hz), 35.6 (d, J = 1.9 Hz), 29.4 (d, J = 2.2 Hz). **^{19}F NMR** (376 MHz, $CDCl_3$) δ −116.4. **HRMS** (ESI+): m/z $[M + H]^+$ calculated for $C_{15}H_{12}FO_4$ 275.0714; found 275.0719. error: 1.8 ppm. **HPLC purity** > 99%.

*(E)-4-(2-Phenoxyphenyl)but-3-en-2-one (**9b**).* (3.56 g; 14.95 mmol; 78%). **^{1}H NMR** (500 MHz, $CDCl_3$) δ 7.90 (d, J = 16.5 Hz, 1H), 7.69 (dd, J = 7.8, 1.6 Hz, 1H), 7.37−7.32 (m, 3H), 7.20−7.12 (m, 2H), 7.06−7.01 (m, 2H), 6.91 (dd, J = 8.3, 1.0 Hz, 1H), 6.80 (d, J = 16.5 Hz, 1H), 2.37 (s, 3H). **^{13}C NMR** (126 MHz, $CDCl_3$) δ 198.9, 156.8, 156.1, 137.9, 131.7, 130.0, 128.5, 128.2, 125.9, 123.8, 123.7, 118.97, 118.95, 27.1.

*5-(2-Phenoxyphenyl)cyclohexane-1,3-dione (**9c**).* (1.41 g; 4.04 mmol; 27%). **^{1}H NMR** (500 MHz, CD_3OD) δ 7.44 (dd, J = 7.7, 1.6 Hz, 1H), 7.39−7.32 (m, 2H), 7.28−7.22 (m, 1H), 7.17 (td, J = 7.5, 1.2 Hz, 1H), 7.14−7.07 (m, 1H), 6.98−6.92 (m, 2H), 6.88 (dd, J = 8.1, 1.2 Hz, 1H), 3.78−3.65 (m, 1H), 2.76 (dd, J = 17.2, 11.7 Hz, 2H), 2.55 (dd, J = 17.3, 4.5 Hz, 2H). **^{13}C NMR** (126 MHz, CD_3OD)

https://doi.org/10.1021/acs.jmedchem.5c03818
J. Med. Chem. 2026, 69, 12099−12121

δ 157.6, 154.4, 133.7, 129.6, 128.0, 127.6, 123.9, 122.8, 119.2, 117.6, 33.6. Two quaternary carbon signals are missing or overlapping. **HRMS** (ESI+): m/z $[M + H]^+$ calculated for $C_{18}H_{17}O_3$ 281.1172; found 281.1170. error: −0.7 ppm.

*4-Oxo-6-(2-phenoxyphenyl)-4,5,6,7-tetrahydrobenzofuran-3-carboxylic Acid (**9**).* (250 mg; 0.717 mmol; 17%). **^{1}H NMR** (400 MHz, $CDCl_3$) δ 13.19 (s, 1H), 8.12 (s, 1H), 7.43−7.25 (m, 4H), 7.16 (t, J = 7.4 Hz, 2H), 7.00 (d, J = 7.8 Hz, 2H), 6.95−6.87 (m, 1H), 4.25−3.88 (m, 1H), 3.42−3.23 (m, 2H), 3.16 (dd, J = 17.2, 12.3 Hz, 1H), 2.97 (dd, J = 17.2, 4.1 Hz, 1H). **^{13}C NMR** (101 MHz, $CDCl_3$) δ 198.3, 170.1, 161.3, 156.6, 155.0, 150.5, 131.3, 130.1, 129.1, 127.8, 123.9, 123.8, 119.0, 118.7, 118.0, 117.1, 42.3, 36.3, 29.5. **HRMS** (ESI+): m/z $[M + H]^+$ calculated for $C_{21}H_{17}O_5$ 349.1071; found 349.1085. error: 4.3 ppm. **HPLC purity** 91%.

*2-Isopropoxybenzaldehyde (**10a**).* (7.87 g; 48 mmol; 80%). **^{1}H NMR** (500 MHz, $CDCl_3$) δ 10.51 (d, J = 0.8 Hz, 1H), 7.84 (dd, J = 7.9, 1.9 Hz, 1H), 7.53 (ddd, J = 8.5, 7.3, 1.9 Hz, 1H), 7.03−6.99 (m, 2H), 4.70 (septet, J = Hz, 1H), 1.42 (d, J = 6.1 Hz, 6H). **^{13}C NMR** (126 MHz, $CDCl_3$) δ 190.2, 160.6, 135.7, 128.3, 125.7, 120.4, 114.0, 71.1, 22.0.

*(E)-4-(2-Isopropoxyphenyl)but-3-en-2-one (**10b**).* (6.2 g; 30.06 mmol; 78%). **^{1}H NMR** (500 MHz, $CDCl_3$) δ 7.92 (d, J = 16.5 Hz, 1H), 7.57 (dd, J = 7.7, 1.7 Hz, 1H), 7.35 (ddd, J = 8.4, 7.4, 1.7 Hz, 1H), 6.96 (t, J = 7.6 Hz, 1H), 6.95 (d, J = 8.4 Hz, 1H), 6.77 (d, J = 16.5 Hz, 1H), 4.64 (septet, J = 6.1 Hz, 1H), 2.40 (s, 3H), 1.42 (d, J = 6.1 Hz, 6H). **^{13}C NMR** (126 MHz, $CDCl_3$) δ 199.1, 156.8, 139.1, 131.6, 128.4, 127.5, 124.3, 120.6, 113.8, 71.0, 27.1, 22.1.

*5-(2-Isopropoxyphenyl)cyclohexane-1,3-dione (**10c**).* (1.18 g; 4.81 mmol; 16%). **^{1}H NMR** (500 MHz, CD_3OD) δ 7.25−7.19 (m, 2H), 6.98 (d, J = 8.1 Hz, 1H), 6.91 (td, J = 7.5, 1.0 Hz, 1H), 4.68 (septet. J = 5.9 Hz, 1H), 3.70 (tt, J = 11.7, 4.5 Hz, 1H), 2.73 (dd, J = 17.2, 11.7 Hz, 2H), 2.53 (dd, J = 17.3, 4.5 Hz, 2H), 1.36 (d, J = 6.0 Hz, 6H). **^{13}C NMR** (126 MHz, CD_3OD) δ 155.2, 131.2, 127.6, 126.9, 120.1, 112.7, 69.5, 47.6, 33.9, 21.0. **HRMS** (ESI+): m/z $[M + H]^+$ calculated for $C_{15}H_{19}O_3$ 247.1329; found 247.1324. error: −1.8 ppm.

*6-(2-Isopropoxyphenyl)-4-oxo-4,5,6,7-tetrahydrobenzofuran-3-carboxylic Acid (**10**).* (300 mg; 0.954 mmol; 20%). **^{1}H NMR** (500 MHz, $CDCl_3$) δ 13.30 (s, 1H), 8.13 (s, 1H), 7.32−7.27 (m, 1H), 7.19 (dd, J = 7.8, 1.6 Hz, 1H), 6.95 (m, 2H), 4.75−4.57 (m, 1H), 4.01−3.88 (m, 1H), 3.32 (dd, J = 17.6, 10.5 Hz, 1H), 3.24 (dd, J = 17.6, 5.5 Hz, 1H), 3.14 (dd, J = 17.2, 12.3 Hz, 1H), 2.90 (dd, J = 17.2, 4.0 Hz, 1H), 1.39 (dd, J = 6.0, 2.6 Hz, 6H). **^{13}C NMR** (126 MHz, $CDCl_3$) δ 199.1, 170.6, 161.4, 155.3, 150.4, 129.2, 128.7, 127.6, 120.5, 118.1, 117.0, 112.7, 69.8, 42.1, 36.6, 29.0, 22.2. **HRMS** (ESI+): m/z $[M + H]^+$calculated for $C_{18}H_{19}O_5$ 315.1227; found 315.1234. error: 2.2 ppm. **HPLC purity** 97%.

*(E)-4-(2-Methoxyphenyl)but-3-en-2-one (**11b**).* (2.19 g; 12.44 mmol; 65%). **^{1}H NMR** (500 MHz, $CDCl_3$) δ 7.91 (d, J = 16.5 Hz, 1H), 7.57 (dd, J = 7.7, 1.6 Hz, 1H), 7.42−7.36 (m, 1H), 7.00 (t, J = 7.5 Hz, 1H), 6.95 (d, J = 8.3 Hz, 1H), 6.78 (d, J = 16.5 Hz, 1H), 3.92 (s, 3H), 2.41 (s, 3H). **^{13}C NMR** (126 MHz, $CDCl_3$) δ 199.1, 158.2, 138.7, 131.8, 128.3, 127.8, 123.3, 120.8, 111.1, 55.5, 27.1.

*5-(2-Methoxyphenyl)cyclohexane-1,3-dione (**11c**).* (164 mg; 0.751 mmol; 7%). **^{1}H NMR** (500 MHz, CD_3OD) δ 7.29−7.21 (m, 2H), 6.99 (dd, J = 8.1, 0.6 Hz, 1H), 6.94 (td, J = 7.5, 1.0 Hz, 1H), 3.87 (s, 3H), 3.74−3.66 (m, 1H), 2.72 (dd, J = 17.2, 11.7 Hz, 2H), 2.53 (dd, J = 17.3, 4.5 Hz, 2H). **^{13}C NMR** (126 MHz, CD_3OD) δ 157.2, 130.4, 127.7, 126.6, 120.4, 110.4, 54.4, 37.7, 33.7.

*6-(2-Methoxyphenyl)-4-oxo-4,5,6,7-tetrahydrobenzofuran-3-carboxylic Acid (**11**).* (108 mg; 0.375 mmol; 50%). **^{1}H NMR** (500 MHz, $CDCl_3$) δ 13.3 (s, 1H), 8.13 (s, 1H), 7.36−7.30 (m, 1H), 7.20 (dd, J = 7.6, 1.6 Hz, 1H), 7.00 (td, J = 7.5, 1.0 Hz, 1H), 6.96 (d, J = 8.3 Hz, 1H), 4.02−3.92 (m, 1H), 3.30 (dd, J = 17.6, 10.3 Hz, 1H), 3.24 (dd, J = 17.6, 5.7 Hz, 1H), 3.12 (dd, J = 17.2, 12.4 Hz, 1H), 2.90 (dd, J = 17.2, 3.8 Hz, 1H). **^{13}C NMR** (126 MHz, $CDCl_3$) δ 198.9, 170.6, 161.4, 157.0, 150.4, 128.9, 128.7, 127.3, 120.9, 118.0, 117.0, 111.0, 55.3, 42.0, 36.3, 29.0. **HRMS** (ESI+): m/z $[M + H]^+$ calculated for $C_{16}H_{15}O_5$ 287.0914; found 287.0912. error: −0.7 ppm. **HPLC purity** 97%.

*(E)-4-(Pyridin-2-yl)but-3-en-2-one (**12b**).* (2.4 g; 16.32 mmol; 85%). **^{1}H NMR** (500 MHz, $CDCl_3$) δ 8.67 (dd, J = 4.7, 0.7 Hz, 1H), 7.74 (td, J = 7.7, 1.8 Hz, 1H), 7.54 (d, J = 16.0 Hz, 1H), 7.50 (d, J = 7.8 Hz, 1H), 7.32−7.27 (m, 1H), 7.16 (d, J = 16.0 Hz, 1H), 2.42 (s, 3H). **^{13}C NMR** (126 MHz, $CDCl_3$) δ 198.5, 153.1, 150.2, 141.9, 136.8, 130.2, 124.3, 124.2, 28.1.

*5-(Pyridin-2-yl)cyclohexane-1,3-dione (**12c**).* (87 mg; 0.46 mmol; 3%). **^{1}H NMR** (500 MHz, CD_3OD) δ 8.54 (ddd, J = 4.9, 1.6, 0.8 Hz, 1H), 7.82 (td, J = 7.7, 1.8 Hz, 1H), 7.42 (d, J = 7.9 Hz, 1H), 7.32 (ddd, J = 7.6, 4.9, 1.1 Hz, 1H), 3.57 (ddd, J = 11.5, 8.1, 4.7 Hz, 1H), 2.83 (dd, J = 17.3, 11.6 Hz, 2H), 2.62 (dd, J = 17.4, 4.7 Hz, 2H). **^{13}C NMR** (126 MHz, CD_3OD) δ 161.4, 148.7, 137.5, 122.3, 122.0, 41.1, 37.6. **HRMS** (ESI+): m/z $[M + H]^+$ calculated for $C_{11}H_{12}NO_2$ 190.0863; found 190.0861. error: −0.8 ppm.

*4-oxo-6-(Pyridin-2-yl)-4,5,6,7-tetrahydrobenzofuran-3-carboxylic Acid (**12**).* (30 mg; 0.116 mmol; 25%). **^{1}H NMR** (500 MHz, $CDCl_3$) δ 13.22 (s, 1H), 8.74−8.39 (m, 1H), 8.12 (s, 1H), 7.72 (td, J = 7.7, 1.8 Hz, 1H), 7.27−7.23 (m, 2H), 3.91−3.80 (m, 1H), 3.50 (dd, J = 17.7, 9.7 Hz, 1H), 3.32 (dd, J = 17.7, 5.3 Hz, 1H), 3.20 (dd, J = 17.3, 11.1 Hz, 1H), 2.96 (dd, J = 17.3, 4.2 Hz, 1H). **^{13}C NMR** (126 MHz, $CDCl_3$) δ 197.9, 169.4, 161.3, 159.4, 150.6, 149.6, 137.1, 122.7, 121.9, 118.0, 117.1, 42.7, 42.3, 29.3. **HRMS** (ESI+): m/z $[M + H]^+$calculated for $C_{14}H_{12}NO_4$ 258.0761; found 258.0764. error: 1.8 ppm. **HPLC purity** > 99%.

*2-(3-Carboxy-4-oxo-4,5,6,7-tetrahydrobenzofuran-6-yl)pyridine 1-Oxide (**13**).* (0.89 mg; 3.25 μmol; 12%). To a solution of **12** (6.8 mg; 0.0264 mmol) in CH_2Cl_2 (0.5 mL) was added mCPBA (6.8 mg; 0.04 mmol) and the mixture stirred at rt for 5h. The solvent was subsequently removed under a stream of nitrogen. The resulting mixture was purified by reversed-phase preparative HPLC (0.1% TFA H_2O/MeCN 2:3 − 1:9) to yield **13** as a white powder. **^{1}H NMR** (500 MHz, $CDCl_3$) δ 8.51 (dd, J = 6.5, 0.9 Hz, 1H), 8.15 (s, 1H), 7.60 (td, J = 7.8, 1.2 Hz, 1H), 7.49−7.44 (m, 1H), 7.39 (dd, J = 7.9, 1.9 Hz, 1H), 4.57−4.33 (m, 1H), 3.52 (dd, J = 17.7, 5.6 Hz, 1H), 3.48 (dd, J = 17.7, 9.0 Hz, 1H), 3.27 (dd, J = 17.1, 10.5 Hz, 1H), 3.08 (dd, J = 17.1, 4.3 Hz, 1H). **^{13}C NMR** (126 MHz, $CDCl_3$) δ 196.7, 168.7, 161.0, 151.0, 140.9, 130.4, 125.5, 124.8, 118.0, 117.1, 39.0, 36.1, 26.1. **HRMS** (ESI+): m/z $[M + H]^+$ calculated for $C_{14}H_{12}NO_5$ 274.0710; found 274.0720. error: 3.5 ppm. **HPLC purity** > 99%.

*6-(2-Hydroxyphenyl)-4-oxo-4,5,6,7-tetrahydrobenzofuran-3-carboxylic Acid (**14**).* (2.63 mg; 9.66 μmol; 12%). To a solution of **11** (24.8 mg; 0.0866 mmol) in CH_2Cl_2 at −78 °C was added a 1 M solution of BBr_3 in CH_2Cl_2 (2.28 eq., 0.197 mmol; 50 mg; 0.2 mL) dropwise and the reaction left to warm to rt and stirred for 24 h. The solvent was removed under a stream of nitrogen and the resulting mixture was purified by reversed-phase preparative HPLC (0.1% TFA H_2O/MeCN 2:3 − 1:9) to yield **14** as a white powder. **^{1}H NMR** (500 MHz, $CDCl_3$) δ 8.15 (s, 1H), 7.25−7.16 (m, 2H), 6.98 (td, J = 7.5, 1.1 Hz, 1H), 6.83 (dd, J = 8.0, 1.0 Hz, 1H), 4.03−3.88 (m, 1H), 3.38 (dd, J = 17.6, 10.7 Hz, 1H), 3.29 (dd, J = 17.6, 5.3 Hz, 1H), 3.20 (dd, J = 17.2, 12.4 Hz, 1H), 2.94 (dd, J = 17.2, 4.0 Hz, 1H). **^{13}C NMR** (126 MHz, $CDCl_3$) δ 198.9, 170.6, 161.7, 153.3, 150.5, 128.8, 127.9, 127.0, 121.3, 117.9, 117.0, 115.9, 41.8, 36.7, 28.8. **HRMS** (ESI+): m/z $[M + H]^+$ calculated for $C_{15}H_{13}O_5$ 273.0757; found 273.0750. error: −2.8 ppm. **HPLC purity** 95%.

*6-([1,1′-Biphenyl]-2-yl)-4-oxo-4,5,6,7-tetrahydrobenzofuran-3-carboxylic Acid (**15**).* (6.9 mg; 0.021 mmol; 35%). **7** (20 mg; 0.06 mmol), phenyl boronic acid (1.2 eq.; 8.8 mg; 0.072 mmol), $Pd(OAc)_2$ (1 mg; 4.45 μmol), s-phos (2.5 mg; 6.0 μmol) and K_3PO_4 (26 mg; 0.12 mmol) were added in toluene (120 μL) and H_2O (18 μL) and heated in the microwave at 60 °C for 18h. The resulting mixture was filtered through Celite, washed with Et_2O (3 × 20 mL) and the solution concentrated in vacuo. The resulting mixture was purified by reversed-phase preparative HPLC (0.1% TFA H_2O/MeCN 2:3 − 1:9) to yield **15** as a white powder. **^{1}H NMR** (500 MHz, $CDCl_3$) δ 8.09 (s, 1H), 7.51−7.35 (m, 6H), 7.32−7.25 (m, 3H), 3.88−3.75 (m, 1H), 3.14 (dd, J = 17.8, 8.3 Hz, 1H), 3.06 (dd, J = 17.8, 5.4 Hz, 1H), 2.98 (dd, J = 17.3, 12.9 Hz, 1H), 2.83 (dd, J = 17.3, 3.7 Hz, 1H). **^{13}C NMR** (126 MHz, $CDCl_3$) δ 197.7, 169.5, 161.3, 150.6, 142.0, 140.5, 138.2, 131.0, 128.9, 128.6, 128.16, 127.6, 127.4, 125.7, 117.9, 117.0,

https://doi.org/10.1021/acs.jmedchem.5c03818
J. Med. Chem. 2026, 69, 12099−12121

43.8, 37.0, 31.1. **HRMS** (ESI+): m/z [M + H]$^+$ calculated for $C_{21}H_{17}O_4$ 333.1121; found 333.1131. error: 3.0 ppm. **HPLC purity** 97%.

*2-Bromo-6-methoxybenzaldehyde (**16a**).* (1.21 g, 5.6 mmol, 75%). A mixture of 6-bromor-2-hydroxybenzaldehyde (1.5 g, 7.5 mmol, 1 equiv), potassium carbonate (3.95 g, 28.6 mmol, 3.8 equiv), methyl iodide (7.9 mL, 126 mmol, 17 equiv) and 40 mL acetone was stirred for 96 h, diluted with H_2O (80 mL) and extracted with ether. The organic extract was dried with anhydrous $MgSO_4$, evaporated and purified by silica gel chromatography (0−60% EtOAc/pet. ether) to yield crystalline 2-bromo-6-methoxybenzaldehyde. R_f = 0.6 (1:1 pet. Ether/EtOAc). **^{1}H NMR** (500 MHz, $CDCl_3$) δ 10.4 (s, 1H), 7.32 (t, J = 8.2 Hz, 1H), 7.24 (dd, J = 8.0, 1.0 Hz, 1H), 6.95 (dd, J = 8.4, 1.0 Hz, 1H), 3.91 (s, 3H). **^{13}C NMR** (126 MHz, $CDCl_3$) δ 190.6, 162.1, 134.9, 126.6, 125.1, 123.6, 111.2, 56.4.

*(E)-4-(2-Bromo-6-methoxyphenyl)but-3-en-2-one (**16b**).* (814 mg; 3.189 mmol; 68%). **^{1}H NMR** (500 MHz, $CDCl_3$) δ 7.82 (d, J = 16.5 Hz, 1H), 7.28 (dd, J = 7.8, 0.9 Hz, 1H), 7.18 (t, J = 8.2 Hz, 1H), 7.08 (d, J = 16.5 Hz, 1H), 6.92 (d, J = 8.4 Hz, 1H), 3.91 (s, 3H), 2.43 (s, 3H). **^{13}C NMR** (126 MHz, $CDCl_3$) δ 199.7, 159.7, 139.0, 133.2, 131.0, 127.1, 125.7, 123.2, 110.3, 55.9, 27.0. **HRMS** (ESI+): m/z [M + H]$^+$ calculated for $C_{11}H_{11}{}^{79}BrO_2$ 255.0015; found 255.0017. error: 0.5 ppm.

*5-(2-Bromo-6-methoxyphenyl)cyclohexane-1,3-dione (**16c**).* (100 mg; 0.336 mmol; 11%). **^{1}H NMR** (500 MHz, d_6-DMSO) δ 7.21 (dd, J = 8.1, 1.1 Hz, 1H), 7.18 (t, J = 8.2 Hz, 1H), 7.07 (dd, J = 8.3, 0.8 Hz, 1H), 3.90 (m, 1H), 3.84 (s, 3H), 3.09 (t, J = 14.6 Hz, 2H), 2.40 (dd, J = 17.4, 4.7 Hz, 2H). **^{13}C NMR** (126 MHz, d_6-DMSO): δ 159.2, 129.4, 128.6, 125.1, 111.8, 103.3, 55.9. **HRMS** (ESI+): m/z [M + H]$^+$ calculated for $C_{13}H_{14}{}^{79}BrO_3$ 297.0121; found 297.0125. error: 1.4 ppm.

*6-(2--6-Methoxyphenyl)-4-oxo-4,5,6,7-tetrahydrobenzofuran-3-carboxylic Acid (**16**).* (35 mg; 0.095 mmol; 28%). **^{1}H NMR** (500 MHz, $CDCl_3$) δ 13.41 (s, 1H), 8.15 (s, 1H), 7.27 (dd, J = 8.1, 1.0 Hz, 1H), 7.18 (t, J = 8.2 Hz, 1H), 6.93 (dd, J = 8.3, 0.8 Hz, 1H), 4.37 (m, 1H), 3.90 (s, 3H), 3.79−3.51 (m, 2H), 3.03 (dd, J = 17.6, 5.4 Hz, 1H), 2.71 (dd, J = 17.5, 4.2 Hz, 1H). **^{13}C NMR** (126 MHz, $CDCl_3$) δ 199.2, 170.7, 161.6, 159.0, 150.4, 129.7, 127.5, 125.9, 125.5, 118.1, 116.9, 110.8, 55.6, 39.5 × 2, 26.4. **HRMS** (ESI+): m/z [M + H]$^+$ calculated for $C_{16}H_{14}{}^{79}BrO_5$ 365.0019; found 365.0030. error: 3.1 ppm. **HPLC purity** > 99%.

*Ethyl 6-(2-bromo-6-methoxyphenyl)-4-oxo-4,5,6,7-tetrahydrobenzofuran-3-carboxylate (**16d**).* (44 mg, 0.11 mmol, 33%). **^{1}H NMR** (500 MHz, $CDCl_3$) δ 7.90 (s, 1H), 7.21 (dd, J = 8.1, 1.1 Hz, 1H), 7.10 (t, J = 8.2 Hz, 1H), 6.87 (dd, J = 8.3, 1.1 Hz, 1H), 4.36 (q, J = 7.1 Hz, 2H), 4.25 (m, 1H), 3.84 (s, 3H), 3.63 (t, J = 14.8 Hz, 1H), 3.42 (t, J = 14.8 Hz, 1H), 2.91 (dd, J = 17.1 Hz, 5.3 Hz, 1H), 2.54 (dd, J = 16.6 Hz, 4.1 Hz, 1H), 1.38 (t, J = 7.1 Hz, 3H). **^{13}C NMR** (126 MHz, $CDCl_3$) δ 192.0, 168.6, 162.2, 159.3, 148.0, 129.3, 128.7, 125.9, 125.7, 118.4, 117.2, 110.9, 61.1, 55.7, 41.7, 39.7, 26.6, 14.4. **HRMS** (ESI+): m/z [M + H]$^+$ neutral calculated $C_{18}H_{17}{}^{79}BrO_5$ 392.02594; neutral found 392.0254. error: −1.4 ppm. **HPLC purity** 95%.

*(E)-4-(2-Chloro-6-fluorophenyl)but-3-en-2-one (**17b**).* (3.25 g; 16.4 mmol; 85%). **^{1}H NMR** (500 MHz, $CDCl_3$) δ 7.75 (d, J = 16.6 Hz, 1H), 7.32−7.22 (m, 2H), 7.13−7.03 (m, 1H), 6.99 (d, J = 16.6 Hz, 1H), 2.43 (s, 3H). **^{13}C NMR** (126 MHz, $CDCl_3$) δ 198.5 (s), 162.0 (d, J = 255 Hz), 136.2 (d, J = 5.1 Hz), 133.4 (d, J = 13.5 Hz), 133.3 (d, J = 2.05 Hz), 130.9 (d, J = 10.4 Hz), 126.01 (d, J = 3.5 Hz), 121.72 (d, J = 13.9 Hz), 115.0 (d, J = 23.5 Hz), 27.9 (s). **^{19}F NMR** (470 MHz, $CDCl_3$) δ −107.6.

*5-(2-Chloro-6-fluorophenyl)cyclohexane-1,3-dione (**17c**).* (685 mg; 2.846 mmol; 17%). **^{1}H NMR** (500 MHz, CD_3OD) δ 7.36−7.26 (m, 2H), 7.18−7.08 (m, 1H), 4.05 (ttd, J = 13.0, 4.5, 1.1 Hz, 1H), 3.02 (dd, J = 17.0, 13.1 Hz, 2H), 2.44 (dd, J = 17.4, 4.6 Hz, 2H). **^{13}C NMR** (126 MHz, CD_3OD) δ 162.5 (d, J = 247 Hz), 134.2 5 (d, J = 7.6 Hz), 129.2 5 (d, J = 10.4 Hz), 127.1 (d, J = 15.1 Hz), 125.8 (d, J = 3.2 Hz), 115.1 (d, J = 23.8 Hz), 35.5 (s), 33.9 (s). **^{19}F NMR** (470 MHz, CD_3OD) δ −110.8. **HRMS** (ESI+): m/z [M + H]$^+$ calculated for $C_{12}H_{11}F^{35}ClO_2$ 241.0426; found 241.0429. error: 1.3 ppm.

*6-(2-Chloro-6-fluorophenyl)-4-oxo-4,5,6,7-tetrahydrobenzofuran-3-carboxylic Acid (**17**).* (102 mg; 0.33 mmol; 12%). **^{1}H NMR** (400 MHz, $CDCl_3$) δ 13.17 (s, 1H), 8.16 (s, 1H), 7.41−7.18 (m, 2H), 7.15−7.04 (m, 1H), 4.32 (ddd, J = 16.6, 12.3, 4.2 Hz, 1H), 3.56 (dd, J = 17.5, 12.0 Hz, 1H), 3.38 (dd, J = 17.2, 13.7 Hz, 1H), 3.17 (dd, J = 17.5, 5.2 Hz, 1H), 2.84 (dd, J = 17.4, 4.1 Hz, 1H). **^{13}C NMR** (101 MHz, $CDCl_3$) δ 197.7 (s), 169.64 (s), 161.2 × 2 (s), 150.6 (s), 134.6 (d, J = 7.1 Hz), 129.7 (d, J = 10.4 Hz), 126.32 (d, J = 3.1 Hz), 118.1 (s), 117.1 (s), 115.55 (d, J = 25 Hz), 40.3 (d, J = 4.4 Hz), 34.9 (s), 27.4 (d, J = 4.5 Hz). **^{19}F NMR** (376 MHz, $CDCl_3$) δ −108.0. **HRMS** (ESI+): m/z [M + H]$^+$ calculated for $C_{15}H_{11}{}^{35}ClFO_4$ 309.0324; found 309.0326. error: 0.5 ppm. **HPLC purity** 99%.

*6-(2-Chloro-6-fluorophenyl)-4-hydroxy-4,5,6,7-tetrahydrobenzofuran-3-carboxylic Acid (**17e**).* $NaBH_4$ (1.47 equiv) was added portion-wise to a stirred solution of 6-(2-chloro-6-fluorophenyl)-4-oxo-4,5,6,7-tetrahydrobenzofuran-3-carboxylic acid **17** (20 mg, 1 equiv) in EtOH (1 mL) at 0 °C. The reaction was warmed to rt and stirred for 3 h before cooling back to 0 °C. The cooled mixture was quenched with HCl (1 M, ≈ 5 drops), extracted with EtOAc (3 × 2 mL), dried over Na_2SO_4 and the organic layer concentrated in vacuo. The crude mixture was purified by reversed-phase column chromatography (H_2O/MeCN 9:1 − 1:1) to yield **17e** as a white powder (4.4 mg, 14 μmol, 40%). **^{1}H NMR** (500 MHz, $CDCl_3$) δ 8.02 (s, 1H), 7.24−7.18 (m, 2H), 7.01 (m, 1H), 5.09 (m, 1H), 3.77 (m, 1H), 3.14 (m, 1H), 2.78 (m, 1H), 2.41 (m, 1H), 2.33 (m, 1H). **^{13}C NMR** (126 MHz, $CDCl_3$) δ 167.4, 163.3, 161.3, 153.0, 149.0, 134.6, 128.6, 125.9, 120.6, 117.2, 115.3, 64.5, 35.2, 34.2, 27.1. **HPLC purity** 96%.

*(E)-4-(2,6-Dimethoxyphenyl)but-3-en-2-one (**18b**).* (2.88 g; 13.96 mmol; 66%). **^{1}H NMR** (500 MHz, $CDCl_3$) δ 8.00 (d, J = 16.6 Hz, 1H), 7.30 (t, J = 8.0 Hz, 1H), 7.19 (d, J = 16.6 Hz, 1H), 6.59 (d, J = 8.4 Hz, 2H), 3.91 (s, 6H), 2.40 (s, 3H). **^{13}C NMR** (126 MHz, $CDCl_3$) δ 200.6, 160.1, 134.8, 131.5, 130.4, 112.2, 103.7, 55.8, 27.0.

*5-(2,6-Dimethoxyphenyl)cyclohexane-1,3-dione (**18c**).* (538 mg; 2.16 mmol; 16%). **^{1}H NMR** (500 MHz, CD_3OD) δ 7.21 (t, J = 8.4 Hz, 1H), 6.66 (d, J = 8.4 Hz, 2H), 4.06 (tt, J = 13.0, 4.6 Hz, 1H), 3.84 (s, 6H), 3.22 (dd, J = 17.4, 13.0 Hz, 2H), 2.18 (dd, J = 17.5, 4.6 Hz, 2H). **^{13}C NMR** (126 MHz, CD_3OD) δ 158.6, 128.0, 117.3, 104.1, 54.7, 47.6, 29.3. **HRMS** (ESI+): m/z [M + H]$^+$ calculated for $C_{14}H_{17}O_4$ 249.1121; found 249.1120. error: −0.4 ppm.

*6-(2,6-Dimethoxyphenyl)-4-oxo-4,5,6,7-tetrahydrobenzofuran-3-carboxylic Acid (**18**).* (61 mg; 0.192 mmol; 10%). **^{1}H NMR** (500 MHz, $CDCl_3$) δ 13.52 (s, 1H), 8.11 (s, 1H), 7.31−7.24 (m, 1H), 6.61 (m, 2H), 4.43−4.30 (m, 1H), 3.85 (s, 6H), 3.74−3.64 (dd, J = 17.6, 11.7 Hz, 1H), 3.60−3.52 (dd, J = 17.6, 13.1 Hz, 1H), 2.94 (dd, J = 17.6, 5.2 Hz, 1H), 2.63 (dd, J = 17.5, 4.1 Hz, 1H). **^{13}C NMR** (126 MHz, $CDCl_3$) δ 200.3, 171.7, 161.7, 150.1, 128.8, 118.1, 116.8, 116.3, 104.2, 55.6, 40.4, 30.8, 27.1. **HRMS** (ESI+): m/z [M + H]$^+$ calculated for $C_{17}H_{17}O_6$ 317.1020; found 317.1026. error: 1.9 ppm. **HPLC purity** 95%.

*(E)-4-(2-Bromo-6-chlorophenyl)but-3-en-2-one (**19b**).* (1.38 g, 5.3 mmol, 83%). **^{1}H NMR** (500 MHz, $CDCl_3$) δ 7.58 (dd, J = 8.0, 1.0 Hz, 1H), 7.56 (d, J = 16.6 Hz, 1H), 7.43 (dd, J = 8.0, 1.0 Hz, 1H), 7.15 (t, J = 8.0 Hz, 1H), 6.74 (d, J = 16.6 Hz, 1H), 2.45 (s, 3H). **^{13}C NMR** (126 MHz, $CDCl_3$): δ 198.0, 139.1, 135.1, 124.4, 133.9, 131.9, 130.3, 129.5, 124.6, 27.6. **HRMS** (ESI+): m/z [M + H]$^+$ calculated for $C_{10}H_8{}^{79}Br^{35}ClO$: 258.95199, found: 258.9528, mass error: 3.1 ppm.

*5-(2-Bromo-6-chlorophenyl)cyclohexane-1,3-dione (**19c**).* (497 mg, 16.5 mmol, 31%). **^{1}H NMR** (500 MHz, CD_3OD) δ 7.45−7.66 (d, 2H), 7.19 (t, J = 8.0 Hz, 1H), 4.41 (m, 1H), 3.45 (dd, J = 17.0, 13.5 Hz, 2H), 2.34 (dd, J = 17.0, 4.5 Hz, 2H). **^{13}C NMR** (126 MHz, CD_3OD) δ 132.4, 131.2, 129.5, 39.6. **HRMS** (ESI+): m/z [M + H]$^+$ calculated for $C_{12}H_{10}{}^{79}Br^{35}ClO_2$: 300.96255, found: 300.9630, mass error: 1.4 ppm.

*6-(2-Bromo-6-chlorophenyl)-4-oxo-4,5,6,7-tetrahydrobenzofuran-3-carboxylic Acid (**19**).* (81 mg, 220 μmol, 14%). **^{1}H NMR** (500 MHz, $CDCl_3$) δ 13.2 (s, 1H), 8.15 (s, 1H), 7.61 (dd, J = 8.0, 1.3 Hz, 1H), 7.40 (dd, J = 8.1, 1.3 Hz, 1H), 7.15 (t, J = 8.1 Hz, 1H), 4.63 (m, 1H), 4.12−3.76 (m, 2H), 3.07 (dd, J = 17.8, 5.7 Hz, 1H), 2.74 (dd, J

https://doi.org/10.1021/acs.jmedchem.5c03818
J. Med. Chem. 2026, 69, 12099−12121

= 17.8, 4.6 Hz, 1H). **^{13}C NMR** (126 MHz, $CDCl_3$) δ 197.9, 169.5, 161.2, 150.8, 135.8, 134.7, 132.7, 131.4, 129.9, 126.6, 118.2, 117.1, 40.3, 38.6, 25.7. **HRMS** (ESI+): m/z $[M + H]^+$ calculated for $C_{15}H_{10}{}^{79}Br^{35}ClO_4$: 368.95238, found: 368.9532, mass error: 2.3 ppm. **HPLC purity** 98%.

*2-Bromo-6-butoxybenzaldehyde (**20a**).* (1.5 g; 5.81 mmol; 78%). **^{1}H NMR** (500 MHz, $CDCl_3$) δ 10.46 (s, 1H), 7.31 (t, J = 8.0 Hz, 1H), 7.24 (dd, J = 8.0, 0.5 Hz, 1H), 6.96 (dd, J = 8.3, 0.7 Hz, 1H), 4.08 (t, J = 6.4 Hz, 2H), 1.89−1.79 (m, 2H), 1.58−1.48 (m, 2H), 1.00 (t, J = 7.4 Hz, 3H). **^{13}C NMR** (126 MHz, $CDCl_3$) δ 190.1, 161.9, 134.6, 126.4, 123.74, 123.66, 111.8, 68.9, 31.0, 19.2, 13.8. **HRMS** (ESI+): m/z $[M + H]^+$ calculated for $C_{11}H_{14}{}^{79}BrO_2$ 257.0172; found 257.0168. error: −1.5 ppm.

*(E)-4-(2-Bromo-6-butoxyphenyl)but-3-en-2-one (**20b**).* (1.14 g; 3.854 mmol; 66%). **^{1}H NMR** (500 MHz, $CDCl_3$) δ 7.83 (d, J = 16.4 Hz, 1H), 7.28 (dd, J = 8.0, 1.0 Hz), 7.15 (t, J = 8.2 Hz), 7.12 (d, J = 16.4 Hz), 6.90 (d, J = 8.3 Hz, 1H), 4.07 (t, J = 6.5 Hz, 2H), 2.41 (s, 3H), 1.86 (tt, J = 12.9, 6.5 Hz, 2H), 1.59−1.49 (m, 2H), 1.01 (t, J = 7.4 Hz, 3H). **^{13}C NMR** (126 MHz, $CDCl_3$) δ 199.5, 159.3, 139.1, 132.9, 130.9, 127.2, 125.4, 123.1, 111.1, 68.7, 31.0, 27.2, 19.3, 13.7.

*5-(2-Bromo-6-butoxyphenyl)cyclohexane-1,3-dione (**20c**).* (618 mg; 1.82 mmol; 47%). **^{1}H NMR** (500 MHz, CD_3OD) δ 7.21 (dd, J = 8.0, 1.0 Hz, 1H), 7.14 (dd, J = 9.5, 6.8 Hz, 1H), 7.03 (d, J = 8.2 Hz, 1H), 4.09 (t, J = 6.4 Hz, 2H), 3.35−3.30 (m, 1H) 3.28 (dd, J = 17.4, 4.8 Hz, 2H), 1.86−1.78 (m, 2H),), 1.60−1.50 (m, 2H), 1.53 (dd, J = 15.1, 7.5 Hz, 2H), 1.00 (t, J = 7.4 Hz, 3H). **^{13}C NMR** (126 MHz, CD_3OD) δ 158.7, 129.0, 128.4, 125.1, 111.4, 31.0, 19.2, 12.7. Some carbon signals are missing. **HRMS** (ESI+): m/z $[M + H]^+$ calculated for $C_{16}H_{19}{}^{79}BrO_3$ 339.0590; found 339.0592. error: 0.6 ppm.

*6-(2-Bromo-6-butoxyphenyl)-4-oxo-4,5,6,7-tetrahydrobenzofuran-3-carboxylic Acid (**20**).* (26 mg; 63.63 μmol; 4%). **^{1}H NMR** (500 MHz, $CDCl_3$) δ 13.35 (s, 1H), 8.15 (s, 1H), 7.25 (dd, J = 8.1, 1.0 Hz, 1H), 7.15 (t, J = 8.2 Hz, 1H), 6.92 (d, J = 7.8 Hz, 1H), 4.37 (m, 1H), 4.07 (t, J = 6.7 Hz, 2H), 3.81−3.55 (m, 2H), 3.02 (dd, J = 17.6, 5.3 Hz, 1H), 2.71 (dd, J = 17.5, 4.1 Hz, 1H), 1.86−1.76 (m, 2H), 1.51−1.39 (m, 2H), 0.97 (t, J = 7.4 Hz, 3H). **^{13}C NMR** (126 MHz, $CDCl_3$) δ 199.2, 170.7, 161.4, 150.4, 129.6, 127.2, 125.6, 118.1, 116.8, 111.3, 68.3, 40.0, 39.7, 31.1, 26.4, 19.3, 13.7. **HRMS** (ESI+): m/z $[M + H]^+$ calculated for $C_{19}H_{19}{}^{79}BrO_5$ 407.0489; found 407.0488. error: −0.1 ppm. **HPLC purity** 96%.

*2-Methoxy-6-(2-methoxyethoxy)benzaldehyde (**21a**).* (1.36 g; 6.48 mmol; 87%). **^{1}H NMR** (500 MHz, $CDCl_3$) δ 10.51 (s, 1H), 7.34 (d, J = 3.3 Hz, 1H), 7.14 (dd, J = 9.0, 3.3 Hz, 1H), 6.98 (d, J = 9.1 Hz, 1H), 4.25−4.19 (m, 2H), 3.82 (s, 3H), 3.81−3.78 (m, 2H), 3.47 (s, 3H). **^{13}C NMR** (126 MHz, $CDCl_3$) δ 189.6, 156.0, 153.9, 125.5, 123.5, 115.0, 110.1, 70.9, 69.1, 59.3, 55.7. **HRMS** (ESI+): m/z $[M + Na]^+$ calculated for $C_{11}H_{14}NaO_4$ 233.0784; found 233.0788. error: 1.7 ppm.

*(E)-4-(2-Methoxy-6-(2-methoxyethoxy)phenyl)but-3-en-2-one (**21b**).* (1.11 g; 5.27 mmol; 81%). **^{1}H NMR** (500 MHz, $CDCl_3$) δ 7.92 (d, J = 16.5 Hz, 1H), 7.08 (d, J = 2.5 Hz, 1H), 6.95−6.89 (m, 2H), 6.75 (d, J = 16.5 Hz, 1H), 4.18−4.13 (m, 2H), 3.81 (s, 3H), 3.80−3.77 (m, 2H), 3.48 (s, 3H), 2.40 (s, 3H). **^{13}C NMR** (126 MHz, $CDCl_3$) δ 199.0, 154.0, 152.0, 138.6, 128.0, 125.0, 117.6, 114.9, 112.3, 71.1, 69.3, 59.2, 55.7, 27.0. **HRMS** (ESI+): m/z $[M + Na]^+$ calculated for $C_{11}H_{14}NaO_4$ 233.0784; found 233.0788. error: 1.7 ppm.

*5-(2-Methoxy-6-(2-methoxyethoxy)phenyl)cyclohexane-1,3-dione (**21c**).* (221 mg; 0.756 mmol; 14%). **^{1}H NMR** (500 MHz, CD_3OD) δ 6.91 (d, J = 8.9 Hz, 1H), 6.82 (d, J = 3.0 Hz, 1H), 6.77 (dd, J = 8.8, 3.0 Hz, 1H), 4.12−4.07 (m, 2H), 3.75 (s, 3H), 3.74−3.72 (m, 2H), 3.72−3.65 (m, 1H), 3.41 (s, 3H), 2.75 (dd, J = 17.1, 11.8 Hz, 2H), 2.53 (dd, J = 17.2, 4.5 Hz, 2H). **^{13}C NMR** (126 MHz, CD_3OD) δ 154.1, 150.5, 132.2, 113.6, 113.2, 111.6, 71.0, 68.1, 57.8, 54.7, 37.5, 34.1. **HRMS** (ESI+): m/z $[M + H]^+$ calculated for $C_{16}H_{21}O_5$: 293.1384; found 293.1388. error: 1.4 ppm.

*6-(2-Methoxy-6-(2-methoxyethoxy)phenyl)-4-oxo-4,5,6,7-tetrahydrobenzofuran-3-carboxylic Acid (**21**).* (60 mg; 0.16 mmol; 22%). **^{1}H NMR** (500 MHz, $CDCl_3$) δ 13.29 (s, 1H), 8.18 (s, 1H), 6.89 (d, J = 8.9 Hz, 1H), 6.81 (dd, J = 8.9, 3.1 Hz, 1H), 6.75 (d, J = 3.1 Hz, 1H), 4.14 (t, J = 4.7 Hz, 2H), 3.98−3.90 (m, 1H), 3.79 (s, 3H), 3.75−3. 71 (m, 2H), 3.40 (s, 3H), 3.32 (dd, J = 17.5, 10.3 Hz, 1H), 3.26 (dd, J = 17.5, 5.7 Hz, 1H), 3.14 (dd, J = 17.5, 12.6 Hz, 1H), 2.91 (dd, J = 17.5, 4.0 Hz, 1H). **^{13}C NMR** (126 MHz, $CDCl_3$) δ 198.9, 170.7, 161.5, 153.9, 150.5, 150.4, 130.4, 118.1, 116.8, 114.4, 113.4, 112.3, 71.0, 68.2, 59.1, 55.7, 40.0, 41.9, 36.7, 28.9. **HRMS** (ESI+): m/z $[M + H]^+$ calculated for $C_{19}H_{20}O_7$ 361.1282; found 361.1284. error: 0.7 ppm. **HPLC purity** 94%.

*(E)-4-(2,3-Dichlorophenyl)but-3-en-2-one (**22b**).* (3.44 g; 16 mmol; 83%). **^{1}H NMR** (500 MHz, $CDCl_3$) δ 7.94 (d, J = 16.3 Hz, 1H), 7.55 (dd, J = 7.9, 1.5 Hz, 1H), 7.52 (dd, J = 7.9, 1.5 Hz, 1H), 7.26 (t, J = 7.9 Hz, 1H), 6.66 (d, J = 16.3 Hz, 1H), 2.45 (s, 3H). **^{13}C NMR** (126 MHz, $CDCl_3$) δ 198.1, 139.1, 135.1, 134.1, 133.1, 131.7, 130.7, 127.6, 125.8, 27.4.

*5-(2,3-Dichlorophenyl)cyclohexane-1,3-dione (**22c**).* (194 mg; 0.754 mmol; 5%). **^{1}H NMR** (500 MHz, d_6-DMSO) δ 7.56 (dd, J = 8.0, 1.5 Hz, 1H), 7.50 (dd, J = 7.9, 1.4 Hz, 1H), 7.39 (t, J = 7.9 Hz, 1H), 5.32 (s, 1H), 3.80−3.70 (m, 1H), 2.70−2.54 (m, 2H), 2.44 (dd, J = 16.5, 3.7 Hz, 2H). Open ring impurities present (20%). **^{13}C NMR** (126 MHz, d_6-DMSO) δ 143.3, 132.5, 131.1, 129.4, 128.9, 127.0, 104.9, 36.9. **HRMS** (ESI+): m/z $[M + H]^+$ calculated for $C_{12}H_{10}{}^{35}Cl_2O_2$ 257.0131; found 257.0137. error: 2.7 ppm.

*6-(2,3-Dichlorophenyl)-4-oxo-4,5,6,7-tetrahydrobenzofuran-3-carboxylic Acid (**22**).* (80 mg; 0.246 mmol; 32%). **^{1}H NMR** (500 MHz, $CDCl_3$) δ 13.05 (s, 1H), 8.16 (s, 1H), 7.49 (dd, J = 8.1, 2.9 Hz, 1H), 7.29 (t, 1H), 7.25 (dd, J = 7.8, 1.6 Hz, 1H), 4.33−4.13 (m, 1H), 3.39 (dd, J = 17.5, 5.1 Hz, 1H), 3.23−3.06 (dd, J_1 = 17.5 Hz, J_2 = 6.9 Hz, 1H), 3.00 (d, J = 8.4 Hz, 2H). **^{13}C NMR** (126 MHz, $CDCl_3$) δ 197.2, 169.1, 161.1, 150.8, 140.2, 134.3, 132.0, 129.9, 127.9, 125.1, 118.1, 117.2, 42.1, 38.3, 29.4. **HRMS** (ESI+): m/z $[M + H]^+$ calculated for $C_{15}H_{11}{}^{35}Cl_2O_4$ 325.0029; found 325.0038. error: 2.9 ppm. **HPLC purity** > 99%.

*(E)-4-(2,3,6-Trichlorophenyl)but-3-en-2-one (**23b**).* (3.00 g, 12.0 mmol, 91%). **^{1}H NMR** (500 MHz, $CDCl_3$) δ 7.56 (d, J = 16.6 Hz, 1H), 7.41 (d, J = 8.7 Hz, 1H,), 7.34 (d, J = 8.7 Hz, 1H), 6.75 (d, J = 16.6 Hz, 1H), 2.45 (s, 3H). **^{13}C NMR** (126 MHz, $CDCl_3$) δ 197.8, 136.8, 135.6, 134.2, 133.2, 132.7, 132.6, 130.3, 129.0, 27.8.

*5-(2,3,6-Trichlorophenyl)cyclohexane-1,3-dione (**23c**).* (419 mg, 1.4 mmol, 12%). **^{1}H NMR** (500 MHz, CD_3OD) δ 7.41−7.53 (d, 2H), 4.49 (m, 1H), 3.45 (dd, J = 17.2, 13.5 Hz, 2H), 2.35 (dd, J = 17.2, 4.3 Hz, 2H).**^{13}C NMR** (126 MHz, CD_3OD) δ 137.9, 130.7, 129.7, 36.8, 33.4. **HRMS** (ESI+): m/z $[M + H]^+$ calculated for $C_{12}H_9{}^{35}Cl_3O_2$: **290.97409**, found: **290.9743**, mass error: 0.6 ppm.

*4-Oxo-6-(2,3,6-trichlorophenyl)-4,5,6,7-tetrahydrobenzofuran-3-carboxylic Acid (**23**).* (91 mg, 250 μmol, 13%). **^{1}H NMR** (500 MHz, $CDCl_3$) δ 13.2 (s, 1H), 8.15 (s, 1H), 7.44 (d, J = 8.7 Hz, 1H), 7.31 (d, J = 8.1 Hz, 1H), 4.74 (m, 1H), 3.95 (dd, J = 17.8, 12.2 Hz, 1H), 3.80 (dd, J = 17.8, 13.7 Hz, 1H), 3.06 (dd, J = 17.8, 6.0 Hz, 1H), 2.72 (dd, J = 17.6, 4.6 Hz, 1H). **^{13}C NMR** (126 MHz, $CDCl_3$) δ 197.6, 169.2, 161.1, 150.9, 136.4, 134.4, 133.3, 133.1, 130.6, 130.4, 118.2, 117.1, 38.4, 37.6, 25.5. **HRMS** (ESI+): m/z $[M + H]^+$ calculated for $C_{15}H_9{}^{35}Cl_3O_4$: 358.96392, found: 358.9568, mass error: 0.5 ppm. **HPLC purity** 95%.

*(E)-4-(4-Chlorophenyl)but-3-en-2-one (**24b**).* (3.4 g, 19 mmol, 88%). **^{1}H NMR** (400 MHz, $CDCl_3$) δ 7.50−7.41 (m, 3H), 7.37 (d, J = 8.6 Hz, 2H), 6.68 (d, J = 16.3 Hz, 1H), 2.40 (s, 3H). **^{13}C NMR** (101 MHz, $CDCl_3$) δ 198.2, 142.0, 136.6, 133.1, 129.4, 129.4, 127.6, 27.8.

*5-(4-Chlorophenyl)cyclohexane-1,3-dione (**24c**).* (662 mg, 2.9 mmol, 36%) **^{1}H NMR** (500 MHz, d_6-DMSO) δ 7.37 (s, 4H), 5.28 (s, 1H), 3.42−3.28 (accounting for overlap with D_2O peak, m, 1H), 2.57 (dd, J = 16.3, 11.9 Hz, 2H), 2.38 (dd, J = 16.3, 2.5 Hz, 2H). **^{13}C NMR** (126 MHz, d_6-DMSO) δ 142.6, 131.1, 128.9, 128.4, 103.6, 38.1. **HRMS** (ESI+): m/z $[M + H]^+$ calculated for $C_{12}H_{11}{}^{35}ClO_2$: 222.04476, found: 222.0450, mass error: 0.9 ppm.

*6-(4-Chlorophenyl)-4-oxo-4,5,6,7-tetrahydrobenzofuran-3-carboxylic Acid (**24**).* (80 mg, 0.27 mmol, 38%). **^{1}H NMR** (500 MHz, $CDCl_3$) δ 13.04 (s, 1H), 8.12 (s, 1H), 7.39−7.35 (m, 2H), 7.25−7.21 (m, 2H), 3.66 (m, 1H), 3.33−3.24 (dd, J = 17.6, 5.0 Hz, 1H), 3.14 (dd, J = 17.6, 11.0 Hz, 1H), 2.99−2.86 (m, 2H). **^{13}C NMR** (126 MHz, $CDCl_3$) δ 197.6, 169.5, 161.2, 150.9, 139.4, 133.9, 129.5, 128.2,

https://doi.org/10.1021/acs.jmedchem.5c03818
J. Med. Chem. 2026, 69, 12099−12121

118.1, 117.4, 43.8, 40.8, 31.1. **HRMS** (ESI+): m/z $[M + H]^+$ neutral calculated for $C_{15}H_{11}{}^{35}ClO_4$ 290.03459; neutral found 290.0341. error: −1.7 ppm. **HPLC purity** > 99%.

*Ethyl 6-(4-Chlorophenyl)-4-oxo-4,5,6,7-tetrahydrobenzofuran-3-carboxylate (**24d**).* (78 mg, 0.24 mmol, 42%). **^{1}H NMR** (700 MHz, $CDCl_3$) δ 7.92 (s, 1H), 7.33 (d, J = 8.4 Hz, 2H), 7.21 (d, J = 8.4 Hz, 2H), 4.35 (q, J = 7.1 Hz, 2H), 3.55 (m, 1H), 3.20 (dd, J = 17.0, 5.2 Hz, 1H), 3.04 (dd, J = 17.0, 11.0 Hz, 1H), 2.84−2.74 (m, 2H), 1.37 (t, J = 7.1 Hz, 3H). **^{13}C NMR** (176 MHz, $CDCl_3$) δ 190.3 (**C**=O), 167.3, 161.9, 148.5, 140.5, 133.3, 129.2, 128.2, 118.9, 117.7, 61.2, 45.9, 40.2, 31.4, 14.3. **HRMS** (ESI+): m/z $[M + H]^+$ neutral calculated for $C_{17}H_{15}{}^{35}ClO_4$ 318.06589; found 318.0643. error: −1.6 ppm. **HPLC purity** 99%.

*(E)-4-(2-Chloro-3-methoxyphenyl)but-3-en-2-one (**25b**).* (3.08 g, 14.6 mmol, 83%). **^{1}H NMR** (500 MHz, $CDCl_3$) δ 7.99 (d, J = 16.2 Hz, 1H), 7.27 (m, 2H), 6.99 (m, 1H), 6.67 (d, J = 16.2 Hz, 1H), 3.95 (s, 3H), 2.44 (s, 3H). **^{13}C NMR** (126 MHz, $CDCl_3$) δ 198.5, 155.6, 139.6, 134.1, 130.1, 127.4, 123.6, 119.3, 113.1, 56.4, 27.2. **HRMS** (ESI+): m/z $[M + H]^+$ calculated for $C_{11}H_{11}{}^{35}ClO_2$: 211.05204, found: 211.0519, mass error: −0.4 ppm.

*5-(2-Chloro-3-methoxyphenyl)cyclohexane-1,3-dione (**25c**).* (450 mg, 1.8 mmol, 14%). **^{1}H NMR** (500 MHz, CD_3OD) δ 7.30 (t, J = 8.0 Hz, 1H), 7.04 (dd, J = 8.0, 1.1 Hz, 1H), 7.01 (dd, J = 8.0, 1.1 Hz, 1H), 3.90 (m, 1H), 3.90 (s, 3H), 2.68 (dd, J = 17.1, 11.4 Hz, 2H), 2.58 (dd, J = 17.1, 4.6 Hz, 2H). **^{13}C NMR** (126 MHz, CD_3OD) δ 155.5, 141.2, 127.4, 121.5, 118.6, 110.5, 55.3, 37.8, 35.9. **HRMS** (ESI+): m/z $[M + H]^+$ calculated for $C_{13}H_{13}{}^{35}ClO_3$: 253.06260, found: 253.0626, mass error: −0.1 ppm.

*6-(2-chloro-3-methoxyphenyl)-4-oxo-4,5,6,7-tetrahydrobenzofuran-3-carboxylic Acid (**25**).* (233 mg, 73 μmol, 46%). **^{1}H NMR** (500 MHz, $CDCl_3$) δ 13.12 (s, 1H), 8.14 (s, 1H), 7.28 (t, J = 8.0 Hz, 1H), 6.94 (2d, 2H), 4.24 (m, 1H), 3.95 (s, 3H), 3.36 (dd, J = 17.6, 5.1 Hz, 1H), 3.16 (dd, J = 17.6, 10.7 Hz, 1H), 2.99 (m, 2H). **^{13}C NMR** (126 MHz, $CDCl_3$) δ 197.8, 169.6, 161.2, 155.7, 150.7, 139.5, 127.9, 122.0, 118.6, 118.0, 117.2, 111.2, 56.4, 42.2, 37.6, 29.4. **HRMS** (ESI+): m/z $[M + H]^+$ calculated for $C_{16}H_{13}{}^{35}ClO_5$: 321.05243, found: 321.0529, mass error: 1.4 ppm. **HPLC purity** 98%.

*(E)-4-(2,5-Dimethoxyphenyl)but-3-en-2-one (**26b**).* (1.00 g, 4.8 mmol, 81%). **^{1}H NMR** (500 MHz, $CDCl_3$) δ 7.88 (d, J = 16.6 Hz, 1H), 7.09 (d, J = 3.0 Hz, 1H), 6.95 (dd, J = 9.0, 3.0 Hz, 1H), 6.88 (d, J = 9.0 Hz, 1H), 6.73 (d, J = 16.6 Hz, 1H), 3.88 (s, 3H), 3.81 (s, 3H), 2.41 (s, 3H). **^{13}C NMR** (126 MHz, $CDCl_3$) δ 199.1, 153.6, 152.8, 138.5, 127.9, 123.9, 117.6, 112.6, 112.4, 56.1, 55.8, 27.1.

*5-(2,5-Dimethoxyphenyl)cyclohexane-1,3-dione (**26c**).* (510 mg, 2.1 mmol, 56%). **^{1}H NMR** (500 MHz, CD_3OD) δ 6.92 (d, J = 8.8 Hz, 1H), 6.82 (m, 1H), 6.80 (m, 1H), 3.82 (s, 3H), 3.76 (s, 3H), 3.67 (m, 1H), 2.71 (dd, J = 17.1, 11.6 Hz, 2H), 2.51 (dd, J = 17.1, 4.5 Hz, 2H). **^{13}C NMR** (126 MHz, CD_3OD) δ 153.8, 151.3, 131.6, 113.5, 111.4, 111.4, 54.9, 54.7, 33.8. **HRMS** (ESI+): m/z $[M + H]^+$ calculated for $C_{14}H_{16}O_4$: 249.11214, found: 249.1120, mass error: −0.4 ppm.

*6-(2,5-Dimethoxyphenyl)-4-oxo-4,5,6,7-tetrahydrobenzofuran-3-carboxylic Acid (**26**).* (12 mg, 37 μmol, 2%). **^{1}H NMR** (500 MHz, d_6-DMSO) δ 8.62 (s, 1H), 6.96 (d, J = 8.9 Hz, 1H), 6.90 (d, J = 3.0 Hz, 1H), 6.83 (dd, J = 8.9, 3.0 Hz, 1H), 3.88 (m, 1H), 3.76 (s, 1H), 3.70 (s, 1H), 3.26 (dd, J = 17.1, 10.8 Hz, 1H), 3.15 (dd, J = 17.1, 5.0 Hz, 1H), 3.05 (dd, J = 16.6, 12.4 Hz, 1H), 2.62 (dd, J = 16.6, 3.8 Hz, 1H). **^{13}C NMR** (126 MHz, d_6-DMSO) δ 196.4, 170.4, 162.0, 153.6, 151.1, 150.5, 131.1, 117.6, 117.2, 114.4, 112.6, 112.4, 56.4, 55.8, 43.1, 34.9, 28.9. **HRMS** (ESI+): m/z $[M + H]^+$ calculated for $C_{17}H_{16}O_6$: 317.10197, found: 317.1024, mass error: 1.3 ppm. **HPLC purity** 94%.

*(E)-4-(4-Chloro-2-methoxyphenyl)but-3-en-2-one (**27b**).* (1.04 g, 4.9 mmol, 74%). **^{1}H NMR** (500 MHz, $CDCl_3$) δ 7.81 (d, J = 16.5 Hz, 1H), 7.49 (d, J = 8.3 Hz, 1H), 6.99 (dd, J = 8.3, 2.0 Hz, 1H), 6.93 (d, J = 2.0 Hz, 1H), 6.75 (d, J = 16.5 Hz, 1H), 3.92 (s, 3H), 2.40 (s, 3H). **^{13}C NMR** (126 MHz, $CDCl_3$) δ 198.8, 158.7, 137.5, 137.3, 129.2, 127.9, 122.1, 121.1, 112.0, 55.9, 27.3.

*5-(4-Chloro-2-methoxyphenyl)cyclohexane-1,3-dione (**27c**).* (255 mg, 1.0 mmol, 21%). **^{1}H NMR** (500 MHz, d_6-DMSO) δ 7.25 (d, J = 8.2 Hz, 1H), 7.05 (d, J = 2.1 Hz, 1H), 6.98 (dd, J = 8.2, 2.1 Hz, 1H), 5.28 (s, 1H), 3.82 (s, 3H), 2.55 (m, 2H), 2.35 (m, 2H). **^{13}C NMR** (126 MHz, d_6-DMSO) δ 158.0, 132.5, 130.4, 128.7, 120.7, 111.9, 103.8, 56.4, 32.8. **HRMS** (ESI+): m/z $[M + H]^+$ calculated for $C_{13}H_{13}{}^{35}ClO_3$: 253.06260, found: 253.0630, mass error: 1.7 ppm.

*6-(4-Chloro-2-methoxyphenyl)-4-oxo-4,5,6,7-tetrahydrobenzofuran-3-carboxylic Acid (**27**).* (17 mg, 50 μmol, 6%). **^{1}H NMR** (500 MHz, $CDCl_3$) δ 13.20 (s, 1H), 8.13 (s, 1H), 7.12 (d, J = 8.2 Hz, 1H), 6.98 (dd, J = 8.2, 2.0 Hz, 1H), 6.94 (d, J = 2.0 Hz, 1H), 3.93 (m, 1H), 3.89 (s, 3H), 3.24 (m, 2H), 3.07 (dd, J = 17.1, 12.6 Hz, 1H), 2.88 (dd, J = 17.1, 4.0 Hz, 1H). **^{13}C NMR** (126 MHz, $CDCl_3$) δ 198.5, 170.2, 161.3, 157.6, 150.5, 134.4, 128.2, 127.3, 121.0, 118.0, 117.1, 55.7, 41.9, 35.9, 28.9. **HRMS** (ESI+): m/z $[M + H]^+$ calculated for $C_{16}H_{13}{}^{35}ClO_5$: 321.05243, found: 321.0527, mass error: 0.8 ppm. **HPLC purity** 93%.

*(E)-4-(4-Chloro-3-methoxyphenyl)but-3-en-2-one (**28b**).* (2.5 g, 12 mmol, 51%). **^{1}H NMR** (500 MHz, $CDCl_3$) δ 7.44 (d, J = 16.2 Hz, 1H), 7.37 (d, J = 8.0 Hz, 1H), 7.11−7.04 (m, 2H), 6.68 (d, J = 16.2 Hz, 1H), 3.93 (s, 3H), 2.38 (s, 3H). **^{13}C NMR** (126 MHz, $CDCl_3$) δ 198.47, 155.70, 142.69, 134.69, 131.03, 127.94, 125.39, 121.92, 111.23, 56.53, 27.98. **HRMS (ESI):** m/z $[M + H]^+$ calculated for $C_{11}H_{11}{}^{35}ClO_2$: 210.04476, found: 210.0447, mass error: −0.4 ppm.

*5-(4-Chloro-3-methoxyphenyl)cyclohexane-1,3-dione (**28c**).* (202 mg, 0.80 mmol, 17%). **^{1}H NMR** (500 MHz, CD_3OD) δ 7.30 (d, J = 8.1 Hz, 1H), 7.03 (d, J = 2.0 Hz, 1H), 6.88 (dd, J = 8.2, 2.0 Hz, 1H), 3.88 (s, 3H), 3.38 (s, 1H), 2.74−2.64 (m, 2H), 2.60−2.52 (m, 2H). **^{13}C NMR** (126 MHz, CD_3OD) δ 156.56, 144.93, 131.14, 121.87, 120.60, 112.38, 56.60, 40.78. **HRMS (ESI+):** m/z $[M + H]^+$ calculated for $C_{13}H_{14}O_3{}^{35}Cl$ 253.0631, found: 253.0631, mass error: 0.0 ppm.

*6-(4-Chloro-3-methoxyphenyl)-4-oxo-4,5,6,7-tetrahydrobenzofuran-3-carboxylic Acid (**28**).* (72 mg, 0.22 mmol, 36%). **^{1}H NMR** (500 MHz, d_6-DMSO): δ 8.45 (s, 1H), 7.38 (d, J = 8.1 Hz, 1H), 7.22 (d, J = 1.9 Hz, 1H), 6.97 (dd, J = 8.2, 2.0 Hz, 1H), 3.86 (s, 3H), 3.67 (m, 1H), 3.28−3.22 (m, 2H), 3.06 (dd, J = 16.5, 12.7 Hz, 1H), 2.69 (dd, J = 16.5, 3.9 Hz, 1H). **^{13}C NMR** (126 MHz, d_6-DMSO): δ 195.27, 169.73, 161.66, 154.57, 150.16, 143.07, 129.83, 119.90, 119.62, 117.26, 117.00, 112.01, 56.14, 44.05, 30.08. **HRMS (ESI):** m/z $[M + H]^+$ calculated for $C_{16}H_{13}{}^{35}ClO_5$: 320.04515, found: 320.0447, mass error: −1.3 ppm. **HPLC purity**: 95%.

*5-(Thiophen-2-yl)cyclohexane-1,3-dione (**29c**).* (276 mg, 14.2 mmol, 21%). **^{1}H NMR** (500 MHz, CD_3OD) δ 7.27 (dd, J = 4.0, 2.5 Hz, 1H), 6.98−6.97 (m, 2H), 5.45 (s, 2H), 3.71 (m, 1H), 2.76 (dd, J = 16.8, 4.8 Hz, 2H), 2.67 (dd, J = 17.1, 10.4 Hz, 2H). **^{13}C NMR** (126 MHz, CD_3OD) δ 146.6, 126.4, 123.3, 123.1, 40.1, 39.3.

*4-oxo-6-(thiophen-2-yl)-4,5,6,7-tetrahydrobenzofuran-3-carboxylic Acid (**29**).* (42 mg, 161 mmol, 16%). **^{1}H NMR** (500 MHz, $CDCl_3$) δ 13.06 (s, 1H), 8.14 (s, 1H), 7.27 (dd, J = 5.0, 1.2 Hz, 1H), 7.02 (dd, J = 5.0, 3.5 Hz, 1H), 6.96 (dd, J = 3.5, 1.2 Hz, 1H), 4.01 (m, 1H), 3.47 (dd, J = 17.6, 5.2 Hz, 1H), 3.24 (dd, J = 17.6, 9.9 Hz, 1H), 3.13 (dd, J = 17.2, 4.1 Hz, 1H), 2.99 (dd, J = 17.2, 11.0 Hz, 1H). **^{13}C NMR** (126 MHz, $CDCl_3$) δ 197.1, 168.9, 161.1, 150.8, 144.4, 127.2, 124.4, 124.3, 118.0, 117.4, 44.6, 36.5, 31.9. **HRMS** (ESI+): m/z $[M + H]^+$ calculated for $C_{13}H_{10}O_4S$: 261.0215, found: 261.0221, mass error: 2.5 ppm. **HPLC purity:** 96%.

*(E)-4-(3-Bromothiophen-2-yl)but-3-en-2-one (**30b**).* (1.50 g, 6.5 mmol, 83%). **^{1}H NMR** (500 MHz, $CDCl_3$) δ 7.70 (d, J = 16.3 Hz, 1H), 7.39 (d, J = 5.3 Hz, 1H), 7.08 (d, J = 5.3 Hz, 1H), 6.58 (d, J = 16.3 Hz, 1H), 2.40 (s, 3H). **^{13}C NMR** (126 MHz, $CDCl_3$) δ 197.6, 134.4, 133.8, 131.6, 128.2, 127.5, 116.7, 27.6. **HRMS** (ESI+): m/z $[M + H]^+$ calculated for C_8H_7BrOS: 230.94738, found: 230.9476, mass error: 1.0 ppm.

*5-(3-Bromothiophen-2-yl)cyclohexane-1,3-dione (**30c**).* (135 mg, 0.5 mmol, 9%). **^{1}H NMR** (500 MHz, CD_3OD) δ 7.40 (d, J = 5.3 Hz, 1H), 7.01 (dd, J = 5.3, 1.0 Hz, 1H), 3.85 (m, 1H), 2.72 (dd, J = 16.9, 5.0 Hz, 2H), 2.62 (dd, J = 16.9, 10.7 Hz, 2H). **^{13}C NMR** (126 MHz, CD_3OD) δ 140.3, 129.8, 123.9, 108.2, 38.6, 34.5. **HRMS** (ESI+): m/z $[M + H]^+$ calculated for $C_{10}H_9{}^{79}BrO_2S$: 272.95794, found: 272.9579, mass error: 0.0 ppm.

*6-(3-Bromothiophen-2-yl)-4-oxo-4,5,6,7-tetrahydrobenzofuran-3-carboxylic Acid (**30**).* (34 mg, 99 μmol, 34%). **^{1}H NMR** (500 MHz, $CDCl_3$) δ 13.03 (s, 1H), 8.17 (s, 1H), 7.28 (d, J = 5.2 Hz, 1H), 7.03

https://doi.org/10.1021/acs.jmedchem.5c03818
J. Med. Chem. 2026, 69, 12099−12121

(d, J = 5.2 Hz, 1H), 4.14 (m, 1H), 3.45 (dd, J = 17.6, 5.1 Hz, 1H), 3.19 (dd, J = 17.6, 10.4 Hz, 1H), 3.09 (dd, J = 17.2, 4.2 Hz, 1H), 2.94 (dd, J = 17.2, 11.6 Hz, 1H). **^{13}C NMR** (126 MHz, $CDCl_3$) δ 195.6, 168.6, 161.0, 150.9, 138.1, 130.6, 124.3, 118.1, 117.2, 109.8, 43.3, 36.0, 30.5. **HRMS (ESI):** m/z $[M + H]^+$ calculated for $C_{13}H_9{}^{79}BrO_4S$: 339.94049, found: 339.9403, mass error: −0.6 ppm. **HPLC purity** > 99%.

*(E)-4-(5-Bromothiophen-2-yl)but-3-en-2-one (**31b**).* (3.25 g, 14.0 mmol, 67%). **^{1}H NMR** (500 MHz, $CDCl_3$) δ 7.52 (d, J = 15.9 Hz, 1H), 7.05 (s, 2H), 6.44 (d, J = 15.9 Hz, 1H), 2.35 (s, 3H). **^{13}C NMR** (126 MHz, $CDCl_3$) δ 197.4, 141.3, 134.7, 131.9, 131.3, 125.9, 116.5, 27.9. **HRMS** (ESI+): m/z $[M + H]^+$ calculated for $C_8H_7{}^{79}BrOS$: 230.94748, found: 230.9475, mass error: 0.4 ppm.

*5-(5-Bromothiophen-2-yl)cyclohexane-1,3-dione (**31c**).* (264 mg, 1.0 mmol, 14%). **^{1}H NMR** (500 MHz, CD_3OD) δ 6.96 (d, J = 3.8 Hz, 1H), 6.78 (dd, J = 3.8, 1.0 Hz, 1H), 3.66 (m, 1H), 2.74 (dd, J = 17.1, 4.8 Hz, 2H), 2.63 (dd, J = 17.1, 10.3 Hz, 2H). **^{13}C NMR** (126 MHz, CD_3OD) δ 148.7, 129.5, 124.2, 109.3, 35.0. **HRMS** (ESI+): m/z $[M + H]^+$ calculated for $C_{10}H_9{}^{79}BrO_2S$: 272.95794, found: 272.9581, mass error: 0.6 ppm.

*6-(5-Bromothiophen-2-yl)-4-oxo-4,5,6,7-tetrahydrobenzofuran-3-carboxylic Acid (**31**).* (12 mg, 34 μmol, 4%). **^{1}H NMR** (500 MHz, d_6-DMSO) δ 8.44 (s, 1H), 7.10 (d, J = 3.8 Hz, 1H), 6.89 (d, J = 3.8, 1.0 Hz, 1H), 3.95 (m, 1H), 3.19 (dd, J = 17.2, 9.6 Hz, 1H), 2.93 (dd, J = 16.5, 10.3 Hz, 1H), 2.87 (dd, J = 16.5, 4.7 Hz, 1H). **^{13}C NMR** (126 MHz, d_6-DMSO): δ 194.3, 169.0, 162.1, 150.5, 148.2, 130.6, 125.9, 117.7, 117.7, 109.6, 44.9, 35.9, 30.9. **HRMS** (ESI+): m/z $[M + H]^+$ calculated for $C_{13}H_9{}^{79}BrO_4S$: 340.94777, found: 340.9481, mass error: 1.0 ppm. **HPLC purity** 90%.

*(E)-4-(5-Chlorothiophen-2-yl)but-3-en-2-one (**32b**).* (0.93 g, 5.0 mmol, 83%). **^{1}H NMR** (500 MHz, $CDCl_3$) δ 7.49 (d, J = 16.0 Hz, 1H), 7.08 (d, J = 3.9 Hz, 1H), 6.90 (d, J = 3.9 Hz, 1H), 6.41 (d, J = 16.0 Hz, 1H), 2.34 (s, 3H). **^{13}C NMR** (126 MHz, $CDCl_3$) δ 197.3, 138.5, 135.0, 133.7, 131.2, 127.6, 125.6, 27.9.

*5-(5-Chlorothiophen-2-yl)cyclohexane-1,3-dione (**32c**).* (439 mg, 1.9 mmol, 42%). **^{1}H NMR** (500 MHz, CD_3OD) δ 6.83 (d, J = 3.8 Hz, 1H), 6.79 (dd, J = 3.8, 1.0 Hz, 1H), 3.63 (m, 1H), 2.73 (dd, J = 17.2, 4.8 Hz, 2H), 2.62 (dd, J = 17.2, 10.2 Hz, 2H). **^{13}C NMR** (126 MHz, CD_3OD) δ 145.9, 127.2, 125.7, 123.1, 39.6, 35.0. **HRMS** (ESI+): m/z $[M + H]^+$ calculated for $C_{10}H_9{}^{35}ClO_2S$: 229.00846, found: 229.0083, mass error: −0.6 ppm.

*6-(5-Chlorothiophen-2-yl)-4-oxo-4,5,6,7-tetrahydrobenzofuran-3-carboxylic Acid (**32**).* (66 mg, 220 μmol, 13%). **^{1}H NMR** (500 MHz, d_6-DMSO) δ 8.44 (s, 1H), 7.00 (d, J = 3.8 Hz, 1H), 6.92 (d, J = 3.8, 1.0 Hz, 1H), 3.93 (m, 1H), 3.16 (dd, J = 17.2, 9.6 Hz, 1H), 2.93 (dd, J = 16.5, 10.4 Hz, 1H), 2.87 (dd, J = 16.5, 4.6 Hz, 1H). **^{13}C NMR** (126 MHz, d_6-DMSO) δ 194.3, 169.0, 162.1, 150.5, 145.5, 127.1, 126.5, 124.9, 117.7, 117.7, 44.9, 35.9, 30.9. **HRMS** (ESI+): m/z $[M + H]^+$ calculated for $C_{13}H_9{}^{35}ClO_4S$: 296.99829, found: 296.9982, mass error: −0.3 ppm. **HPLC purity** 95%.

*(E)-4-(4-Bromothiophen-2-yl)but-3-en-2-one (**33b**).* (2.37 g, 10.2 mmol, 89%). **^{1}H NMR** (500 MHz, $CDCl_3$) δ 7.54 (d, J = 16.0 Hz, 1H,), 7.31 (br s, 1H), 7.22 (br s, 1H), 6.55 (d, J = 16.0 Hz, 1H), 2.36 (s, 3H). **^{13}C NMR** (126 MHz, $CDCl_3$) δ 197.3, 140.5, 134.1, 132.9, 126.6, 125.6, 111.1, 27.9.

*5-(4-Bromothiophen-2-yl)cyclohexane-1,3-dione (**33c**).* (1.40 g, 5.2 mmol, 61%). **^{1}H NMR** (500 MHz, CD_3OD) δ 7.27 (s, 1H), 6.94 (s, 1H), 3.70 (m, 1H), 2.75 (dd, J = 17.0, 4.8 Hz, 2H), 2.63 (dd, J = 17.0, 10.3 Hz, 2H). **^{13}C NMR** (126 MHz, CD_3OD) δ 148.4, 126.3, 120.8, 108.8, 39.5, 34.6. **HRMS** (ESI+): m/z $[M + H]^+$ calculated for $C_{10}H_9{}^{79}BrO_2S$: 272.95794, found: 272.9580, mass error: 0.0 ppm.

*6-(4-Bromothiophen-2-yl)-4-oxo-4,5,6,7-tetrahydrobenzofuran-3-carboxylic Acid (**33**).* (26 mg, 76 μmol, 3%). **^{1}H NMR** (500 MHz, d_6-DMSO) δ 13.01 (s, 1H), 8.46 (s, 1H), 7.56 (d, J = 1.5 Hz, 1H), 7.10 (dd, J = 1.5, 1.0 Hz, 1H), 3.98 (m, 1H), 3.43 (dd, J = 17.2, 5.4 Hz, 1H & D_2O peak), 3.22 (dd, J = 17.2, 9.8 Hz, 1H), 2.96 (dd, J = 16.5, 10.8 Hz, 1H), 2.86 (dd, J = 16.5, 4.4 Hz, 1H). **^{13}C NMR** (126 MHz, d_6-DMSO) δ 194.2, 169.1, 162.1, 150.5, 148.1, 127.3, 122.4, 117.6, 117.7, 108.8, 44.8, 35.6, 30.8. **HRMS** (ESI+): m/z $[M + H]^+$ calculated for $C_{13}H_9{}^{79}BrO_4S$: 340.94777, found: 340.9482, mass error: 1.3 ppm. **HPLC purity 95** %.

*Ethyl 6-(4-Bromothiophen-2-yl)-4-oxo-4,5,6,7-tetrahydrobenzofuran-3-carboxylate (**33d**).* (140 mg, 0.38 mmol, 15%). **^{1}H NMR** (500 MHz, d_6-DMSO) δ 7.95 (s, 1H), 7.14 (d, J = 1.3 Hz, 1H), 6.86 (d, J = 1.3, 0.9 Hz, 1H), 4.37 (q, J = 7.2 Hz, 2H), 3.83 (m, 1H), 3.37 (dd, J = 17.0, 5.0 Hz, 1H), 3.11 (dd, J = 17.0, 10.0 Hz, 1H), 2.96 (dd, J = 16.1, 4.1 Hz, 1H), 2.81 (dd, J = 16.1, 11.6 Hz, 1H), 1.39 (t, J = 7.2 Hz, 3H). **^{13}C NMR** (126 MHz, d_6-DMSO) δ 198.1, 166.3, 161.6, 148.5, 146.9, 126.8, 121.2, 118.9, 117.6, 109.6, 61.1, 46.2, 35.9, 31.8, 14.2. **HRMS (ESI):** m/z $[M + H]^+$ calculated for $C_{15}H_{13}{}^{79}BrO_4S$: 390.96101, found: 390.9613, mass error: 0.7 ppm. **HPLC purity** 95%.

*(E)-4-(4,5-Dibromothiophen-2-yl)but-3-en-2-one (**34b**).* (3.08 g, 9.9 mmol, 89%). **^{1}H NMR** (500 MHz, $CDCl_3$) δ 7.45 (dd, J = 16.1, 0.5 Hz, 1H), 7.10 (s, 1H), 6.46 (d,, J = 16.1 Hz, 1H), 2.35 (s, 3H). **^{13}C NMR** (126 MHz, $CDCl_3$) δ 197.0, 140.5, 133.5, 133.1, 126.6, 115.3, 114.7, 28.1. **HRMS** (ESI+): m/z $[M + H]^+$ calculated for $C_8H_6{}^{79}Br_2OS$: 308.85789, found: 308.8580, mass error: 0.3 ppm.

*5-(4,5-Dibromothiophen-2-yl)cyclohexane-1,3-dione (**34c**).* (508 mg, 1.4 mmol, 11%). **^{1}H NMR** (500 MHz, d_6-DMSO): δ 6.98 (s, 1H), 5.28 (s, 1H), 2.48−2.63 (m, 4H). **^{13}C NMR** (126 MHz, d_6-DMSO): δ 149.8, 127.4, 113.3, 108.5, 104.2, 34.8. **HRMS** (ESI+): m/z $[M + H]^+$ calculated for $C_{10}H_8{}^{79}Br_2O_2S$: 350.86846, found: 250.8680, mass error: −1.2 ppm.

*6-(4,5-Dibromothiophen-2-yl)-4-oxo-4,5,6,7-tetrahydrobenzofuran-3-carboxylic Acid (**34**).* (26 mg, 62 μmol, 5%). **^{1}H NMR** (500 MHz, d_6-DMSO) δ 12.97 (s, 1H), 8.46 (s, 1H), 7.12 (s, 1H), 3.95 (m, 1H), 3.41 (dd, J = 17.1, 5.1 Hz, 1H), 3.21 (dd, J = 17.6, 10.2 Hz, 1H), 2.94 (dd, J = 16.4, 10.7 Hz, 1H), 2.87 (dd, J = 16.4, 4.4 Hz, 1H). **^{13}C NMR** (126 MHz, d_6-DMSO) δ 193.8, 168.8, 162.1, 150.5, 148.4, 127.9, 117.7, 117.7, 113.5, 109.1, 44.5, 36.0, 30.5. **HRMS** (ESI+): m/z $[M + H]^+$ calculated for $C_{13}H_8{}^{79}Br_2O_4S$: 418.85829, found: 418.8577, mass error: −1.3 ppm. **HPLC purity** 90%.

*Ethyl 2-(1-Oxo-1,2,3,4-tetrahydronaphthalen-2-yl)acetate (**36**).* A solution of 2.5 M nBuLi (7.3 mL, 18.3 mmol, 1.1 equiv) in hexane was slowly added to a cold (−78 °C) solution of diisopropylamine (2.569 mL, 18.3 mmol, 1.1 equiv) in THF (8.3 mL). After 0.5 h, alpha tetralone **35** (2.22 mL, 16.7 mmol, 1 equiv) in THF (0.83 mL) was added dropwise, followed by addition of dry ethyl bromopyruvate (2.03 mL, 18.3 mmol, 1.1 equiv). The reaction was allowed to warm from -78 °C to rt and stirred for 16 h. The reaction was quenched by dilution with H_2O, extracted with EtOAc, dried over anhydrous $MgSO_4$ and purified by reversed-phase column chromatography (H_2O/MeCN 9:1 − 9:11) to yield ester **36** as a white powder (555 mg, 2.39 mmol, 14.3%). **^{1}H NMR** (500 MHz, $CDCl_3$) δ 8.05 (dd, J = 7.9, 1.3 Hz, 1H), 7.49 (t, J = 7.7 Hz, 1H), 7.33 (t, J = 7.7 Hz, 1H), 7.27 (d, J = 7.6 Hz, 1H), 4.21 (m, 2H), 3.15 (m, 1H), 3.10 (m, 1H), 3.07 (m, 1H), 3.02 (m, 1H), 2.44 (m, 1H), 2.27 (m, 1H), 1.99 (m, 1H), 1.31 (t, J = 7.1 Hz, 3H). **^{13}C NMR** (126 MHz, $CDCl_3$) δ 198.4, 172.6, 144.0, 133.4, 132.2, 128.8, 127.5, 126.7, 60.6, 44.8, 35.2, 29.3, 14.2.

*2-(1-Oxo-1,2,3,4-tetrahydronaphthalen-2-yl)acetic Acid (**37**).* To a solution of the ester **36** (555 mg, 2.39 mmol, 1 equiv) in a 2:1 mix of THF/MeOH (8 mL) was added 3 M NaOH (2.39 mL, 7.17 mmol, 3 equiv) and the reaction was stirred for 2 days at rt. The crude mixture was subjected to a stream of N_2 to remove the solvent and dissolved in water (26 mL). An orangey/pink solution resulted and was acidified to pH 2 (6 M HCl) before extraction with EtOAc, drying over anhydrous Na_2SO_4 and purification by HPLC to yield the product of the hydrolysis as a white powder (175 mg, 0.86 mmol, 36%). **^{1}H NMR** (500 MHz, $CDCl_3$) δ 8.05 (dd, J = 7.6, 1.3 Hz, 1H), 7.50 (t, J = 7.7 Hz, 1H), 7.33 (t, J = 7.7 Hz, 1H), 7.27 (d, J = 7.6 Hz, 1H), 3.16 (m, 1H), 3.10 (m, 1H), 3.07 (m, 1H), 3.02 (m, 1H), 2.52 (m, 1H), 2.30 (m, 1H), 2.02 (m, 1H). **^{13}C NMR** (126 MHz, $CDCl_3$) δ 198.5, 178.3, 144.1, 133.6, 132.0, 128.8, 127.6, 126.8, 44.7, 35.0, 29.3. **HPLC purity** 95%.

https://doi.org/10.1021/acs.jmedchem.5c03818
J. Med. Chem. 2026, 69, 12099−12121

■ ASSOCIATED CONTENT

Supporting Information

The Supporting Information is available free of charge at https://pubs.acs.org/doi/10.1021/acs.jmedchem.5c03818.

Crystallographic data statistic tables, supplemental figures, ^{1}H NMR, ^{13}C NMR, and HPLC spectra for the compounds, as well as mass spectrometry and MALDI-TOF spectra, raw data from differential scanning fluorimetry, statistical analysis and supercritical fluid chromatography spectra of enantiomers, and data from pK_a value estimation (PDF)

Molecular formula strings (CSV)

Covalent docking outputs publication (ZIP)

Accession Codes

PDB code for BTK PH domain with bound **1** is 6TUH; PDB code for BTK PH domain with bound **2** is 7I9I; PDB code for BTK PH domain with bound **4** is 7I96; PDB code for BTK PH domain with bound **5** is 9T23; PDB code for BTK PH domain with bound **7** is 7I90; PDB code for BTK PH domain with bound **8** is 7I97; PDB code for BTK PH domain with bound **9** is 7I92; PDB code for BTK PH domain with bound **10** is 7I98; PDB code for BTK PH domain with bound **11** is 9T3M; PDB code for BTK PH domain with bound **12** is 973G; PDB code for BTK PH domain with bound **13** is 7I91; PDB code for BTK PH domain with bound **14** is 7I9D; PDB code for BTK PH domain with bound **16** is 7I9F; PDB code for BTK PH domain with bound **17** is 9T1V; PDB code for BTK PH domain with bound **18** is 7I9E; PDB code for BTK PH domain with bound **19** is 9T0T; PDB code for BTK PH domain with bound **22** is 7I99; PDB code for BTK PH domain with bound **24** is 7I9B; PDB code for BTK PH domain with bound **25** is 7I95; PDB code for BTK PH domain with bound **26** is 7I9H; PDB code for BTK PH domain with bound **27** is 7I93; PDB code for BTK PH domain with bound **28** is 7I9G; PDB code for BTK PH domain with bound **29** is 9T21; PDB code for BTK PH domain with bound **30** is 7I9C; PDB code for BTK PH domain with bound **31** is 9RM0; PDB code for BTK PH domain with bound **32** is 7I9B; PDB code for BTK PH domain with bound **33** is 9RN5. Authors will release the atomic coordinates upon article publication.

■ AUTHOR INFORMATION

Corresponding Authors

David R. Spring − *Yusuf Hamied Department of Chemistry, University of Cambridge, Cambridge CB2 1EW, U.K.*; Email: spring@ch.cam.ac.uk

Marko Hyvönen − *Department of Biochemistry, University of Cambridge, Cambridge CB2 1GA, U.K.*; orcid.org/0000-0001-8683-4070; Email: mh256@cam.ac.uk

Authors

Rebekah M. West − *Yusuf Hamied Department of Chemistry, University of Cambridge, Cambridge CB2 1EW, U.K.*; orcid.org/0000-0002-8621-7184

Radu Costin Bizga Nicolescu − *Yusuf Hamied Department of Chemistry, University of Cambridge, Cambridge CB2 1EW, U.K.*

Paul Brear − *Department of Biochemistry, University of Cambridge, Cambridge CB2 1GA, U.K.*; orcid.org/0000-0002-4045-0474

James Wagstaff − *Department of Biochemistry, University of Cambridge, Cambridge CB2 1GA, U.K.*

Beata K. Blaszczyk − *Department of Biochemistry, University of Cambridge, Cambridge CB2 1GA, U.K.*

Tomas Deingruber − *Yusuf Hamied Department of Chemistry, University of Cambridge, Cambridge CB2 1EW, U.K.*

Matthew G. Sanders − *Oncology Targeted Discovery, Oncology R&D, The Discovery Centre, AstraZeneca, Cambridge CB2 0AA, U.K.*

Francisco Javier Pérez-Areales − *Yusuf Hamied Department of Chemistry, University of Cambridge, Cambridge CB2 1EW, U.K.*; orcid.org/0000-0001-9525-9346

Complete contact information is available at: https://pubs.acs.org/10.1021/acs.jmedchem.5c03818

Author Contributions

M.H. conceptualized the project. The first draft was written by R.C.B.N. and R.M.W., with P.B. contributing the X-ray crystallography section. The manuscript was written through contributions of all authors. All authors contributed to proof reading and have given approval to the final version of the manuscript. R.M.W., R.C.B.N., and P.B. contributed equally to this work.

Notes

The authors declare no competing financial interest.

■ ACKNOWLEDGMENTS

The authors would like to thank Peter Gierth, Andrew Mason, and Duncan Howe for their support in NMR analysis; Dijana Matak-Vinkovic, Roberto Canales, and Asha Boodhun for maintaining the instruments and methods for the protein mass spectrometry; Kristina Kostadinova (Spring Group) for the MALDI spectra; and Linwei Zeng (Spring Group) for the analytical chiral LCMS of compound **19** and Arqum Anwar (Babraham Institute) for conducting biological studies. The authors thank X-ray crystallographic and Biophysics facilities at the Department of Biochemistry for access to instrumentation and support. The authors are grateful for access to beamlines I04, I03, and I04-1 at Diamond Light Source (Proposals mx14043, mx25402, mx33658, and mx40158). The project was supported by MRC Confidence in Concept award. R.M.W. acknowledges support from the UK Engineering and Physical Sciences Research Council (EPSRC) Centre of Doctoral Training in Automated Chemical Synthesis Enabled by Digital Molecular Technologies (SynTech) [EP/S024220/1]. R.C.B.N. acknowledges support from Trinity College Cambridge. T.D. acknowledges a studentship from AstraZeneca. F.J.P.-A. acknowledges Fundación Ramón Areces (reference BEVP31A6160) and Marie Skłodowska-Curie Individual Fellowships (MSCA-IF-2020, grant number 101025271). The Spring group research was supported by grants from UKRI (EP/P020291/1). For the purpose of Open Access, the author has applied a CC BY public copyright licence to any Author Accepted Manuscript (AAM) version arising.

■ ABBREVIATIONS

ATP	adenosine triphosphate
BTK	Bruton's Tyrosine Kinase
DCM	dichloromethane
DMF	dimethyl formamide

https://doi.org/10.1021/acs.jmedchem.5c03818
J. Med. Chem. 2026, 69, 12099−12121

DMSO	dimethyl sulfoxide
DSF	differential scanning fluorimetry
ERBB4	erythroblastic leukemia viral oncogene 4
FCC	flash column chromatography
FDA	Food and Drug Administration
HEPES	4-(2-hydroxyethyl)-1-piperazineethanesulfonic acid
HPLC	high-performance liquid chromatography
HRMS	high resolution mass spectrometry
IC_{50}	half maximal inhibitory concentration
IP4	inositol 1,3,4,5-tetrakisphosphate
ITC	isothermal titration calorimetry
K_d	dissociation constant
LCMS	liquid chromatography−mass spectrometry
LDA	lithium diisopropylamide
MALDI-TOF	matrix-assisted laser desorption/ionization time of flight
MOE	molecular operating environment
NMR	nuclear magnetic resonance
PDB	Protein Data Bank
PE	petroleum ether
PH	Pleckstrin Homology
PIP3	phosphatidylinositol (3,4,5)-trisphosphate
PLC	phospholipase C
rt	room temperature
SH2	Src Homology 2
SH3	Src Homology 3
SFC	supercritical fluid chromatography
s-phos	2-dicyclohexylphosphino-2′,6′-dimethoxybiphenyl
TCEP	tris(2-carboxyethyl)phosphine
THF	tetrahydrofuran
TLC	thin layer chromatography
WT	wildtype

REFERENCES

(1) Wylie, A. A.; Schoepfer, J.; Jahnke, W.; Cowan-Jacob, S. W.; Loo, A.; Furet, P.; Marzinzik, A. L.; Pelle, X.; Donovan, J.; Zhu, W.; Buonamici, S.; Hassan, A. Q.; Lombardo, F.; Iyer, V.; Palmer, M.; Berellini, G.; Dodd, S.; Thohan, S.; Bitter, H.; Branford, S.; Ross, D. M.; Hughes, T. P.; Petruzzelli, L.; Vanasse, K. G.; Warmuth, M.; Hofmann, F.; Keen, N. J.; Sellers, W. R. The Allosteric Inhibitor ABL001 Enables Dual Targeting of BCR−ABL1. *Nature* **2017**, *543* (7647), 733−737.

(2) Stockwell, S. R.; Scott, D. E.; Fischer, G.; Guarino, E.; Rooney, T. P. C.; Feng, T.-S.; Moschetti, T.; Srinivasan, R.; Alza, E.; Asteian, A.; Dagostin, C.; Alcaide, A.; Rocaboy, M.; Blaszczyk, B.; Higueruelo, A.; Wang, X.; Rossmann, M.; Perrior, T. R.; Blundell, T. L.; Spring, D. R.; McKenzie, G.; Abell, C.; Skidmore, J.; Venkitaraman, A. R.; Hyvönen, M. Selective Aurora A-TPX2 Interaction Inhibitors Have In Vivo Efficacy as Targeted Antimitotic Agents. *J. Med. Chem.* **2024**, *67* (17), 15521−15536.

(3) Powis, G.; Meuillet, E. J.; Indarte, M.; Booher, G.; Kirkpatrick, L. Pleckstrin Homology [PH] Domain, Structure, Mechanism, and Contribution to Human Disease. *Biomedicine & Pharmacotherapy* **2023**, *165*, No. 115024.

(4) Jo, H.; Lo, P.-K.; Li, Y.; Loison, F.; Green, S.; Wang, J.; Silberstein, L. E.; Ye, K.; Chen, H.; Luo, H. R. Deactivation of Akt by a Small Molecule Inhibitor Targeting Pleckstrin Homology Domain and Facilitating Akt Ubiquitination. *Proc. Natl. Acad. Sci. U. S. A.* **2011**, *108* (16), 6486−6491.

(5) Hyvonen, M. Structure of the PH Domain and Btk Motif from Bruton's Tyrosine Kinase: Molecular Explanations for X-Linked Agammaglobulinaemia. *EMBO J.* **1997**, *16* (12), 3396−3404.

(6) Bradshaw, J. M. The Src, Syk, and Tec Family Kinases: Distinct Types of Molecular Switches. *Cell. Signal.* **2010**, *22* (8), 1175−1184.

(7) Tsukada, S.; Saffran, D. C.; Rawlings, D. J.; Parolini, O.; Allen, R. C.; Klisak, I.; Sparkes, R. S.; Kubagawa, H.; Mohandas, T.; Quan, S.; Belmont, J. W.; Cooper, M. D.; Conley, M. E.; Witte, O. N. Deficient Expression of a B Cell Cytoplasmic Tyrosine Kinase in Human X-Linked Agammaglobulinemia. *Cell* **1993**, *72* (2), 279−290.

(8) Wang, X.; Kokabee, L.; Kokabee, M.; Conklin, D. S. Bruton's Tyrosine Kinase and Its Isoforms in Cancer. *Front. Cell Dev. Biol.* **2021**, *9*, No. 668996.

(9) Chung, J. K.; Nocka, L. M.; Decker, A.; Wang, Q.; Kadlecek, T. A.; Weiss, A.; Kuriyan, J.; Groves, J. T. Switch-like Activation of Bruton's Tyrosine Kinase by Membrane-Mediated Dimerization. *Proc. Natl. Acad. Sci. U. S. A.* **2019**, *116* (22), 10798−10803.

(10) Teocchi, M. A.; Domingues Ramalho, V.; Abramczuk, B. M.; D'Souza-Li, L.; Santos Vilela, M. M. *BTK* Mutations Selectively Regulate BTK Expression and Upregulate Monocyte *XBP1* MRNA in XLA Patients. *Immun. Inflamm. Dis.* **2015**, *3* (3), 171−181.

(11) Rawlings, D. J.; Saffran, D. C.; Tsukada, S.; Largaespada, D. A.; Grimaldi, J. C.; Cohen, L.; Mohr, R. N.; Bazan, J. F.; Howard, M.; Copeland, N. G.; Jenkins, N. A.; Witte, O. N. Mutation of Unique Region of Bruton's Tyrosine Kinase in Immunodeficient XID Mice. *Science* **1979**, *261* (5119), 358−361.

(12) Sampath, D.; Malik, A.; Plunkett, W.; Nowak, B.; Williams, B.; Burton, M.; Verstovsek, S.; Faderl, S.; Garcia-Manero, G.; List, A. F.; Sebti, S.; Kantarjian, H. M.; Ravandi, F.; Lancet, J. E. Phase I Clinical, Pharmacokinetic, and Pharmacodynamic Study of the Akt-Inhibitor Triciribine Phosphate Monohydrate in Patients with Advanced Hematologic Malignancies. *Leuk. Res.* **2013**, *37* (11), 1461−1467.

(13) Deyle, K. M.; Farrow, B.; Qiao Hee, Y.; Work, J.; Wong, M.; Lai, B.; Umeda, A.; Millward, S. W.; Nag, A.; Das, S.; Heath, J. R. A Protein-Targeting Strategy Used to Develop a Selective Inhibitor of the E17K Point Mutation in the PH Domain of Akt1. *Nat. Chem.* **2015**, *7* (5), 455−462.

(14) Park, J.; Zhang, H.; Kwak, H. J.; Gadhe, C. G.; Kim, Y.; Kim, H.; Noh, M.; Shin, D.; Ha, S.-J.; Kwon, Y.-G. A Novel Small Molecule, CU05−1189, Targeting the Pleckstrin Homology Domain of PDK1 Suppresses VEGF-Mediated Angiogenesis and Tumor Growth by Blocking the Akt Signaling Pathway. *Front. Pharmacol.* **2023**, *14*, No. 1275749.

(15) Nawrotek, A.; Benabdi, S.; Niyomchon, S.; Kryszke, M.-H.; Ginestier, C.; Cañeque, T.; Tepshi, L.; Mariani, A.; St Onge, R. P.; Giaever, G.; Nislow, C.; Charafe-Jauffret, E.; Rodriguez, R.; Zeghouf, M.; Cherfils, J. PH-Domain-Binding Inhibitors of Nucleotide Exchange Factor BRAG2 Disrupt Arf GTPase Signaling. *Nat. Chem. Biol.* **2019**, *15* (4), 358−366.

(16) Zhang, Z.; Morstein, J.; Ecker, A. K.; Guiley, K. Z.; Shokat, K. M. Chemoselective Covalent Modification of K-Ras(G12R) with a Small Molecule Electrophile. *J. Am. Chem. Soc.* **2022**, *144* (35), 15916−15921.

(17) Baraldi, E.; Carugo, K. D.; Hyvönen, M.; Surdo, P. L.; Riley, A. M.; Potter, B. V.; O'Brien, R.; Ladbury, J. E.; Saraste, M. Structure of the PH Domain from Bruton's Tyrosine Kinase in Complex with Inositol 1,3,4,5-Tetrakisphosphate. *Structure* **1999**, *7* (4), 449−460.

(18) Cai, Z.; Peng, H.; Sun, S.; He, J.; Luo, F.; Huang, Y. DeepKa Web Server: High-Throughput Protein pK_a Prediction. *J. Chem. Inf. Model.* **2024**, *64* (8), 2933−2940.

(19) Reis, P. B. P. S.; Vila-Viçosa, D.; Rocchia, W.; Machuqueiro, M. PypKa: A Flexible Python Module for Poisson−Boltzmann-Based pK_a Calculations. *J. Chem. Inf. Model.* **2020**, *60* (10), 4442−4448.

(20) Abbasov, M. E.; Kavanagh, M. E.; Ichu, T.-A.; Lazear, M. R.; Tao, Y.; Crowley, V. M.; Am Ende, C. W.; Hacker, S. M.; Ho, J.; Dix, M. M.; Suciu, R.; Hayward, M. M.; Kiessling, L. L.; Cravatt, B. F. A Proteome-Wide Atlas of Lysine-Reactive Chemistry. *Nat. Chem.* **2021**, *13* (11), 1081−1092.

(21) GraphPad Software *GraphPad Prism, Version 10*; GraphPad Software: San Diego, CA, 2023.

(22) PerkinElmer (now Revvity Signals) *ChemDraw Professional*; PerkinElmer: Waltham, MA, 2023.

https://doi.org/10.1021/acs.jmedchem.5c03818
J. Med. Chem. 2026, 69, 12099−12121

(23) McCoy, A. J.; Grosse-Kunstleve, R. W.; Storoni, L. C.; Read, R. J. Likelihood-Enhanced Fast Translation Functions. *Acta Crystallogr. D Biol. Crystallogr.* **2005**, *61* (4), 458−464.
(24) Winn, M. D.; Ballard, C. C.; Cowtan, K. D.; Dodson, E. J.; Emsley, P.; Evans, P. R.; Keegan, R. M.; Krissinel, E. B.; Leslie, A. G. W.; McCoy, A.; McNicholas, S. J.; Murshudov, G. N.; Pannu, N. S.; Potterton, E. A.; Powell, H. R.; Read, R. J.; Vagin, A.; Wilson, K. S. Overview of the *CCP* 4 Suite and Current Developments. *Acta Crystallogr. D Biol. Crystallogr.* **2011**, *67* (4), 235−242.
(25) Murshudov, G. N.; Vagin, A. A.; Dodson, E. J. Refinement of Macromolecular Structures by the Maximum-Likelihood Method. *Acta Crystallogr. D Biol. Crystallogr.* **1997**, *53* (3), 240−255.
(26) Bricogne, G.; Blanc, E.; Brandl, M.; Flensburg, C.; Keller, P.; Paciorek, W.; Roversi, P.; Sharff, A.; Smart, O. S.; Vonrhein, C.; Womack, T. O. *BUSTER Version X.Y.Z.*; Global Phasing Ltd: Cambridge, United Kingdom, 2017.
(27) Emsley, P.; Cowtan, K. *Coot*: Model-Building Tools for Molecular Graphics. *Acta Crystallogr. D Biol. Crystallogr.* **2004**, *60* (12), 2126−2132.
(28) Long, F.; Nicholls, R. A.; Emsley, P.; Gražulis, S.; Merkys, A.; Vaitkus, A.; Murshudov, G. N. *AceDRG*: A Stereochemical Description Generator for Ligands. *Acta Crystallogr. D Struct. Biol.* **2017**, *73* (2), 112−122.
(29) Schrödinger LLC *Schrödinger Release 2025-2*; Schrödinger LLC: New York, NY, 2025.
(30) Schrödinger LLC *Maestro Schrödinger Release 2025-3*; Schrödinger LLC: New York, NY, 2025.

https://doi.org/10.1021/acs.jmedchem.5c03818
J. Med. Chem. 2026, 69, 12099−12121